ISSN: 2153-1196 Volume 14, Number 13, December 2023

Scientific Research Publishing

Journal of Modern Physics

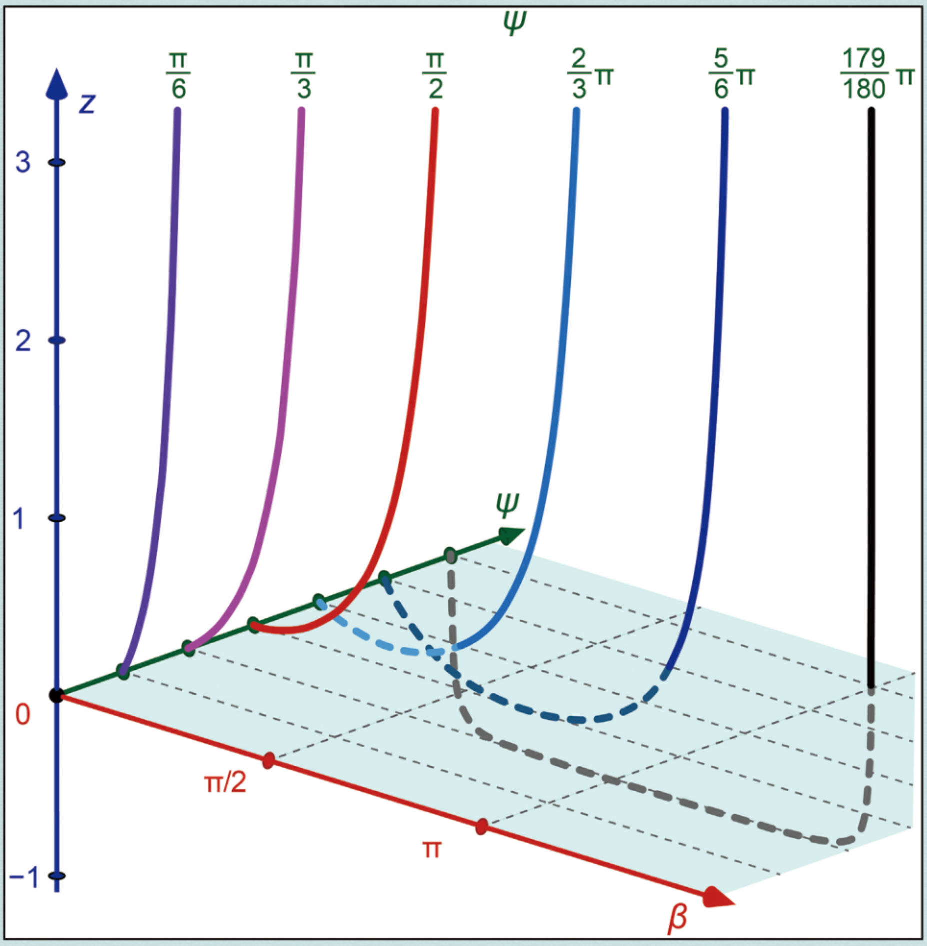

ISSN: 2153-1196
9 772153 119007 13

https://www.scirp.org/journal/jmp

Journal Editorial Board

ISSN: 2153-1196 (Print) ISSN: 2153-120X (Online)
https://www.scirp.org/journal/jmp

Editorial Board

Scientific Research Publishing

Journal of Modern Physics, 2023, 14, 1693-1782
https://www.scirp.org/journal/jmp
ISSN Online: 2153-120X
ISSN Print: 2153-1196

Table of Contents

Volume 14 Number 13 December 2023

The figure on the front cover is from the article published in Journal of Modern Physics, 2023, Vol. 14, No. 13, pp. 1693-1702 by Hitoshi Shibata and Norio Ogata.

Journal of Modern Physics (JMP)
Journal Information

SUBSCRIPTIONS

The *Journal of Modern Physics* (Online at Scientific Research Publishing, https://www.scirp.org/) is published monthly by Scientific Research Publishing, Inc., USA.

Subscription rates:
Print: $89 per issue.
To subscribe, please contact Journals Subscriptions Department, E-mail: sub@scirp.org

SERVICES

Advertisements
Advertisement Sales Department, E-mail: service@scirp.org

Reprints (minimum quantity 100 copies)
Reprints Co-ordinator, Scientific Research Publishing, Inc., USA.
E-mail: sub@scirp.org

COPYRIGHT

PRODUCTION INFORMATION

For manuscripts that have been accepted for publication, please contact:
E-mail: jmp@scirp.org

Journal of Modern Physics, 2023, 14, 1693-1702
https://www.scirp.org/journal/jmp
ISSN Online: 2153-120X
ISSN Print: 2153-1196

Apparent Accelerated Expansion of the Three-Dimensional Spherical Universe Observed during Its Contraction Phase

Hitoshi Shibata[1], **Norio Ogata**[2*]

[1]Taiko Pharmaceutical Company, Limited, Osaka, Japan
[2]R & D Department, Taiko Pharmaceutical Company, Limited, Seikacho, Japan
Email: *nogata7@yahoo.co.jp

How to cite this paper: Shibata, H. and Ogata, N. (2023) Apparent Accelerated Expansion of the Three-Dimensional Spherical Universe Observed during Its Contraction Phase. *Journal of Modern Physics*, **14**, 1693-1702.
https://doi.org/10.4236/jmp.2023.1413099

Received: November 2, 2023
Accepted: December 10, 2023
Published: December 13, 2023

Abstract

In recent years, it has been thought that the expansion of the universe has begun to accelerate. However, there are other views against this. Here we propose a new theory based on the three-dimensional spherical (S^3) universe wherein the same observations as the present universe can also be found by the accelerated *contraction* of the universe. According to our theory, the expansion velocity of the S^3 universe slowed down after the Big Bang, and all the kinetic energy was converted into potential energy to reach the great sphere. After that, accelerated contraction begins, and the universe finally converges to an original single point. In the S^3 universe, the passage of time (referred to as "proper time") changes depending on its expansion velocity. The frequency of light emitted from celestial bodies is determined by their proper time on emission, and when the light is observed by observers having different proper time, a redshift or blueshift is observed. Observers in the expansion phase observe redshifts, because the proper time of the observer progresses faster than that of emitted light, but observers in the contraction phase observe an accelerated delay of the proper time, so the progress of the proper time is reversed based upon its order from nearby celestial bodies, a blueshift is observed, and its range of observable distance increases. The results of this early contraction phase are consistent with the observations of the current universe. In conclusion, the S^3 universe may be able to explain the geometrical structure of the current universe.

Keywords

Three-Dimensional Universe, Spherical Universe, Redshift, Big Bang

1. Introduction

Since the discovery of Hubble, the universe is expanding in an accelerated fashion according to the current cosmology [1] [2] [3] [4] [5]. The most reliable rationale of this expansion is the redshift of the light emitted from celestial bodies, where the extent of the redshift is larger if the celestial body is farther away [6]-[12]. Recently, the observation precision of the cosmic microwave background (CMB) radiation and the redshift of large galaxies has increased, and the measurement of the expansion velocity of the universe has become more accurate [13]. However, a basic question of what occurred at the beginning of the universe and an ultimate fate of the universe are still unknown [13]. Furthermore, the observation data of more distant celestial bodies are welcome, because they let us know what happened in the past universe. For instance, Chen *et al.* reported a redshift of $z = 6.68$ in their observation data of a distant celestial body [14]. However, Stern *et al.* claim that it may be impossible to observe the redshift of wavelengths less than 9300 Å at such a distance, because the intensity of the light is too weak to observe [15]. Although the observation data of very distant celestial bodies are important, there are questions relative to the data's reliability [15].

A question has also been raised against the accelerated expansion of the universe first pointed out by Hubble [1] [4]. Barrow *et al.* also pointed out a question of whether the expansion of the universe is accelerating or decelerating [16] [17]. Furthermore, although the primary force of the currently believed accelerated expansion of the universe derives from the "repulsive gravity" of dark energy [4], some researchers doubt even the existence of dark energy [18]. We hereby present the following proposal to construct a clearer theory regarding such a problem. Lehoucq *et al.* presented the existence of a 3-dimensional spherical universe as a basic structure of the universe [19]. The 3-dimensional sphere is a manifold having a spherical structure that exists in 4-dimensional space time, and the universe is considered to exist on its surface according to Shibata *et al.* [20]. We think that the universe began explosively from a tiny Big Bang and expanded soon after in an accelerated way. Next, the expansion velocity decreases and ceases, begins to contract in an accelerated fashion, and finally ends with the Big Crunch with contraction to a single point. According to our proposal, it is possible to explain the current structure of the universe without considering the dark energy, and to explain the expansion and contraction of the universe. Focusing on this point, we present a new concept of the current structure of the universe.

2. Three-Dimensional Spherical Universe

The 3-dimensional spherical (S^3) universe model we propose in this paper is composed of four dimensions, in which they are shown by 3-dimensional *x*-, *y*-, and z-coordinates that represent a space and a *w*-coordinate that has a dimension of distance by coordinate time *t* multiplied by light speed c (Equations (1) and (2)). In Equation (2), R represents the maximum radius of the S^3 universe.

$$w = ct, \tag{1}$$

and

$$w^2 + x^2 + y^2 + z^2 = R^2. \tag{2}$$

In this S^3 universe, the space expands and contracts while the coordinate time t advances from the birth of the universe ($w = -R$) to its end ($w = R$) in one direction (**Figure 1(a)**). At arbitrary coordinate time t, the S^3 universe can be observed as a 2-dimensional sphere of radius r mapped in a 3-dimensional space when it is observed from one direction outside of the S^3 universe fixing one of the space coordinates to zero (**Figure 1(a)**). On the other hand, for an observer inside the hypersphere S^3 universe, the universe is observed as a 3-dimensional observer-centred filled-in sphere, and numerous lights from celestial bodies scattered at each distance are observed as if they are coming straight to us (**Figure 1(b)**). This observed universe is a map of the light from a light source of a hypersphere of observer-centred space inside of the 3-dimensional sphere (**Figure 1(b)**).

3. Mathematical Characteristics of the S³ Universe

When the S^3 universe is represented in polar coordinates, it is written as shown in Equations (3) - (6). ψ is elevation angle of space coordinate against the w coordinate axis, and it represents the expansion of the observable universe. It changes from zero to π upon the passage of coordinate time t. This ψ will be

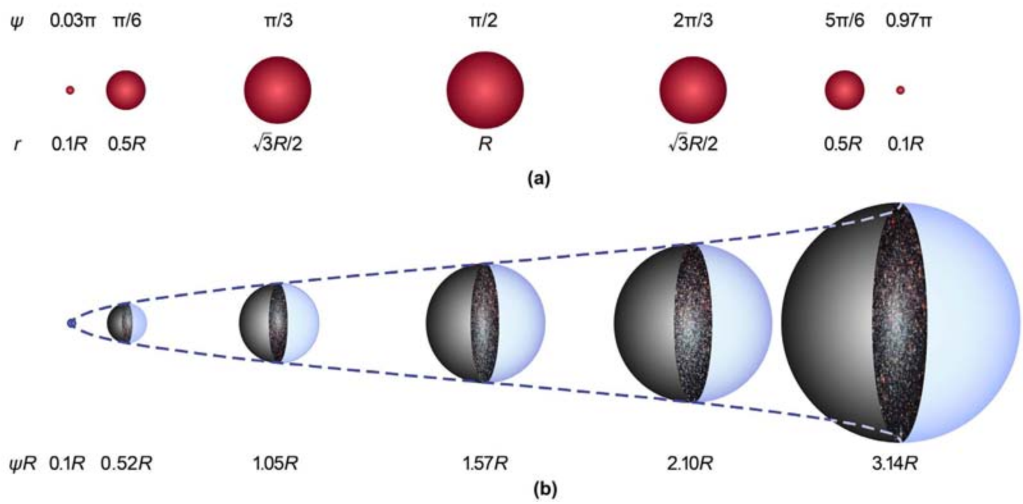

Figure 1. Expansion of the universe that accompanies the expansion contraction of the observable universe. (a) This shows expansion contraction of the universe from the birth to its end as a 2-dimensional sphere that follows the passage of coordinate time t with one dimension omitted. Upon the passage of coordinate time t, the expansion angle ψ of the S^3 universe increases, the radius r expands to R, but then returns to zero. (b) The three-dimensional spherical universe demonstrated as a 2-dimensional sphere. The balls represent cross sections of the observable universe at a respective expansion angle ψ of the S^3 universe with an arbitrary observation point in its centre. Upon increasing expansion angle ψ, radius ψR also increases, not only during the expansion but also during its contraction phase.

called expansion angle hereafter. θ is zenith angle at an arbitrary ψ, when the direction of the z-axis is facing upward, and the zenith top is zero and the zenith bottom is π. Likewise, η shows a deflection angle from the x-axis; it is positive when a right screw rotated clockwise goes ahead. This variable moves from zero to 2π.

$$w = -R\cos(\psi), \tag{3}$$

$$x = R\sin(\psi)\sin(\theta)\cos(\eta), \tag{4}$$

$$y = R\sin(\psi)\sin(\theta)\sin(\eta), \tag{5}$$

$$z = R\sin(\psi)\cos(\theta) \tag{6}$$

and

$$\psi = \cos^{-1}\left(\frac{-ct}{R}\right), \tag{7}$$

where $0 \le \psi \le \pi$, $0 \le \theta \le \pi$, and $0 \le \eta \le 2\pi$.

A radius r of the S^3 universe is shown in Equation (8), and it becomes the maximal R at a great sphere. The expansion velocity v of the S^3 universe at coordinate time t is shown in Equation (9).

$$r = R\sin(\psi) \tag{8}$$

and

$$\frac{\mathrm{d}r}{\mathrm{d}t} = v = -\mathrm{c}\cot(\psi). \tag{9}$$

The minute distance that light runs in the S^3 universe becomes cosec(ψ)-times larger than that when it runs on a flat space time, because the radius of the S^3 universe changes upon the passage of coordinate time t. This increase of the geodesic can be explained by the increase of the passage of proper time τ on the S^3 hypersphere against the passage of proper time τ on the expansion angle ψ, if the concept that light speed is always constant holds (Equation (11)). Therefore, if the ratio cosec(ψ) is integrated by coordinate time t, the ratio of the passage of proper time τ against that of coordinate time t from its origin ($-R/c$) to the coordinate time t is obtained (Equation (12)).

$$\mathrm{c}\Delta\tau = \operatorname{cosec}(\psi)\mathrm{c}\Delta t, \tag{10}$$

$$\frac{\mathrm{d}\tau}{\mathrm{d}t} = \operatorname{cosec}(\psi) \tag{11}$$

and

$$\frac{\mathrm{c}}{R}\int_{-\frac{R}{\mathrm{c}}}^{t} \operatorname{cosec}(\psi)\,\mathrm{d}t = \frac{\mathrm{c}}{R}\int_{-\frac{R}{\mathrm{c}}}^{t}\left[\cos^{-1}\left(\frac{-\mathrm{c}t}{R}\right)\right]\mathrm{d}t = \cos^{-1}\left(\frac{-\mathrm{c}t}{R}\right) = \psi. \tag{12}$$

4. Geodesic of Light in the S^3 Universe

The result of this integration indicates that the angular distance of the light of the Big Bang (CMB) that ran in the S^3 universe is the same as the expansion angle ψ of the S^3 universe. Therefore, this expansion angle ψ is the angular distance that CMB runs, and the geodesic distance S_ψ is the same as the arc length ψR of the great sphere of radius R and angle ψ as shown in **Figure 2** (Equation (13)). The geodesic distance S_β that light reaches the observation point from a celestial body born after the Big Bang is βR, if the angular distance between an observation point and a space coordinate of the celestial body is β (Equation (14)). As shown in **Figure 2**, angular distance and the geodesic of a celestial body that remains in the S^3 universe are always constant despite the expansion·contraction of the S^3 universe.

$$S_\psi = \psi R \tag{13}$$

and

$$S_\beta = \beta R. \tag{14}$$

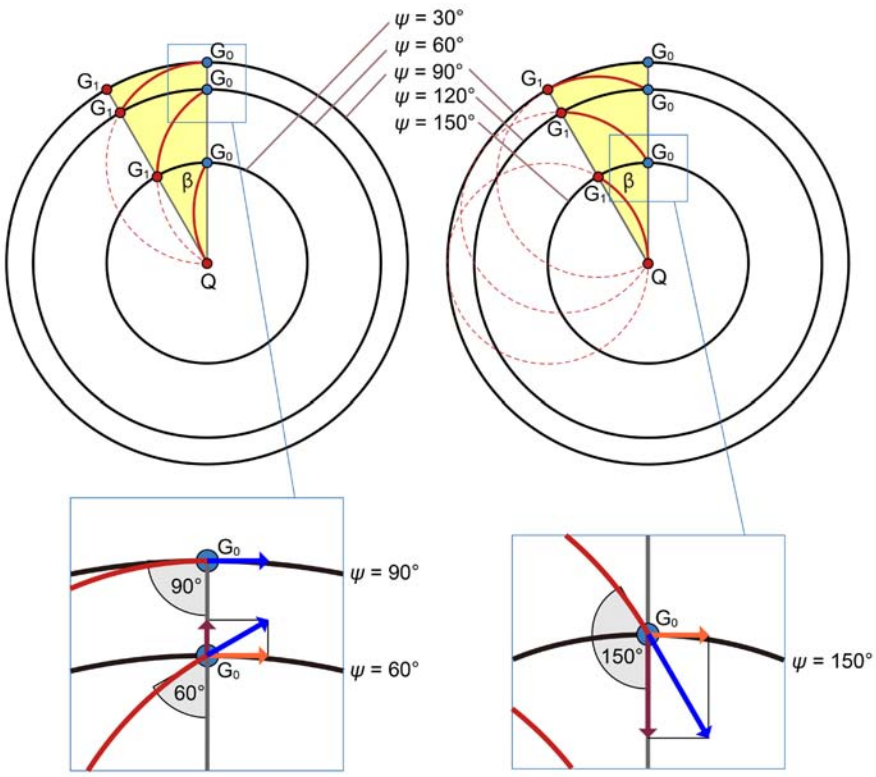

Figure 2. The geodesic of light in the S^3 universe. The concentric circles of the left upper panel show cross sections during expansion, and those in the right upper panel show cross sections during contraction of the S^3 universe at respective expansion angles ψ. The angular distance (longitude difference β) of the space coordinate formed between the stationary celestial bodies G_1 and G_0 is always constant despite the changes in expansion angle ψ. The red arcs are the geodesic of light that reaches from G_1 to G_0, and their distances are always constant in the course of the light, because the radius of the S^3 universe changes during the time it runs. The enlarged figures in the lower panels show that the incident angle of the light that reaches G_0 is the expansion angle ψ. The orange arrow shows the distance $c\Delta t$ that light runs during the passage of minute coordinate time t in a flat space time, the brown arrow shows the expansion $v\Delta t$ of the universe, and the blue arrow shows the elongation $c\Delta t\,\mathrm{cosec}(\psi)$ of the geodesic of light due to the expansion of the S^3 universe.

5. Observable Universe

The observable universe that can be observed at the expansion angle ψ in the S^3 universe is an image mapped in the 3-dimensional sphere of the radius ψR with its center in the observation point. The radius ψR of the observable universe becomes large soon after the Big Bang, but then the expansion velocity slows down. Thereafter, when the S^3 universe enters the contraction phase, the expansion velocity decreases and the radius ψR becomes $\pi R/2$ in the great sphere of the S^3 universe and the expansion velocity increases again. The radius ψR then reaches maximal πR immediately before the end of the S^3 universe (Equation (13) and Figure 3).

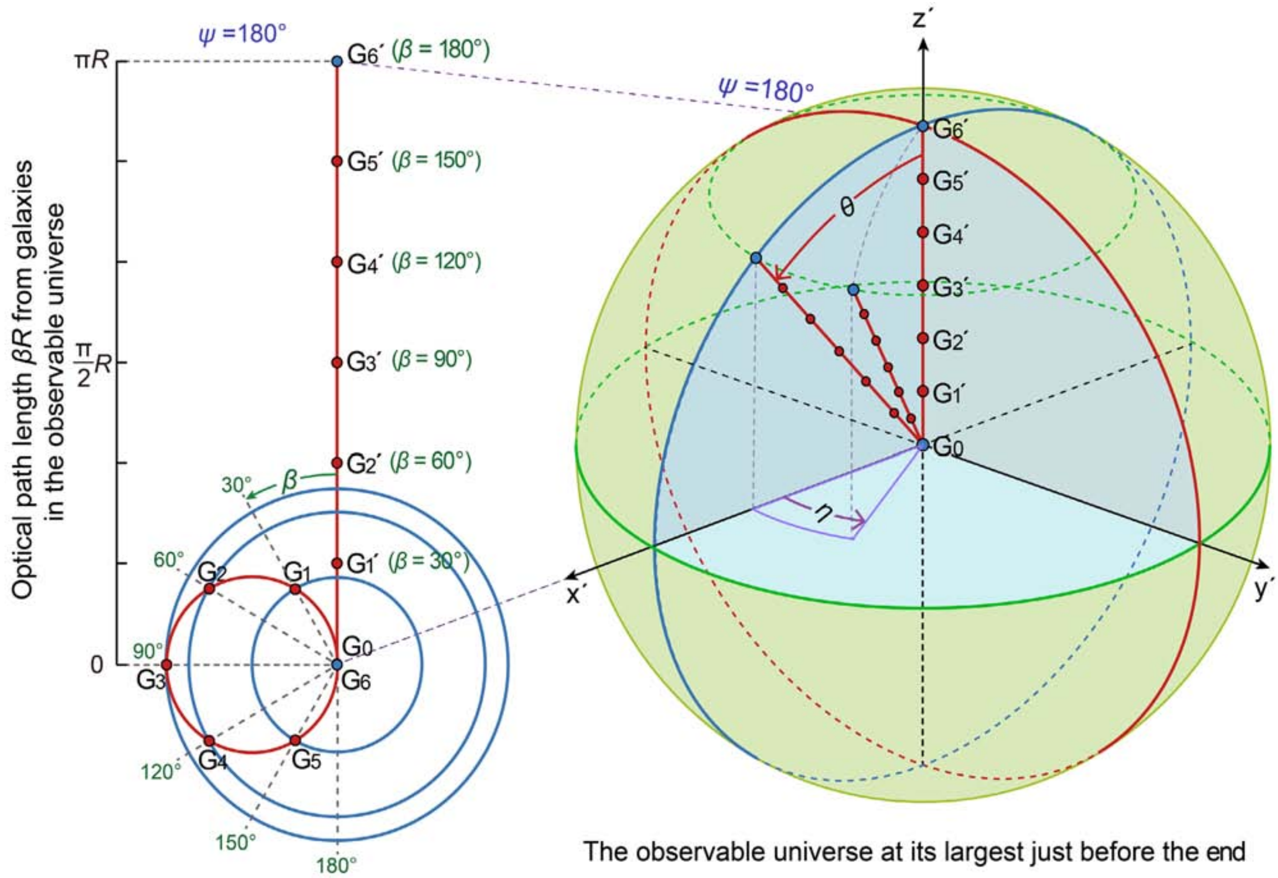

Figure 3. The observable universe that has become maximal just before the end of the S^3 universe. This figure shows the observable universe observed at an arbitrary observation point G_0 inside the S^3 universe just before it ends at an expansion angle $\psi = 180˚$. The left lower red circle that inscribes the outermost concentric circle shows optical paths of light that reach the observation point G_0 from the same direction just before the end of the S^3 universe, and the red points G_0 through G_6 on the circumference of the red circle show light sources of the galaxies of longitude difference (β) 30˚, 60˚, 90˚, 120˚, 150˚, and 180˚ (CMB), respectively. The points G_1' through G_6' on the red straight vertical line in the left figure are the points on the extended line of the light straight from the observation G_0 to the direction of the incident angle of the red circle, and are the mappings of the celestial bodies of the respective optical path length βR from G_0 in the observable universe. The sphere in the right figure shows the observable universe that has become a maximal size just before the end of the S^3 universe as a 3-dimensional space of x', y', and z' coordinates, and it shows the red segments of the line of the left figure which are expanded from observation point G_0 to all the directions of the observable universe. θ is a zenith angle of a celestial body mapped in the observable universe, and η is a deviation angle. The distance to a celestial body is shown as βR, if the longitude difference between the observation point to the celestial body is β.

6. Redshift of Light from Celestial Bodies

The optical path light reaches from an arbitrary celestial body to an observation point is always constant despite the expansion of the observable universe (**Figure 2**). However, a redshift (or blueshift when minus) is observed due to a difference in the wavelength of light between the time of emission and that of observation, because the passage of the proper time of the light at the time of emission and that of observation differs. The redshift z is shown in Equation (15), when the longitude difference of the space coordinate between the light source and the observation points is β. λ_s is the wavelength of the light source and λ is the wavelength of light at the observation point. The ratio between them is a ratio of the inverse of the elongation of the proper time (Equation (12)).

$$z = \frac{\lambda}{\lambda_s} - 1 = \frac{\operatorname{cosec}(\psi - \beta)}{\operatorname{cosec}(\psi)} - 1 = \frac{\sin(\psi)}{\sin(\psi - \beta)} - 1. \quad (15)$$

The redshift is observed in a flat space due to the receding velocity of the light source, but it is observed due to the difference of the proper times between those of emission and observation, both stationary, in the S^3 universe. From Equation (15), it can be concluded that the blueshift begins successively from neighbouring stars of smaller to larger longitudinal difference β when the S^3 universe enters the contraction phase (**Figure 4**).

This result agrees very well with the current observation of the universe that the universe apparently turned from decelerated to accelerated expansion [21]. In fact, the S^3 universe is contracting in an accelerated way, and is not expanding. In view of our theory, it would be important to mention the report of Lombriser [22]. He found that the redshift of galaxies can be interpreted to be an evolution of particle masses as a consequence of conformal transformation of the FLRW (Friedmann Lemaître Robertson Walker) metric to a Minkowski space [22]. Although his rationale behind the theory is different from that of our theory, he pointed out that the current universe may not be expanding based upon his theory. The conclusion of his theory is basically same as our conclusion.

Welch *et al.* recently reported observations of a distant star of redshift 6.2 ± 0.1 and 900 million years after the Big Bang [23]. Based upon their observations we calculated from Equation (13) that R is $13.8/\psi$ billion light years. The expansion angle of the light source is $9 = \psi_s R$ from Equation (13). Therefore, ψ_s is $9/R$ radians and $\psi_s = (9/138)\psi = 0.0652\psi$. If we assume that the expansion angle of a star at the time of emission is ψ_s, Equation (15) becomes

$$z = \frac{\lambda}{\lambda_s} - 1 = \frac{\sin(\psi)}{\sin(\psi_s)} - 1. \quad (16)$$

By substituting $z = 6.2$ and $\psi_s = 0.0652$ in the above equation, we obtain

$$6.2 = \frac{\sin(\psi)}{\sin(0.0652\psi)} - 1. \quad (17)$$

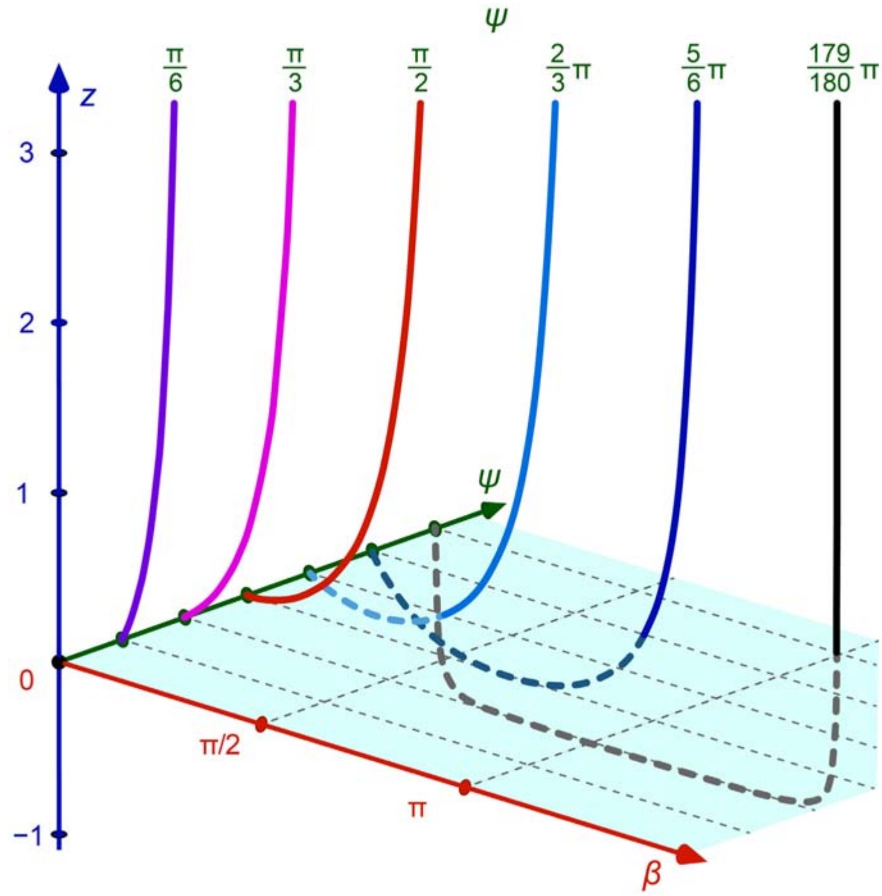

Figure 4. Redshift observed in the S^3 universe. This figure shows redshifts of celestial bodies that are observed on observation points at expansion angles $\psi = 30˚, 60˚, 90˚, 120˚, 150˚$, and $179˚$, and changes of redshift z at longitude difference β from the observation point up to the celestial bodies. The redshift is defined by the ratio $d\tau/dt$ (Equation (11)) of the passage of proper time of light at the time of observation against that of coordinate time t at emission minus one (Equation (15)). The above ratio of the passage of proper times is larger when the longitude difference β becomes larger, because the expansion velocity of the observation point becomes slower than that of the light source at its emission during the expansion phase of the S^3 universe. During the contraction phase ($\psi > \pi/2$), the redshift changes to blueshift ($z < 0$, broken lines) successively from the light of celestial bodies that have become slower in the passage of proper time of the emission than that at observation, because the observed recession velocity of celestial bodies increases due to the increase of the contraction velocity of the observation point. The blueshift of the light increases from neighbouring celestial bodies up to those close to the great sphere and then begins to decrease when they reach the great sphere. The redshift of the light from celestial bodies that are farther away from those of the light source of the same proper time as that at the observation point ($z > 0$, solid line) increases.

From this equation we obtain $\psi \approx 113$ deg (1.97 rad), indicating that the universe is in a stage after the beginning of the contraction.

In summary, we theoretically demonstrated that the increase in receding velocity of the observable universe is observed when the universe is contracting in an accelerated fashion even though it is not expanding. In our theory, the so-called unknown energy that expands the universe in an accelerated fashion in terms of the energy balance of the entire universe is unnecessary. Our results suggest that this model can be a potential candidate demonstrating the geometrical structure of the current universe.

7. Conclusion

We proposed in this paper a novel view of redshifts of the lights emitted from celestial bodies based upon the structure of the three-dimensional spherical (S^3) universe. Contrary to the common interpretation of the redshift that the universe is expanding in an accelerated fashion, we theoretically demonstrated that the redshift of the celestial bodies can also be observed in a *contraction* phase of the universe. In our theory, the so-called unknown energy, which is known to expand the universe in an accelerated fashion in terms of the energy balance of the entire universe, is not necessary. Our result suggests that our model can be a potential candidate that clearly explains the geometrical structure of the current universe, and it will open a new concept of the current status of the universe.

Conflicts of Interest

The authors declare no conflicts of interest regarding the publication of this paper.

References

[1] Hubble, E. (1929) *Proceeding of the National Academy of Science USA*, **15**, 168-173. https://doi.org/10.1073/pnas.15.3.168

[2] Bahcall, N.A., Ostriker, J.P., Perlmutter, S. and Steinhardt, P.J. (1999) *Science*, **284**, 1481-1488. https://doi.org/10.1126/science.284.5419.1481

[3] Freese, K. and Lewis, M. (2002) *Physics Letters B*, **540**, 1-8. https://doi.org/10.1016/S0370-2693(02)02122-6

[4] Frieman, J.A., Turner, M.S. and Huterer, D. (2008) *Annual Review of Astronomy and Astrophysics*, **46**, 385-432. https://doi.org/10.1146/annurev.astro.46.060407.145243

[5] Myrzakulov, R. (2011) *The European Physical Journal C*, **71**, Article No. 1752. https://doi.org/10.1140/epjc/s10052-011-1752-9

[6] Harrison, E. (1993) *The Astrophysical Journal*, **403**, 28-31. https://doi.org/10.1086/172179

[7] Li, C. and White, S.D.M. (2009) *Monthly Notices of the Royal Astronomical Society*, **398**, 2177-2187. https://doi.org/10.1111/j.1365-2966.2009.15268.x

[8] Mei, X. and Yu, P. (2012) *International Journal of Astronomy and Astrophysics*, **2**, 183-193. https://doi.org/10.4236/ijaa.2012.23023

[9] Zucker, S., Alexander, T., Gillessen, S., Eisenhauer, F. and Genzel, R. (2006) *The Astrophysical Journal*, **639**, L21-L24. https://doi.org/10.1086/501436

[10] Futamase, T. and Sasaki, M. (1989) *Physical Review D*, **40**, 2502-2510. https://doi.org/10.1103/PhysRevD.40.2502

[11] Kaiser, N. (2014) *Monthly Notices of the Royal Astronomical Society*, **438**, 2456-2465. https://doi.org/10.1093/mnras/stt2362

[12] O'Raifeartaigh, C. and O'Keeffe, M. (2020) *Physics in Perspective*, **22**, 215-225.

https://doi.org/10.1007/s00016-020-00263-z

[13] Kipreos, E.T. (2014) *PLOS ONE*, **9**, e115550. https://doi.org/10.1371/journal.pone.0115550

[14] Chen, H.-W., Lanzetta, K.M. and Pascarelle, S. (1999) *Nature*, **398**, 586-588. https://doi.org/10.1038/19251

[15] Stern, D., Eisenhardt, P., Spinrad, H., Dawson, S. and van Breugel, W. (2000) *Nature*, **408**, 560-562. https://doi.org/10.1038/35046027

[16] Linder, E.V. (2003) *Physical Review Letters*, **90**, Article ID: 091301. https://doi.org/10.1103/PhysRevLett.90.091301

[17] Barrow, J.D., Bean, R. and Magueijo, J. (2000) *Monthly Notices of the Royal Astronomical Society*, **316**, L41-L44. https://doi.org/10.1046/j.1365-8711.2000.03778.x

[18] White, S.D.M. (2007) *Reports on Progress in Physics*, **70**, 883-897. https://doi.org/10.1088/0034-4885/70/6/R01

[19] Lehoucq, R., Weeks, J., Uzan, J.-P., Gausmann, E. and Luminet, J.-P. (2002) *Classical and Quantum Gravity*, **19**, 4683-4708. https://doi.org/10.1088/0264-9381/19/18/305

[20] Shibata, H. and Ogata, N. (2022) *Journal of Modern Physics*, **13**, 1253-1266. https://doi.org/10.4236/jmp.2022.139074

[21] Moresco, M., Pozzetti, L., Cimatti, A., Jimenez, R. and Maraston, C. (2016) *Journal of Cosmology and Astroparticle Physics*, **2016**, 014. https://doi.org/10.1088/1475-7516/2016/05/014

[22] Lombriser, L. (2023) *Classical and Quantum Gravity*, **40**, Article ID: 155005. https://doi.org/10.1088/1361-6382/acdb41

[23] Welch, B., Coe, D., Diego, J.M., Zitrin, A. and Zackrisson, E. (2022) *Nature*, **603**, 815-818. https://doi.org/10.1038/s41586-022-04449-y

Scientific Research Publishing

Journal of Modern Physics, 2023, 14, 1703-1720
https://www.scirp.org/journal/jmp
ISSN Online: 2153-120X
ISSN Print: 2153-1196

Large Scale Fundamental Interactions in the Universe

Qiao Bi

Department of Physics, Science School, Wuhan University of Technology, Wuhan, China
Email: biqiao@gmail.com

How to cite this paper: Bi, Q. (2023) Large Scale Fundamental Interactions in the Universe. *Journal of Modern Physics*, **14**, 1703-1720.
https://doi.org/10.4236/jmp.2023.1413100

Received: November 6, 2023
Accepted: December 10, 2023
Published: December 13, 2023

Abstract

The author of this paper once attempted to propose a unified framework for gauge fields based on the mathematical and physical picture of the principal fiber bundle: that is, to believe that our universe may have more fundamental interactions than the four, and these fundamental gauge fields are only components on the bottom manifold (*i.e.* our universe) projected by a unified gauge potential of the principal fiber bundle manifold; these components can satisfy the transformation of gauge potential, or even be transformed from one basic interaction gauge potential to another basic interaction gauge potential, and can be summarized into a unified equation, namely the generalized gauge equation expression, corresponding to gauge transformation invariance; so the invariance of gauge transformation is a necessary condition for unified field theory, and the four (or more) fundamental interaction fields of the universe are unified in a unified gauge field defined by the connection on the principal fiber bundle. In this paper, the author continues to propose a model of large-scale (gravitational) fundamental interactions in the universe based on the mathematical and physical picture of the principal fiber bundle, attempting to explain that dark matter and dark energy are merely reflections of these gravitational fundamental interactions that deviate in intensity from the gravitational fundamental interactions of the solar system at galaxy scales or some cosmic scales which are much larger than the solar system. All these "gravitational" fundamental interactions originate from the unified gauge field of the universe, namely the connection or curvature on the principal fiber bundle. These interactions are their projected representations on the bottom manifold (*i.e.* our universe) by different cross-sections (gauge transformations). These projection representations of the universe certainly are described by the generalized gauge equation or curvature similarity equation, and under the guidance of curvature gauge transformation factors, oscillate and evolve between the curvatures $1 \to 0 \to -1 \to 0 \to 1$ of the universe.

Keywords

Principal Bundle, Gauge Similarity Transformation, Dark Matter and Dark Energy, Large-Scale Fundamental Interaction, Evolution of Universe

1. Introduction

Dark matter and dark energy are the two biggest secrets and important frontier issues in the cosmology of physics in our era. Currently, this topic can be mainly divided into two major academic viewpoints. The first viewpoint holds that dark matter and dark energy are the main components of matter and energy in the universe; in the composition of the entire universe, conventional matter (*i.e.* baryonic matter) accounts for only 4.9%, while dark matter accounts for 26.8%, and 68.3% is dark energy (mass energy equivalent) [1] [2] [3]. Dark matter does not interact with electromagnetic forces, that is, it does not absorb, reflect, or emit light. At present, people can only know through the effects generated by gravity, which are mysterious and universally distributed. The detection of dark matter is a hot research field in contemporary particle physics and astrophysics. For massive weakly interacting particles, physicists may directly detect them by placing detectors in underground laboratories with extremely low background noise, or indirectly detect other particles generated by the annihilation of these particles at the center of galaxies, sun, or Earth through ground or space telescopes. In November 2015, Gary Prézeau, a scientist at NASA's Jet Propulsion Laboratory, also used the Lambda Cold Dark Matter model to simulate the flow of dark matter through planets such as Earth and Jupiter in the Milky Way. He found that this would significantly increase the density of the dark matter flow (for example, Earth is: 10^7 times, Jupiter is: 10^8 times), and exhibit a hairlike outward radiation distribution structure [4] [5]. However, although dark matter is currently the most popular theory in explaining observations of various galaxies and galaxy clusters, there is still no direct observational evidence to support the existence of dark matter [6]. As for dark energy, the main evidence is currently believed to be that the observed universe is accelerating expansion. Currently, it is generally assumed that dark energy is isotropic in the universe, has a very low density, and only interacts with gravity without electromagnetic, strong, or weak forces. The density of dark energy is as low as approximately 10^{-29} g/cm^3, making it difficult for laboratories on Earth to directly detect it. However, because dark energy fills all space, accounting for 68.3% of the total mass and energy of the universe, it significantly affects the overall evolution of the universe [7] [8] [9].

The second viewpoint holds that dark matter and dark energy do not exist at all, but are merely illusory manifestations of human cognitive or measurement errors; perhaps the Newton or Einstein theory of gravity, which we believe to be absolutely correct, is not complete, and gravity behaves differently at different scales of time and space. Among them, the interesting one is the Gravity Theory Correction (MOND) hypothesis, which modifies Newton's formula of universal gravitation as an alternative dark matter theory to explain the problem of galaxy rotation. This theory was founded by Israeli physicist Modze Milgrom in 1983 [10]. Currently, there are two main types of dark matter theories to explain dark energy, namely the cosmological constant theory and the basic scalar field theory, and both contain two important properties of dark energy, namely uniformity and negative pressure [11] [12] [13] [14] [15]. But at present, physics still cannot truly explain which type of energy by dark energy acts on the spatiotemporal structure itself, and how does this sort of energy also generate uniform negative pressure, leading to accelerated expansion of the spatiotemporal structure? What is the mechanism behind this [16]?

For the first viewpoint, the author does not want to make a negative evaluation, but the author believes that the biggest problem with it is that it has been going through many years, with humans spending a huge amount of money, scientists spending a huge amount of energy and time, and so far there is no direct evidence of dark matter or dark energy. What does it mean that a universal distribution of matter and energy, which accounts for over 95% of the universe, should exist in large quantities around us but cannot be detected?

The author agrees with the second viewpoint in terms of direction. But the problem is that the theoretical hypotheses related to systematicity still need to be updated and developed. For example, why does Newton's Second Law fail at the scale of galaxies? What is the physical meaning of adding the cosmological constant term to the Einstein equation? Is there an overall connection between the dark matter problem and the dark energy problem? That's exactly what this paper aims to explore and answer. Moreover, this paper aims to construct a structural picture of large-scale basic interactions in the universe from a holistic perspective, exploring the sources of dark matter and dark energy, as well as the direction of cosmic evolution.

The tool used in this paper is the mathematical and physical theory of the principal fiber bundle [17] [18] [19]. The author believes that our universe, in a sense, is like a bottom manifold of principal bundle and various interactions are like connections or curvature on this bottom manifold, corresponding to the physical essence of gauge potential or gauge field strength. These gauge potentials or gauge field strengths are influenced by the scale of the manifold region, and their relationship with each other is given by the generalized gauge equation or the gauge similarity transformation [17] [18] [19]. The real determining factor in the universe is the principal bundle structure built on this bottom manifold. It can also be seen as a direct product manifold of the universe (*i.e.* bottom manifold) and the rules of universe (*i.e.* structure group), combined with numerous complicated mappings, which is a manifold with higher dimensions than the universe. Its connection or curvature just corresponds to a unified gauge field in the universe, which is invariant to the gauge transformation [17].

The remaining parts of this paper are organized as follows: Section 2 describes the physical and mathematical landscape of the Principle Bundle. In Section 3, the physical essence of dark matter and dark energy are studied in detail. The two branch evolution of universe is detail proposed. In Section 4, a brief discussion on the large-scale kinematic equations of the universe is presented. In Sections 5 - 6, the secret of the cosmic term in the Einstein equation is discussed. Lastly, conclusions and expectation are given in Section 7.

2. The Physical and Mathematical Picture of the Principal Bundle

The differential geometric representation of the mathematical and physical picture of the principal bundle mentioned above in this paper can be referred to references [17] [18] [19] [20], and will not be repeated here for simplicity. But here, in order to ensure that the calculations related to general relativity can be directly applied without being affected, it is possible to assume that the bottom manifold M in the frame bundle $P(M,G)$ has an adapted metric field, and this frame field can have orthogonal normalization properties. That is, if the dimension of M is $n=4$, the adapted Riemann metric field or Lorentz metric field can be applied on it, and $P \equiv \left\{ (x, \hat{e}_\mu) \mid x \in M \right\}$, where $\hat{e}_\mu$ represents an orthogonal normalized basis in the tangent space $T_x M$, and then selecting matrix groups $SO(4)$ or $O(1,3)$ as a structure group, the group elements can undergo orthogonal normalized frame transformations, so that obtained principal bundle can be defined as an orthogonal normalized frame bundle.

A connection on the principal bundle $P(M,G)$ is a C^∞ 1-form field $\boldsymbol{\omega}_U$ of the Lie algebra $\mathcal{G}$-value specified by a local trivial $T_U : \pi^{-1}[U] \to U \times G$ on U, namely it is a connection on $U \subset M$. At this time, if $T_V : \pi^{-1}[V] \to V \times G$ is another local trivial, $U \cap V \neq \varnothing$, and $\exists$ the conversion function g_{UV} from the local trivial T_U to T_V, then the generalized Gauge equation is held [15], namely

$$\boldsymbol{\omega}_V(Y) = \mathcal{A}d_{g_{UV}(x)^{-1}} \boldsymbol{\omega}_U(Y) + L^{-1}_{g_{UV}(x)*} g_{UV*}(Y), \forall x \in U \cap V, Y \in T_x M \tag{1}$$

where $L^{-1}_{g_{UV}(x)}$ is an inverse mapping of left translation $L_{g_{UV}(x)}$ generated by $g_{UV}(x) \in G$, and the asterisk represents the forward mapping with $L^{-1}_{g_{UV}(x)*} \equiv \left(L^{-1}_{g_{UV}(x)} \right)_*$.

Furthermore, this principal bundle structure consists of a structure group, a principal bundle manifold, and a base manifold. The cross-section of the principal bundle is the gauge potential, and the curvature is the gauge field strength, satisfying the curvature gauge transformation relationship between two different regions U and V. For example, generally speaking, if $g_{UV} : U \cap V \to G$ is a conversion function of local trivial transition from T_U to T_V, and $\boldsymbol{\Omega}_V$ and $\boldsymbol{\Omega}_U$ is the curvature of the V region or the U region on the bottom manifold, then on $U \cap V$ there is

$$\boldsymbol{\Omega}_V = \mathcal{A}d_{g_{UV}^{-1}} \boldsymbol{\Omega}_U \tag{2}$$

where, $\mathcal{A}d_{g_{UV}^{-1}}$ is the forward mapping from Lie algebra $\mathcal{G}$ to $\mathcal{G}$, which is induced by the adjoin isomorphism $I_{g_{UV}^{-1}}$ defined by the group element g_{UV}^{-1} of structure group G with Lie algebra $\mathcal{G}$.

If the structure group is a matrix group, then Equation (2) can be further expressed as:

$$\boldsymbol{\Omega}_V = g_{UV}^{-1} \boldsymbol{\Omega}_U g_{UV} \tag{3}$$

Therefore, under the cross-section transformation $\boldsymbol{\sigma}$, there is $\boldsymbol{\omega}_U \to \boldsymbol{\omega}_V$ on the bottom manifold (that is, the world we assume), namely, Equation (1) holds, and here g_{UV}^{-1} and g_{UV} are related to a gauge transformation.

Furthermore, it can be proven that Equation (3) is equivalent to the following "similarity" transformation Equation (4) [19]:

$$\boldsymbol{\Omega}_V = g_{UV}^{-1} \boldsymbol{\Omega}_U g_{UV} \Leftrightarrow \hat{F}'_{\mu\nu} = W \hat{F}_{\mu\nu} W^{-1} \tag{4}$$

where $\hat{F}'_{\mu\nu}$ is defined as the gravitational gauge field strength on the V region of the bottom manifold; $\hat{F}_{\mu\nu}$ is defined as the gravitational gauge field strength on the U region of the bottom manifold. W^{-1} or W can be regarded as the matrix expression of some kind of gauge transformation. The author suggests calling it as the gauge similarity transformation.

We should emphasize that this gauge similarity transformation is influenced by regional scale, or rather depends on changes in regional scale. The scale of U or V in different regions determines different gauge potentials or field strengths. The generalized gauge equation or the gauge similarity transformation above refers to the transformation relationship between the gauge potentials or field strengths of two different regions at the same spatiotemporal point in the bottom manifold (our universe). Moreover, after careful consideration, the author also believes that if the structure group is a general linear group ($GL(m,\mathbb{C})$), the generalized gauge transformation over basic interactions should corresponds to the gauge transformations between several subgroups (such as $U(1)$, $SU(2)$, $SU(3)$, $O(1, 3)$), while the gauge transformation within a basic interaction (such as electromagnetic force) only corresponds to gauge transformations within a subgroup (such as $U(1)$ or $SU(2)$). These components are just a "representation" of the original connection or curvature on the principal bundle in the real world (bottom manifold); in this sense, "quantization" or "classicalization" is just a natural "picture representation" of the original connection or curvature selection in different regions of the real world, and cannot be replaced by each other, or not every physical field can or needs be quantized, especially gravity. It should be emphasized that the original connection (gauge potential) or curvature (gauge field strength) on the principal bundle is gauge invariant, while the gauge potential or field strength on the bottom manifold is only the projection component mapped (gauge selection) from different cross-sections of the original connection or curvature of the principal bundle, which is the physical meaning of the unity of the "four" basic interactions in the world [17] [18] [19].

3. The Physical Essence of Dark Matter and Dark Energy

Based on the above assumptions, this paper believes that dark matter and dark energy are both fictitious hypotheses generated by the differences in the gauge transformation of the gravitational gauge potential or gauge field strength between different regional scales on the bottom manifold. There is no dark matter or dark energy, but only changes in the bottom manifold relative to the original gauge potential or field strength caused by gauge transformation. The original Einstein's equation or Newton's second law may change its form under such a transformation, and may be different from the form before the transformation, and there is a difference, so this difference is blurred into the existence of some kind of dark matter or dark energy.

The specific mathematical and physical foundations and related gauge transformation that make our "theory" valid are constructed as follows:

$$\begin{array}{ccc} \hat{F}'_{\mu\nu} & = & W\hat{F}_{\mu\nu}W^{-1} \\ \hat{F}'_{\mu\nu} \equiv \text{Gauge field strength in } V & \leftarrow & \hat{F}_{\mu\nu} \equiv \text{Gauge field strength in } U \\ & \downarrow\downarrow & \\ & \hat{F}'_{\mu\nu} = \gamma\left(\dfrac{|a|}{a_0}\right)\hat{F}_{\mu\nu} & \end{array} \tag{5}$$

where, $\gamma\left(\dfrac{|a|}{a_0}\right)$ can be defined as a function of $\dfrac{|a|}{a_0}$. The author suggests that it can be called the gauge similarity transformation factor, where $|a|$ is the absolute value of acceleration related to the region and can be defined as the acceleration of a particle relative to a basic framework determined by distant matter in the universe. a_0 is an acceleration constant related to our galaxy, and experiments [10] have found that is approximately $a_0 \sim cH_0 = 2\times10^{-8}\ \text{cm}\cdot\text{s}^{-2} \sim 5\times10^{-8}\ \text{cm}\cdot\text{s}^{-2}$. What is very surprising is that a_0 is very consistent with the measured value of the acceleration of the solar system in the gravitational field of the Milky Way $(2.32 \pm 0.16) \times 10^{-8}\ \text{cms}^{-2}$ [21], indicating that the regional scale corresponding to a_0 is just the scale of our solar system! Therefore, the solar system can be used as a reference system to judge the applicable scope of relativity and Newtonian mechanics. Generally speaking, as the scale of the region corresponding to a_0 increases, it should be more difficult for the regional matter as a whole to change acceleration $|a|$ under the gravitational field of galaxy. Therefore, on average, if the acceleration a_0 as the benchmark, then the larger the scale of the galaxy, the smaller its overall acceleration $|a|$ should be. For example, if a_0 is set as the benchmark, the corresponding solar system region scale is U_{sun}, and the galaxy is V_{uni}, there should be an inverse relationship,

$$\frac{|a|}{a_0} \sim \frac{U_{sun}}{V_{uni}} \tag{6}$$

Obviously, when the galaxy scale V_{uni} tends to the universe scale, the above equation tends to 0. If the galaxy scale shrinks to the U_{sun} scale, the above equation becomes to 1. When the galaxy scale is much smaller than the base system scale, the above equation tends to ∞. The corresponding acceleration shows: when $|a| \ll a_0$, $\gamma\left(\frac{|a|}{a_0}\right) \to \frac{|a|}{a_0} \to 0$, and when $|a| = a_0$, $\gamma\left(\frac{|a|}{a_0}\right) \to \gamma(1)$, while when $|a| \gg a_0$, $\gamma\left(\frac{|a|}{a_0}\right) \to 1$, so the gauge similarity transformation factor γ changes between 0 and 1. In order to reflect this law, we speculatively choose the $\gamma\left(\frac{|a|}{a_0}\right) \equiv th\left(\frac{|a|}{a_0}\right)$ function to "simulate" this change. But this does not take into account the fact that Einstein's law of gravity and Newton's second law normally hold true within the scale of the solar system. Therefore, the author generally believes that when $|a| \ge a_0$, there should be $th\left(\beta\frac{|a|}{a_0}\right) \to 1$. At this time, the reference system should include the scale of our solar system, and an appropriate coefficient β should be introduced, so that when $|a| \ge a_0$,

$$th\left(\beta\frac{|a|}{a_0}\right) \to 1 \tag{7}$$

To ensure that within the scale of the solar system, Einstein's law of gravitational attraction remains unchanged and Newton's law of gravity (second law) remains unchanged, the gauge similarity transformation should be given by

$$\hat{F}'_{\mu\nu} = \hat{F}_{\mu\nu} \tag{8}$$

In other cases, such as $|a| < a_0$, then $0 < th\left(\beta\frac{|a|}{a_0}\right) < 1$, one gets

$$\hat{F}'_{\mu\nu} = th\left(\beta\frac{|a|}{a_0}\right)\hat{F}_{\mu\nu} < \hat{F}_{\mu\nu} \tag{9}$$

At this point, from the perspective of our solar system, Newton's Second Law becomes

$$m\,th\left(\beta\frac{|a|}{a_0}\right)\boldsymbol{a} < m\boldsymbol{a} = \boldsymbol{F} \tag{10}$$

Newton's Second Law no longer seems to hold true, which is consistent with MOND's viewpoint [21] [22] [23].

In fact, from the perspective that the strength of the gauge field is the curvature of the bottom manifold, considering the Newton approximation, the linear Einstein equation can give [24] [25],

$$m\frac{\mathrm{d}^2 x^i}{\left(\mathrm{d}x^0\right)^2} = -m\Gamma^i_{00} \tag{11}$$

where, Γ^i_{00} is the Christoffel symbols, which is approximated by Newton's condition, $g_{ab} = \eta_{ab} + h_{ab}$, etc., can be transformed into

$$\Gamma^{i}_{00}=\frac{1}{2}\eta^{i\mu}\left(h_{\mu0,0}+h_{\mu0,0}-h_{00,\mu}\right)=\frac{1}{2}h_{00,i} \tag{12}$$

Hence one can obtain

$$m\frac{\mathrm{d}^2x^i}{\left(\mathrm{d}x^0\right)^2}=-m\frac{1}{2}h_{00,i} \tag{13}$$

Further consideration of Newton's second law in the classical field of universal gravitation can be written as

$$m_I\frac{\mathrm{d}^2x^i}{\mathrm{d}t^2}=m_g\left(-\frac{\partial\varphi}{\partial x^i}\right) \tag{14}$$

where φ is Newton's gravitational potential. Comparing the above two formulas one gets:

$$\varphi=\frac{1}{2}h_{00}+\text{const} \tag{15}$$

Assume that the gravitational field disappears at infinity as $\varphi=0$, then the metric should return to the Minkowski metric at this time, $h_{00}=0$, so that the constant in the above formula is 0, which gives

$$g_{00}=-1+h_{00}=-\left(1+\frac{2\varphi}{c^2}\right) \tag{16}$$

But considering gauge transformation and Newton approximation one can have

$$\hat{F}_{\mu\nu}\to\gamma\hat{F}_{\mu\nu}\to\gamma\hat{F}_{\mu\nu}\to\gamma\Gamma^{i}_{00}\to\gamma g_{00}\to\gamma h_{00}\to\gamma\varphi \tag{17}$$

Therefore, Newton's second law in the above classical gravitational field becomes

$$m\left(-\frac{\partial\gamma\varphi}{\partial x^i}\right)=m\gamma\boldsymbol{a}<m\boldsymbol{a}=\boldsymbol{F} \tag{18}$$

This difference in gravitation is the origin of the dark matter hypothesis.

In addition, if $V_{uni}\gg$ base system scale, or $\gg$ galaxy scale, then $\frac{|a|}{a_0}\ll 1$, $th\left(\beta\frac{|a|}{a_0}\right)\to 0$, its physical meaning is that the gravitational gauge field strength is $\hat{F}'_{\mu\nu}=th\left(\beta\frac{|a|}{a_0}\right)\hat{F}_{\mu\nu}\to 0$, which corresponds to the zero gravitational gauge field strength of the manifold region on the cosmic scale. So that Equation (18) means that Newton's second law becomes:

$$\lim_{\frac{|a|}{a_0}\to 0}\left[mth\left(\beta\frac{|a|}{a_0}\right)\boldsymbol{a}\right]\to 0 \tag{19}$$

This reveals that the curvature of the entire region at the scale of the universe is 0, and the attraction disappears. The author speculates that at this scale, the universe may be driven by the energy converted from the initial kinetic energy of the original big bang and the disappearing attraction to accelerate expansion, and producing repulsive forces are also possible. This part of the conversion energy from the disappearance of gravity plus the initial kinetic energy left behind by the Big Bang of the original universe may be the origin of dark energy, thus forming a structure of regional distribution of large-scale basic interactions, that is

$$\begin{cases} th\left(\beta\frac{|a|}{a_0}\right)\to 1 & \Rightarrow \text{Newton's second law holds}\left(\text{such as our solar system}\right) \\ 0<th\left(\beta\frac{|a|}{a_0}\right)<1 & \Rightarrow \text{Dark matter}\left(\text{"region"}\ge\text{galaxy}\right) \\ th\left(\beta\frac{|a|}{a_0}\right)\to 0 & \Rightarrow \text{Dark energy}\left(\text{such as the universe currently measured}\right) \end{cases} \tag{20}$$

Furthermore, the above picture is just a branch of the evolution of the universe if considering original $\hat{F}_{\mu\nu}$ as a unit (such as the gauge field strength of the solar system). In the process of $th\left(\beta\frac{|a|}{a_0}\right)$ causing the curvature of the universe to become 0, as the gravitational gauge field of attraction disappears, its energy may be converted into repulsive force, that is $\hat{F}'_{\mu\nu}=th\left(\beta\frac{|a|}{a_0}\right)\hat{F}_{\mu\nu}\to 0^-$ may tend to be negative, causing the curvature to become negative, gradually increasing the repulsive force, and in driven by the initial kinetic energy of the Big Bang, the universe may continue to develop in the direction of negative curvature and accelerate its expansion (this is consistent with the current measurement evidence that extragalactic galaxies are accelerating red shifts [26] [27] [28] [29]), thus evolving into another branch, namely universe with negative curvature:

$$\begin{cases} th\left(\beta\frac{|a|}{a_0}\right)\to -1 & \Rightarrow \text{Applicable regions of Newton's second law} \\ -1<th\left(\beta\frac{|a|}{a_0}\right)<0 & \Rightarrow \text{"Dark matter" region} \\ th\left(\beta\frac{|a|}{a_0}\right)\to 0 & \Rightarrow \text{"Dark energy" universe} \end{cases} \tag{21}$$

where a negative value is taken by β.

Which branch is the universe currently on? Obviously, the gravity in areas smaller than the scale of the universe are still dominated by attraction, that is, the gauge similarity factor is $0<th\left(\beta\frac{|a|}{a_0}\right)<1$, so the universe is in the first branch. However, it is not impossible for the universe to evolve to a second branch in the distant future. The measurement evidence that extragalactic galaxies are generally accelerating their red shifts is a possible interpretation of the negative gauge similarity transformation of the curvature of the bottom manifold (*i.e.* our universe).

Then the universe will continue to oscillate and develop, oscillating back and forth among the curvature of −1, 0, and 1… see the hyperbolic tangent curve shown in **Figure 1**. The hypotheses of these two branches can obtain some support from the solutions of the Friedmann equation, that is, the curvature of the universe evolves possible three scenarios are 0, 1 and −1, which also have similar cyclic characteristics to Penrose's model of conformal cyclic cosmology [17] [25] [30] [31] [32] [33]. The evolution of the universe may be oscillation, cycle, and development among three curvature images of −1, 0, and 1.

But the author needs to emphasize that $\gamma\left(\frac{|a|}{a_0}\right) \equiv th\left(\beta\frac{|a|}{a_0}\right)$ is just a speculation, and whether it is correct or not depends on experiments and observations. The more confident one is still the setting: $\gamma\left(\frac{|a|}{a_0}\right)$ is just certain function of $\frac{|a|}{a_0}$ which satisfies the following graph:

$$\begin{cases} \gamma\left(\frac{|a|}{a_0}\right) \to 1 & \Rightarrow \text{For } |a| \gg a_0, \text{Newton's second law holds (i.e. solar system)} \\ 0 < \gamma\left(\frac{|a|}{a_0}\right) < 1 & \Rightarrow v(r) = \sqrt{\frac{GM}{\gamma r}} > \sqrt{\frac{GM}{r}} \text{ ("Dark matter" regions} \geq \text{galaxies)} \\ \gamma\left(\frac{|a|}{a_0}\right) \to \frac{|a|}{a_0} \to 0 & \Rightarrow \text{For } |a| \ll a_0, \text{Dark energy (accelerated expansion of the universe)} \end{cases} \tag{22}$$

where if $v(r)$ is the rotation curve of the galaxy, *i.e.* $\sqrt{\frac{GM}{\gamma r}}$, then after being

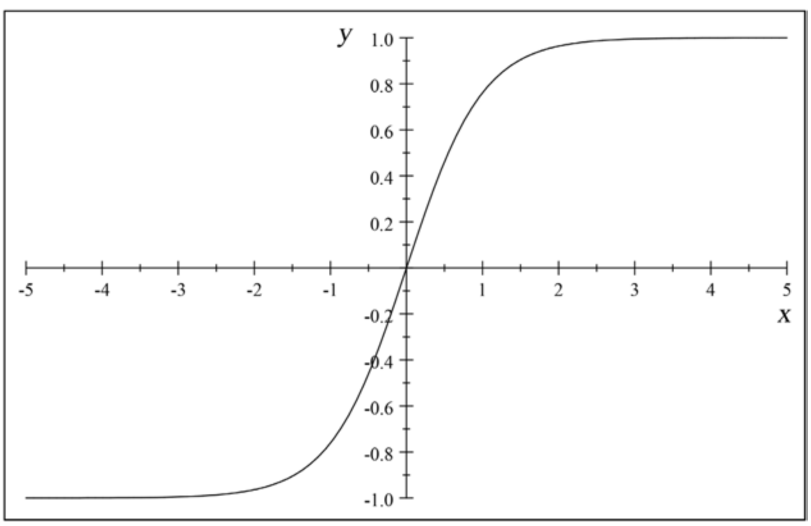

Figure 1. One possible oscillation or evolution of our universe in two branches: $y = th(x)$, $x = \frac{|a|}{a_0}$; $|a| \gg a_0$, $y \to \pm 1$; $|a| \ll a_0$, $y \to 0$; Other, 0 < y < 1, or −1 < y < 0.

account by $0<\gamma\left(\frac{|a|}{a_0}\right)<1$ in the denominator, as r increases, the observation result is greater than the original $\sqrt{\frac{GM}{r}}$, which well explains no existence of "dark matter" and is consistent with the observation and calculation results of MOND [21] [22] [23]. While for the "dark energy", the following two sections can give more clear analysis.

4. Connection or Curvature Determines the Equation of Motion

In the previous analysis and discussion, we can draw an important conclusion: that is, the connection or curvature of large-scale space-time in the universe affects the evolutionary landscape of the universe. Here, the author briefly discusses the kinematic equations related to the large-scale structure of universe:

An important idea in the theory of principal bundles is the connection of principal bundle $\tilde{\boldsymbol{\omega}}$ can induce a derivative operator ∇ on the bottom manifold, and this principal bundle is just the frame bundle *FM*, that is

$$(M,\nabla)\leftrightarrow(FM,\tilde{\boldsymbol{\omega}}) \tag{23}$$

Fortunately, the principal bundle in our universe's diagram is just the frame bundle, so the connection of this frame bundle will have a derivative operator effect on the gauge field in the corresponding region of the bottom manifold, which displays certain geometric kinematic features. Let the cross-section of the constructed associated bundle be $\hat{\boldsymbol{\sigma}}$ representing a physical gauge field, the kinematic equation of this physical gauge field in this cosmic scale region can be determined by obtaining its covariant derivative (see [17]):

$$\nabla_T\hat{\boldsymbol{\sigma}}=\boldsymbol{\sigma}(0)\cdot\left\{\left.\frac{\mathrm{d}}{\mathrm{d}t}\right|_{t=0} f(t)+\left[\rho_*\left(\boldsymbol{\omega}(T)\right)\right]f(0)\right\} \tag{24}$$

where, $f(t)$ and $f(0)$ are arrays composed by the components of a certain gauge field tensor, $\rho_*\left(\boldsymbol{\omega}(T)\right)$ is a square matrix, T is a tangent vector in the base manifold, $\boldsymbol{\omega}$ is the connection on the bottom manifold. Therefore the equation of motion is determined by the following equation:

$$\begin{cases}\nabla_T\hat{\boldsymbol{\sigma}}=0\to\text{Geodesic equation}\\ \nabla_T\hat{\boldsymbol{\sigma}}\neq0\to\text{Equations of motion driven by connections}\end{cases} \tag{25}$$

For example, if the principal bundle $P=FM$ and the tangent bundle is the associated bundle $Q=TM$, then the associated bundle cross-section $\hat{\boldsymbol{\sigma}}:U\to Q$ is the tangent field, and let a coordinate system in the bottom manifold region U be $\{x^\mu\}$, utilizing auxiliary cross-sections $\boldsymbol{\sigma}:U\to P$, then it can be calculated as

$$T^b\nabla_b v^a=T^\sigma\left[\left(\frac{\partial}{\partial x^\mu}\right)^a\left(\frac{\partial v^\mu}{\partial x^\sigma}+\omega^\mu_{\nu\sigma}v^\nu\right)\right]_{x_0} \tag{26}$$

where $\forall x_0 \in U$, T is a vector along point x_0, v^a represents the vector field corresponding to $\hat{\boldsymbol{\sigma}}$, and $\nabla_T \hat{\boldsymbol{\sigma}} = T^b \nabla_b v^a$. For example, if taking $v^\mu = T^\mu = \frac{\mathrm{d}x^\mu}{\mathrm{d}t}$, $T^\sigma \frac{\partial v^\mu}{\partial x^\sigma} = \frac{\mathrm{d}v^\mu}{\mathrm{d}t}$, then the equation of motion can be:

$$T^b \nabla_b T^a = 0 \rightarrow \frac{\mathrm{d}T^\mu}{\mathrm{d}t} + \omega^\mu_{\nu\sigma} T^\sigma T^\nu = 0 \tag{27}$$

The geodesic equation is thus obtained:

$$\frac{\mathrm{d}^2 x^\mu}{\mathrm{d}t^2} + \Gamma^\mu_{\nu\sigma} \frac{\mathrm{d}x^\nu}{\mathrm{d}t} \frac{\mathrm{d}x^\sigma}{\mathrm{d}t} = 0 \tag{28}$$

In addition, considering Equation (25), it can be determined that Equation (26) is the general equation of kinematics of the frame bundle contact action gauge vector field. At this point view, the frame bundle connection is a derivative operator on the bottom manifold, and the associated bundle cross-section is a physical field, and the effect of the connection on the physical field is to obtain covariant derivatives of the physical field. When this physical field is a tangent vector and the direction is consistent with the derivative operator, the covariant derivative of the tangent vector is 0, and then the equation of motion becomes a geodesic equation.

5. The Secret of the Universal Term in Einstein's Equation

The connections or curvature of large-scale space-time can certainly affect the dynamical equations. In fact, the physical essence reflected in the gauge similarity transformation Formula (4) can be realized by introducing a factor that changes with space-time scale in the universal term of Einstein's equation, for example

$$G_{ab} + \Lambda\left(\frac{|a|}{a_0}\right) g_{ab} = 8\pi T_{ab} \tag{29}$$

where G_{ab} is the Einstein tensor, g_{ab} is the metric tensor, T_{ab} is the energy and momentum tensor, Λ is originally the cosmological constant, and now it is related to $\gamma\left(\frac{|a|}{a_0}\right)$, that is

$$-\Lambda g_{ab} = 8\pi\left(\frac{1-\gamma}{\gamma}\right) T_{ab} \tag{30}$$

Proof: From the gauge similarity transformation and Einstein's equation, let $\gamma = th\left(\beta \frac{|a|}{a_0}\right)$, we have

$$\gamma R_{ab} - \frac{1}{2}\gamma R g_{ab} = 8\pi T_{ab} \tag{31}$$

So we can get

$$R_{ab} - \frac{1}{2} R g_{ab} = \frac{8\pi}{\gamma} T_{ab} \tag{32}$$

Consider again Einstein's equation with the cosmological constant Λ

$$R_{ab}-\frac{1}{2}Rg_{ab}+\Lambda g_{ab}=8\pi T_{ab} \tag{33}$$

And because the above equation can become

$$8\pi T_a^a=R_a^a-\frac{1}{2}\delta_a^a R+\delta_a^a\Lambda=R-2R+4\Lambda=-R+4\Lambda$$

namely

$$R=-8\pi T+4\Lambda \tag{34}$$

So (33) can be reduced to

$$\begin{aligned}R_{ab}&=8\pi T_{ab}+\frac{1}{2}Rg_{ab}-\Lambda g_{ab}\\&=8\pi T_{ab}+\frac{1}{2}\left(-8\pi T+4\Lambda\right)g_{ab}-\Lambda g_{ab}\\&=8\pi\left(T_{ab}-\frac{1}{2}Tg_{ab}\right)+\Lambda g_{ab}\end{aligned} \tag{35}$$

Then bring Equation (34) and (35) into Equation (32), we get

$$\begin{aligned}\frac{8\pi}{\gamma}T_{ab}&=R_{ab}-\frac{1}{2}Rg_{ab}\\&=8\pi\left(T_{ab}-\frac{1}{2}Tg_{ab}\right)+\Lambda g_{ab}-\frac{1}{2}\left(-8\pi T+4\Lambda\right)g_{ab}\\&=8\pi T_{ab}-\Lambda g_{ab}\end{aligned} \tag{36}$$

Hence we have Equation (30) established, that is

$$-\Lambda g_{ab}=8\pi\left(\frac{1-\gamma}{\gamma}\right)T_{ab}$$

Under condition (30), Equation (31) can be reduced to

$$\begin{aligned}R_{ab}-\frac{1}{2}Rg_{ab}&=\frac{8\pi}{\gamma}T_{ab}=\frac{8\pi}{\gamma}T_{ab}-\frac{\gamma}{\gamma}8\pi T_{ab}+8\pi T_{ab}\\&=8\pi\left(\frac{1-\gamma}{\gamma}\right)T_{ab}+8\pi T_{ab}\\&=-\Lambda g_{ab}+8\pi T_{ab}\end{aligned} \tag{37}$$

So we have the Einstein Equation (33) with the cosmological term.

Therefore, a conclusion can be drawn: when condition (30) is established, the Einstein equation with gauge similarity transformation and the original Einstein equation can be derived from each other, that is, we have

$$\begin{gathered}\gamma R_{ab}-\frac{1}{2}\gamma Rg_{ab}=8\pi T_{ab}\\\downarrow\uparrow\\R_{ab}-\frac{1}{2}Rg_{ab}+\Lambda g_{ab}=8\pi T_{ab}\end{gathered} \tag{38}$$

Let me emphasize again that γ is defined here as the gauge similarity transformation factor, Λ is the cosmological constant of Einstein's equation, and the relationship between the both is Equation (30).

So the gauge similarity transformation $R_{ab}\to\gamma R_{ab}$ is equivalent to adding the cosmological constant Λ to Einstein's equations. This shows that in a certain sense, adding a certain cosmological constant to the Einstein equation is equivalent to applying a certain gauge similarity transformation to the curvature. The cosmological constant is no longer a constant, and is related to the coefficient γ of the gauge field strength after the gauge similarity transformation, which is the physical meaning of the cosmological constant. Not only that, Λ is affected by $\gamma\left(\frac{|a|}{a_0}\right)$, Λ is also a function of the space-time scale, that is, it becomes larger as the time-space scale becomes larger; when the time-space scale tends to the cosmic scale, $\gamma\left(\frac{|a|}{a_0}\right) \to \frac{|a|}{a_0} \to 0$, $\Lambda \to -\infty$, the gauge gravitational field strength is 0, and Einstein's equation fails; when the space-time scale is smaller than the scale of the solar system, $\gamma\left(\frac{|a|}{a_0}\right) \to 1$, $\Lambda \to 0$, the gravitational field strength remains unchanged after gauge transformation, the original Einstein equation holds, and Newton's second law holds. The conditions that must be met for the specific change of Λ are determined by Equation (30).

6. The Λ Variable Affects the Einstein Equation

From the above analysis of the Einstein equation's cosmological constant, the author found that since the cosmological constant is now not a constant but a function that varies with the scale of the universe region, or the ratio to regional acceleration $\frac{|a|}{a_0}$ is related, so the Einstein equation will vary with the size of the universe region, and take on different forms. Therefore, the Newton's law or the law of universal gravitation that appears in the U region observed at the same point in the bottom manifold (*i.e.* our universe) may not necessarily be the same as the Newton's law or the law of universal gravitation observed in the V region at the same point. The transformation between them satisfies a gauge similarity transformation (or generalized gauge equation); and it is precisely the difference between the both to cause the virtual origin of hypothesis for the dark matter and the dark energy.

In fact, from Equation (36), the Einstein equation containing the cosmological term becomes

$$R_{ab} - \frac{1}{2} R g_{ab} = 8\pi T_{ab} - \Lambda g_{ab} = 8\pi \frac{T_{ab}}{\gamma\left(\frac{|a|}{a_0}\right)} \tag{39}$$

namely

$$G_{ab} = 8\pi \frac{T_{ab}}{\gamma\left(\frac{|a|}{a_0}\right)} \tag{40}$$

Here G_{ab} certainly is the Einstein tensor. Therefore, the large-scale Einstein equation of the universe is suggested to be given by the following formula:

$$G_{ab} = R_{ab} - \frac{1}{2} R g_{ab} + \Lambda\left(\frac{|a|}{a_0}\right) g_{ab} = 8\pi T_{ab} \tag{41}$$

Therefore, the evolution law of Einstein's equation in the large-scale universe is affected by $\Lambda\left(\frac{|a|}{a_0}\right)$ or $\gamma\left(\frac{|a|}{a_0}\right)$ and is expressed as follows:

$$\begin{cases} G_{ab} = 8\pi T_{ab}, |a| \gg a_0, \gamma \to 1, (\text{The area where Einstein equation and Newton gravity hold}) \\ G_{ab} = 8\pi \dfrac{T_{ab}}{\gamma}, 0 < \gamma < 1, (\text{dark matter, Einstein's equation and Newton gravity deviation area}) \\ -\Lambda g_{ab} = 8\pi\left(\dfrac{1-\gamma}{\gamma}\right) T_{ab} \to \infty, |a| \ll a_0, \gamma \to 0, (\text{A chaotic region where gravity disappears} \\ \qquad\qquad\qquad\qquad \text{or repulsive force appears}) \end{cases} \tag{42}$$

In terms of details, the relevant mechanism of the two limit points with curvature 0 and 1 in the above picture can also be explained as follows:

The interval with a curvature of 0 is the fluctuation or chaos region where all gravitational or repulsive forces disappear or begin to occur. At the limit point of 0, neither Einstein's equation nor Newton's second law completely holds. The repulsive energy converted from the disappearance of gravity is the source of dark energy. So "the problem of cosmological constant for physicists" has not existed [17].

Whether the universe ultimately continues to evolve depends on which part of the force disappears much more. Obviously, from the first branch to point 0, gravity disappears much more, so repulsive forces will inevitably occur much more, and the universe will evolve towards the second branch. On the contrary, there is a high probability that universe will evolve towards the first branch. It is not impossible for the universe to oscillate and evolve repeatedly in a branch with a certain probability. In the process of the curvature of the first branch of the universe tending towards 1, as $|a| \gg a_0$, and the simultaneous surface gradually tend to a closed 3-dimensional circular sphere, with its spatiotemporal scale compressed until it becomes a singularity, and then the Big Bang begins a new curvature evolution from 1 to 0; in the second branch, the author speculates that as the curvature of the universe tends towards −1, the simultaneous surface of the universe presents a continuously compressed and reduced 3-dimensional saddle surface under the constraint that its overall energy must be conserved, until the time-space becomes a singularity, and then the kinetic energy of the Big Bang drives the evolution of its curvature from −1 to 0. At the +1 limit point, both the Einstein equation and Newton's second law hold. At the −1 limit point, the Einstein equation and Newton's second law require sign changes. But it is still unclear whether that is a world dominated by "universal repulsion"…

In the first branch: $0 < \gamma < 1$, or second branch: $-1 < \gamma < 0$ compared with the Einstein equation and Newton's second law of the solar system, both the Einstein equation and the Newton's second law are partially valid. The difference between those is just the source of dark matter hypothesis.

7. Conclusions and Outlook

In this paper, the author proposes a hypothesis about the structure of large-scale gravitational interactions in the universe and the oscillatory evolution of the universe with a hyperbolic tangent function. These hypotheses are based on the theory of principal bundles and gauge similarity transformations. The author believes that our universe is a bottom manifold under the principal bundle, and the laws of cosmic evolution are hidden in the principal bundle above the bottom manifold. The structure group and relevant gauge transformations provide a similarity transformation of the gauge field, which can reflect the connection between the strength of the physical gauge field and the large space-time scale of the universe, as well as the mutual relationship between the gauge field strengths in the two different space-time regions. The results obtained are unexpected:

1) The unified understanding of the hypothesis of dark matter and dark energy is caused by data biases between the measured massive galaxy system and solar system from the calculations of the Einstein equation or Newton's second law. Actual dark matter, dark energy does not exist!

2) The Einstein equation and Newton's second law can only be partially true for these massive galaxies. Its correction can be given by the cosmological constant term of the Einstein equation. But this cosmic constant actually varies with the size of the universe and is related to the gauge similarity transformation factor. The overall acceleration of the "solar system" a_0 can be selected as benchmark, which is 2.5×10^{-8} cm/s^2; then the cosmological constant Λ varies with the absolute value $|a|$ of the overall acceleration of the large-scale cosmological structure by comparing to a_0, *i.e.* $\Lambda\left(\frac{|a|}{a_0}\right)$.

3) If the gauge field strength of the datum system is defined as the unit, then the universe oscillates and evolves according to the function type of the gauge similarity transformation factor $\gamma\left(\frac{|a|}{a_0}\right)$, which can be divided into two branches, *i.e.* $0 \le \gamma\left(\frac{|a|}{a_0}\right) \le 1$ and $-1 \le \gamma\left(\frac{|a|}{a_0}\right) \le 0$. The corresponding curvatures are 1, 0, −1, and the universe oscillates and develops among these curvatures of 1, 0, and −1. A curvature of ±1 corresponds to the two singularities before the Big Bang, and a curvature of 0 corresponds to the chaotic region where gravity and repulsion disappear or arise.

4) The above results have covered almost all the most important difficult issues on basic interaction theory and cosmology in current theoretical physics, and the progresses are obvious. They once again illustrate that the principal bundle picture about the evolution of universe [18] [19] based on the principal and associated bundles of differential geometry and the generalized gauge transformation or the gauge similarity transformation may be a very important founda-

tion and starting point for studying the basic interaction structure of large-scale gravity in the universe, and are expected to shine in future research on cosmology.

Conflicts of Interest

The author declares no conflicts of interest regarding the publication of this paper.

References

[1] Ade, P.A.R., Aghanim, N., Armitage-Caplan, C., *et al.* (2015) *Astronomy and Astrophysics*, **571**, A1.

[2] Ade, P.A.R., Aghanim, N., Armitage-Caplan, C., *et al.* (2014) *Astronomy and Astrophysics*, **571**, A16.

[3] First Planck Results: The Universe Is Still Weird and Interesting (2013).

[4] Prézeau, G. (2015) *The Astrophysical Journal*, **814**, 122. https://doi.org/10.1088/0004-637X/814/2/122

[5] Landau, E. (2015) Earth Might Have Hairy Dark Matter. NASA's Jet Propulsion Laboratory, Pasadena.

[6] Misiaszeka, M. and Rossi, N. (2023) Direct Detection of Dark Matter: A Critical Review.

[7] Steinhardt, P.J. and Turok, N. (2006) *Science*, **312**, 1180-1183. https://doi.org/10.1126/science.1126231

[8] "Dark Energy". Hyperphysics.

[9] Ferris, T. (2015) Dark Matter (Dark Energy).

[10] Milgrom, M. (1983) *The Astrophysical Journal*, **270**, 365-370. https://doi.org/10.1086/161130

[11] Moon Findings Muddy the Water.

[12] Carroll, S. (2001) *Living Reviews in Relativity*, **4**, 1. https://doi.org/10.12942/lrr-2001-1

[13] Ratra, P. and Peebles, L. (1988) *Physical Review D*, **37**, 3406-3427. https://doi.org/10.1103/PhysRevD.37.3406

[14] Wetterich, C. (1988) *Nuclear Physics B*, **302**, 668-696. https://doi.org/10.1016/0550-3213(88)90193-9

[15] Doran, M., *et al.* (2001) *The Astrophysical Journal*, **559**, 501-506. https://doi.org/10.1086/322253

[16] Zhang, Y.Y., Golden-Marx, J.B., Ogando, R.L.C., Yanny, B., Rykoff, E.S., *et al.* (2023) Dark Energy Survey Year 6 Results: Intra-Cluster Light from Redshift 0.2 to 0.5.

[17] Lian, C.B. and Zhou, B. (2019) Introduction to Differential Geometry and General Relativity. 2nd Edition, Vol. I, II, III, Science Press, Beijing.

[18] Qiao, B. (2023) *Journal of Modern Physics*, **14**, 212-326. https://doi.org/10.4236/jmp.2023.143016

[19] Qiao, B. (2023) *Journal of Modern Physics*, **14**, 604-622. https://doi.org/10.4236/jmp.2023.145035

[20] Duan, Y.S. (2020) General Relativity and Gravity Gauge Theory. Science Press, Beijing.

[21] Klioner, S.A., Mignard, F., Lindegren, L., Bastian, U., McMillan, P.J., Hernández, J., Hobbs, D., Ramos-Lerate, M., Biermann, M., *et al.* (2021) *A&A*, **649**, A9. https://doi.org/10.1051/0004-6361/202039653

[22] Milgrom, M. (1983) *The Astrophysical Journal*, **270**, 371. https://doi.org/10.1086/161131

[23] Milgrom, M. (1983) *The Astrophysical Journal*, **270**, 384-389. https://doi.org/10.1086/161132

[24] Zhao, Z. and Liu, W.B. (2010) Fundamentals of General Relativity. Tsinghua University Press, Beijing.

[25] Misner, C.W., Thorne, K.S. and Wheeler, J.A. (2017) Gravitation. Princeton University Press, Princeton and Oxford.

[26] Riess, A., *et al.* (1998) *Astronomical Journal*, **116**, 1009. https://doi.org/10.1086/300499

[27] Perlmutter, S., *et al.* (1999) *Astrophysical Journal*, **517**, 565.

[28] Riess, A.G., *et al.* (2004) *Astrophysical Journal*, **607**, 665.

[29] Nobel Physics Prize Honours Accelerating Universe Find. BBC News.

[30] Wald, R.M. (1984) General Relativity. The University of Chicago Press, Chicago. https://doi.org/10.7208/chicago/9780226870373.001.0001

[31] Palmer, J. (2010) Cosmos May Show Echoes of Events before Big Bang. BBC News.

[32] Penrose, R. (2006) Before the Big Bang: An Outrageous New Perspective and Its Implications for Particle Physics. *Proceedings of the EPAC* 2006, Edinburgh, 26-30 June 2006, 2759-2762.

[33] Gurzadyan, V.G. and Penrose, R. (2013) *The European Physical Journal Plus*, **128**, Article No. 22. https://doi.org/10.1140/epjp/i2013-13022-4

Journal of Modern Physics, 2023, 14, 1721-1734
https://www.scirp.org/journal/jmp
ISSN Online: 2153-120X
ISSN Print: 2153-1196

Meissner Exclusion of Gravito-Magnetic Energy from a Momentum-Space Crystal

Edwin Eugene Klingman

Cybernetic Micro Systems, Inc., San Gregorio, CA, USA
Email: klingman@geneman.com

How to cite this paper: Klingman, E.E. (2023) Meissner Exclusion of Gravito-Magnetic Energy from a Momentum-Space Crystal. *Journal of Modern Physics*, **14**, 1721-1734.
https://doi.org/10.4236/jmp.2023.1413101

Received: November 8, 2023
Accepted: December 12, 2023
Published: December 15, 2023

Abstract

A primordial field theory of Quantum Gravity resolves a number of century-old paradoxes associated with general relativity and quantum mechanics. It allows re-interpretation of major experiments such as Michelson-Gale (1925) and Q-bounce (1999). I address herein an unexplained anomalous experiment by Martin Tajmar (2006), in terms of a gravitomagnetic-based Meissner effect.

Keywords

Quantum Gravity, Meissner Exclusion, Momentum Space Crystal, Gravitomagnetism, Tajmar Anomaly

1. Introduction

Any theory of Quantum Gravity faces an uphill climb, as evidenced in Arma's "*Conversations on Quantum Gravity*" [1]. A century of paradox accompanies 20th Century relativity and quantum theory, much of this due to the attempt to base the physics of space-time on geometry. Ashtekar says: "… *if in fact geometry is a physical entity, as Einstein has taught us… geometry should have an atomic structure*." Yet, Field states: "*Spacetime is just an abstraction… I believed all my life that spacetime exists, but I no longer do so*." Einstein early concluded [2] that space and time are abstractions; "*there is no vacuum* (aka 'empty space') *absent field*." Feynman, Weinberg and others, state that geometry is unnecessary as a means of understanding gravity, so much quantum gravity is based on geometrical concepts deemed inappropriate by some of our greatest physicists.

Every theory is intended to describe or explain physical reality. Instead of pursuing highly abstract conceptions, effectively divorced from physical reality, we assume that a fundamental physical field, the primordial field, came into existence at the Creation, the only physical reality in existence. The plan of this paper is:

1) Introduction

2) The Primordial Field of the Universe

3) Local C-field induced structure and energy distribution

4) Definition of Momentum-space Crystal

5) Meissner-exclusion of Gravitomagnetic field from Momentum-space Crystal

6) Primordial field explanation of Tajmar effect

7) Summary

8) Conclusions.

2. The Primordial Field of the Universe

If nothing else exists, evolution of the primordial field ψ can occur only through self-interaction, and this principle is reflected in the self-interaction equation:

$$\nabla\psi = \psi\psi : \left\{\psi(\xi) = -\xi^{-1}, \psi(\boldsymbol{\xi}) = \boldsymbol{\xi}^{-1}\right\} \tag{1}$$

where solutions are simply presented, and ∇ represents the change operator $\nabla = \partial_\xi$. Defining primordial field $\psi = \boldsymbol{G}(\boldsymbol{r},t) + i\boldsymbol{C}(\boldsymbol{r},t)$ with corresponding operator $\nabla = \boldsymbol{\nabla} + \partial_t$, Equation (1) becomes [3].

$$(\boldsymbol{\nabla} + \partial_t)(\boldsymbol{G} + i\boldsymbol{C}) = (\boldsymbol{G} + i\boldsymbol{C})(\boldsymbol{G} + i\boldsymbol{C}) \tag{2}$$

A Hestenes' Geometric Calculus expansion of this equation immediately leads to the following:

$$\begin{array}{ll} \textbf{Self-Interaction equations} & \textbf{Heaviside equations} \\ \boldsymbol{\nabla}\cdot\boldsymbol{G} = \boldsymbol{G}\cdot\boldsymbol{G} - \boldsymbol{C}\cdot\boldsymbol{C} & \boldsymbol{\nabla}\cdot\boldsymbol{G} = -\rho \\ i\boldsymbol{\nabla}\cdot\boldsymbol{C} = i2\boldsymbol{G}\cdot\boldsymbol{C} & \boldsymbol{\nabla}\cdot\boldsymbol{C} = 0 \\ \partial_t\boldsymbol{G} - \boldsymbol{\nabla}\times\boldsymbol{C} = \boldsymbol{G}\times\boldsymbol{C} \pm \boldsymbol{C}\times\boldsymbol{G} & \boldsymbol{\nabla}\times\boldsymbol{C} = -\rho\boldsymbol{v} + \partial_t\boldsymbol{G} \\ i\boldsymbol{\nabla}\times\boldsymbol{G} + i\partial_t\boldsymbol{C} = 0 & \boldsymbol{\nabla}\times\boldsymbol{G} = -\partial_t\boldsymbol{C} \end{array} \tag{3}$$

Heaviside's generalization of Newtonian gravity is equivalent (under iteration) to Einstein's GR. Terms on the left are given *field energy density* interpretation leading to Heaviside's (1893) formulation [4] of the right side of (3). The concept of *field strength* is absent in the derivation, other than the implicit assumption of ultra-strong fields existing at the big bang. The fields are shown in **Figure 1**. *Encoding Energy-Density as Geometry* [5] analyzes the mismatch between primordial field ontology and "geometric reality" and discusses the physical reality associated with such. After the conceptual basis of the theory has been developed, the theory has been used to re-interpret key experiments of physics such as the well-known (1925) Michelson-Gale [6] and (1999) Q-bounce experiments [7]. This paper advances the theory by applying it to an anomalous (2006) experiment by Martin Tajmar [8].

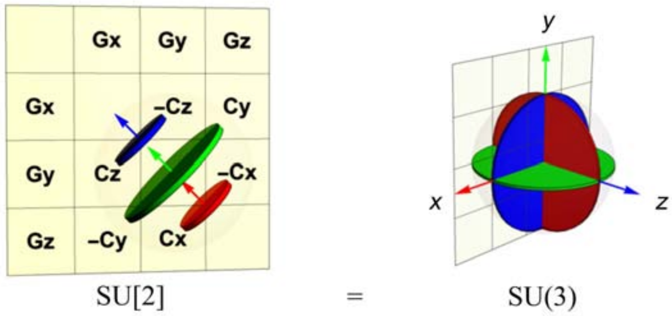

Figure 1. The circulating field, the C-field, can be labeled by the (row, col) component or by the orthogonal axis about which the (row, col) component circulates. For example, the (*x*, *z*) element is labeled C_y and the (*z*, *x*) element is labeled $-C_y$ since both of these terms rotate about the y-axis; similarly for the other components. These rotations are shown abstractly in the representation of the field strength $F_{\mu\nu}$ matrix on the left. The right-hand illustration maps the three bivector diagrams into 3-space. Colors are used for visual convenience and for suggested correlation with SU(3) × SU(2) × U(1) symmetry.

3. Local C-Field-Induced Structure and Energy Distribution

$$\boldsymbol{C}(x,y,z)=\sum\nolimits_{i=1}^{N}\boldsymbol{p}_i\times\boldsymbol{r}_i\Big/\int \mathrm{d}r_i^3 \qquad (4)$$

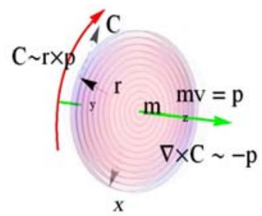

Consider a slice of local C-field induced by a momentum density $\boldsymbol{p}=\rho\boldsymbol{v}$. The diagram in Equation (4) depicts mass m, momentum $\boldsymbol{p}$ (green), circulating-C-field-slice (pinkish), and C-field circulation direction (red, curved arrow). C-fields are additive, however circulation is strongest near the momentum, so consider the fields of two relatively independent entities. As is evident from the red C-field curved arrow, for adjacent co-parallel momenta the chirality of the fields is such that they tend to cancel on the axis between them when added, as shown in **Figure 2(b)**, in which two momenta point out of the page, with their induced C-field calculated at surrounding points. On the line between two identical momenta, the field at the midpoint of the axis will be zero.

We make full use of the most powerful tools available to physicists [9] including Hestenes' *Geometric Calculus* (GC) [10] and Wolfram's *Mathematica 13+*, and potentially *ChatGPT-4* [11]; Although GC can be extended to arbitrary dimensions, ontological analysis implies that we are concerned only with three spatial dimensions $\{\hat{x},\hat{y},\hat{z}\}$ plus scalar time. Points are labelled $\{x,y,z,t\}$; GC-objects function in coordinate-free space and support scalars, 1D-points, 2D-bivectors, 3D-trivectors, and a pseudoscalar or duality operator, *i*, as in $\boldsymbol{a}\wedge\boldsymbol{b}=-i(\boldsymbol{a}\times\boldsymbol{b})$, which projects a plane into an orthogonal (dual) vector. Unlike most math, which does not mix apples and oranges, <u>all</u> GC-objects interoperate and interact algebraically. Arfken [12] shows that sometimes the local integral of an infinitesimal volume is equal to

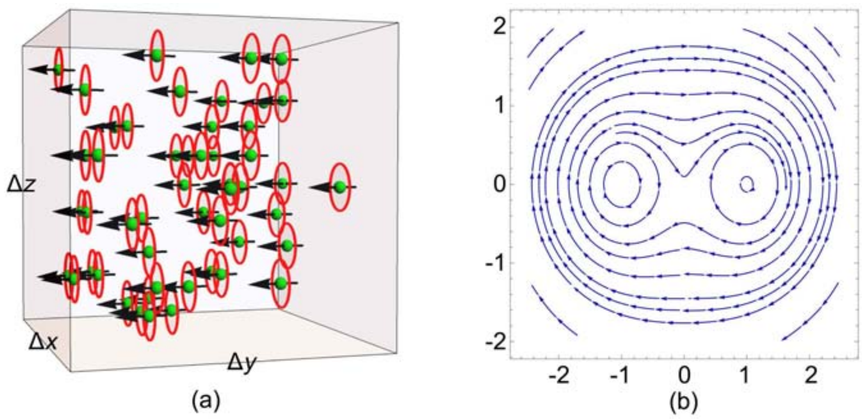

Figure 2. (a) Random atomic nuclei with common momentum density vectors distributed in local cube. (b) The C-field is summed around two nuclei with parallel momentum, perpendicular to the page. C-field cancellation occurs at the midpoint, but circulation around both particles form left-handed loops. The asymmetry is an artifact of the sampling instruction used to create the plot.

$$\int d^3x = \Delta x \Delta y \Delta z = \text{trivector} \tag{5}$$

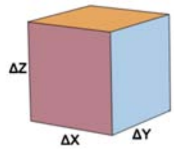

Thus, integration over a volume is sometimes equivalent to multiplying by the scaled volume. In Equation (5) we show the infinitesimal volume as integral formulation, as differential volume, as trivector, and geometrical equivalent. Specific boundary value problems defined on a volume containing distributed sources often require exquisite analytical integrations making use of Gauss' theorem, Stokes' theorem, and Cauchy's theorem. On the other hand, a region containing many particles and associated (entangled) fields, with density n per unit volume, need only be multiplied by the relevant volume. Therefore, when appropriate, we will explicitly depict the trivector in integral form, as in Equation (4).

Consider mass flowing through an infinitesimal volume: the momentum of any mass is essentially the momentum of the nuclei comprising the mass as seen in Figure 2(a) where particles are randomly distributed with all nuclei moving in $\boldsymbol{p}$ direction, but the nuclei are not locked in a lattice configuration; *thermal* motion is allowed in the plane perpendicular to $\boldsymbol{p}$. Integrating meaningful information sometimes equates to simply counting particles in a given region of space, each of which induces a local momentum-based field; interacting particles interact through their fields. Fields of left-handed co-parallel momenta conflict with each other, and vanish at the midpoint between the two, as shown in Figure 2(b).

Let us examine the way in which we plan to display the relevant C-field energy. Figure 3 depicts a number of momenta, located at $[x = \{1, 2, 3, 4\}, y = 0, z = 0]$ and a line through the 2-D plane perpendicular to $\boldsymbol{p}$, left to right. We calculate the C-field vector at every point on the line by summing the contribution at

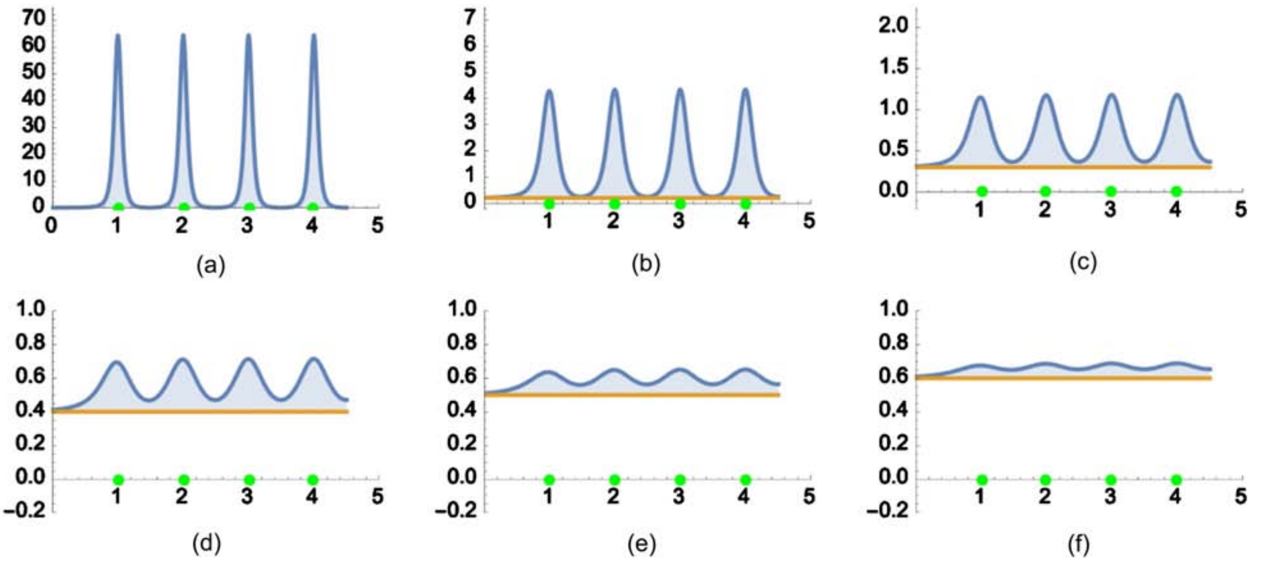

Figure 3. (a)-(f) C-field energy density for four (green) momenta on x-axis.

this point from each of the nuclei in the plane. The energy of the field is $\boldsymbol{C}(x,y,z)\cdot\boldsymbol{C}(x,y,z)$ sampled on the intersection of the $y=k$ plane and the $z=0$ plane.

C-field energy surrounding mass in motion is shown around individual nuclei; local field energy is largely contained inside the cube. Figure 2(b) shows two parallel momenta perpendicular to the plane of the page, each inducing a left-handed C-field circulation, such that fields vanish exactly halfway between the particles, while above and below the particles the field circulates more or less in the same direction, indicated by arrows on the contour lines. Having computed $\boldsymbol{C}(x)$ for every point on a line, we compute local energy density at the points on the line by calculating $|\boldsymbol{C}(x)\cdot\boldsymbol{C}(x)|$. In Figure 3, the base line is orange, drawn at height k above the momenta, and amplitude of the C-field energy density at the point on the orange line is given by the blue curve. The sampling curve vanishes midway between two momenta, as shown for two momenta in Figure 2(b), due to y-components of neighboring momenta cancelling each other. As we rise above the momenta, up and down C-field components tend to cancel, whereas horizontal C-field components add in the $+x$ direction (above the momenta), and in the $-x$ direction if we are sampling below the momenta.

It is easy to visualize the density contours for two source fluxes (momentum density $\rho\boldsymbol{v}$). It is more difficult to study the density contours for all of the momenta in the cube in Figure 2(a). Figure 4 shows three rows of diagrams, each a random displacement from lattice points. Each row shows density profiles across four slices.

4. Definition of Momentum-Space Crystal

Ontologically, a cube of mass is not solid mass, but consists of atoms with electrons

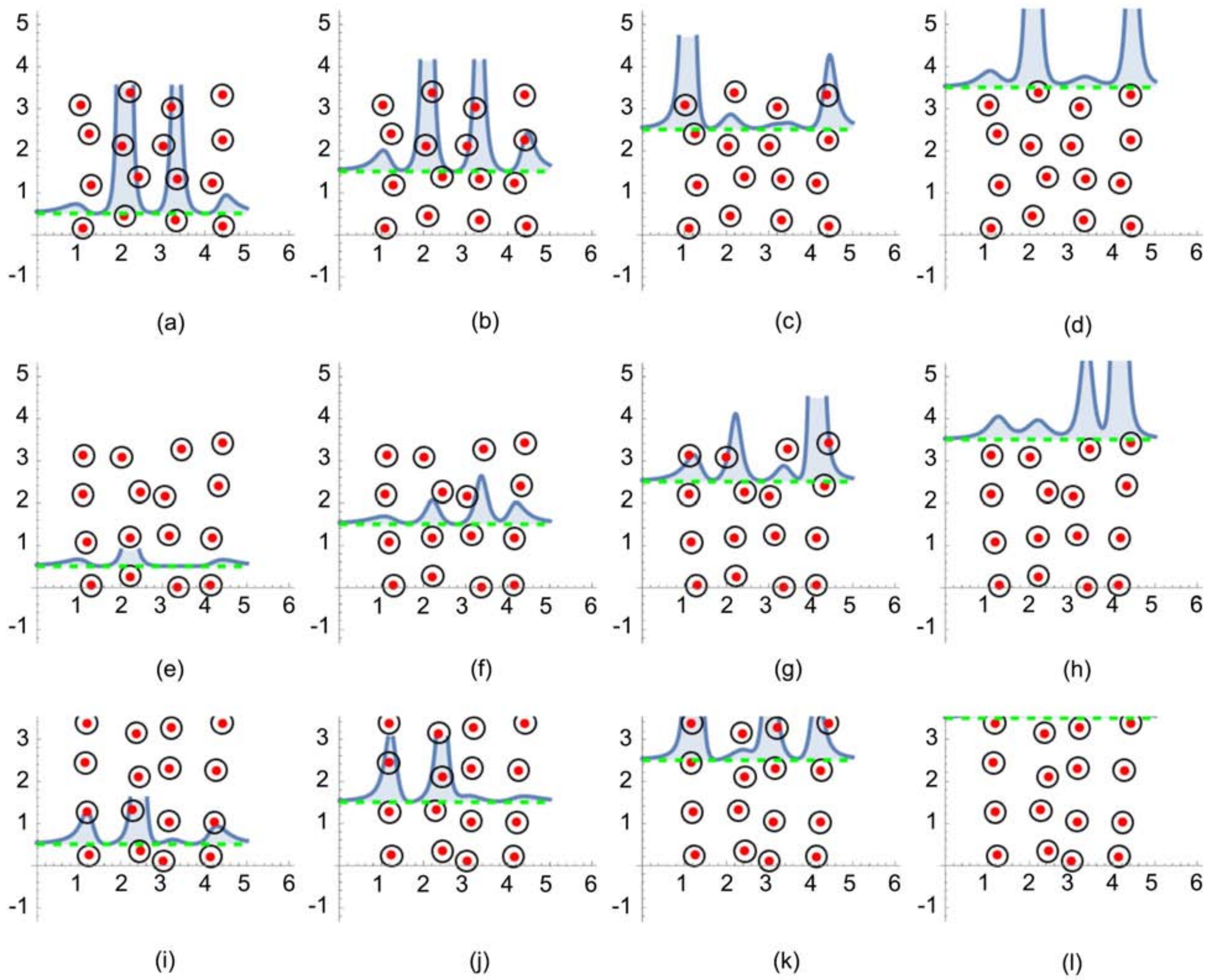

Figure 4. (a)-(l): A 4 × 4-array with random displacements from the 4 × 4 lattice points. The C-field energy density is sampled on lines midway between rows of lattice points. Randomly arranged momenta yield random C-field energy density distributions across the array, that is, the C-field energy varies within the material.

and nuclei. Clouds of electrons keep nuclei distributed evenly over local space but contribute very little to momentum density $\rho \boldsymbol{v}$ where $\rho = m \big/ \int \mathrm{d}^3 x$ and $m = \sum m_{nucleus}$. Ideally, the nuclei are positioned at equidistant lattice points, however the ideal is frustrated by thermal motion. Thus, if we cool the material, we expect the average positions of nuclei to move closer to the lattice points. In the limit, identical momenta located at the lattice points define a momentum-space crystal. Depending upon constitution of the lattice, different lattices "freeze" at different temperatures, for example, Wang *et al.* [13] describe a particular lattice freezing below 50 K. To investigate the C-field behavior of momenta at the lattice points, we consider two rows of momenta, located at $y = 0$ and $y = 1$ as shown in **Figure 5(a)**, sampled as described by Equation (6), with $k = \frac{1}{2}$.

$$\boldsymbol{C}(x, y, z) = \sum_{i=1}^{ncol} \sum_{j=1}^{nrow} r3\left[x - x_{ij}, y = k, 0\right] \times \{0, 0, p_z\} \tag{6}$$

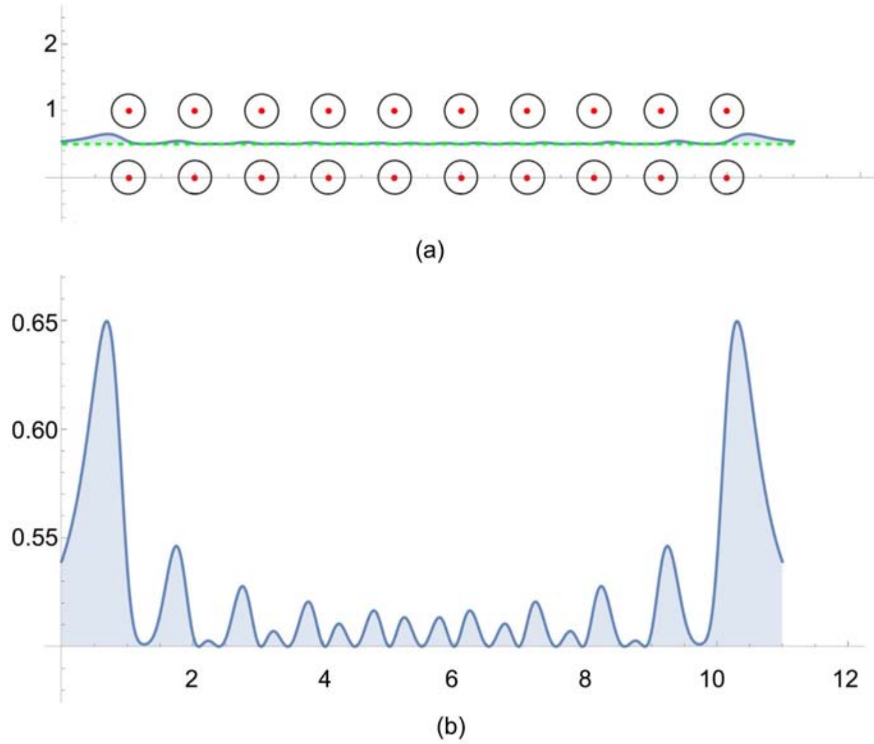

Figure 5. (a) C-field sampled online midway between rows of momenta shows cancellation of circulation. In (b) the sampled energy density diagram is expanded (from $y = 0.5$ to $y = 0.64$) demonstrating that much of the C-field energy density has been excluded from the material.

5. Discussion of Tajmar Effect

Martin Tajmar and de Matos began exploring gravitomagnetism in conjunction with the London moment of superconductivity. The BCS Theory of superconducting related "Cooper pairs" of electrons whose anomalous mass was not understood; electron's charge and mass occurs in relevant equations, but it's unclear whether electron mass or *bare* mass accounts for apparent mass increase of niobium Cooper pairs, though they differ by about three orders of magnitude.

Tajmar and others spun rings of various materials in a cryogenically cooled container and used accelerometers and later laser gyroscopes to detect the gravitomagnetic field generated when the angular velocity of the spinning ring is varied. These detectors are positioned inside the ring and at three positions above the rings with detectors in mirror pairs (the "curl configuration") to cancel mechanical signals. The spin vector of the disk points down and establishes the clockwise or counterclockwise direction of the field. The experiment varied the materials, the temperatures, and the velocity profiles, as seen in **Figure 6**. As expected, the gravitomagnetic field varies directly proportional to the applied angular acceleration of the ring, and the direction of the peak signal changes with the sense of rotation. Niobium gave the strongest acceleration in the tangential direction when angularly accelerated, with gravitational peaks observed when the superconductor passed its critical temperature while rotating.

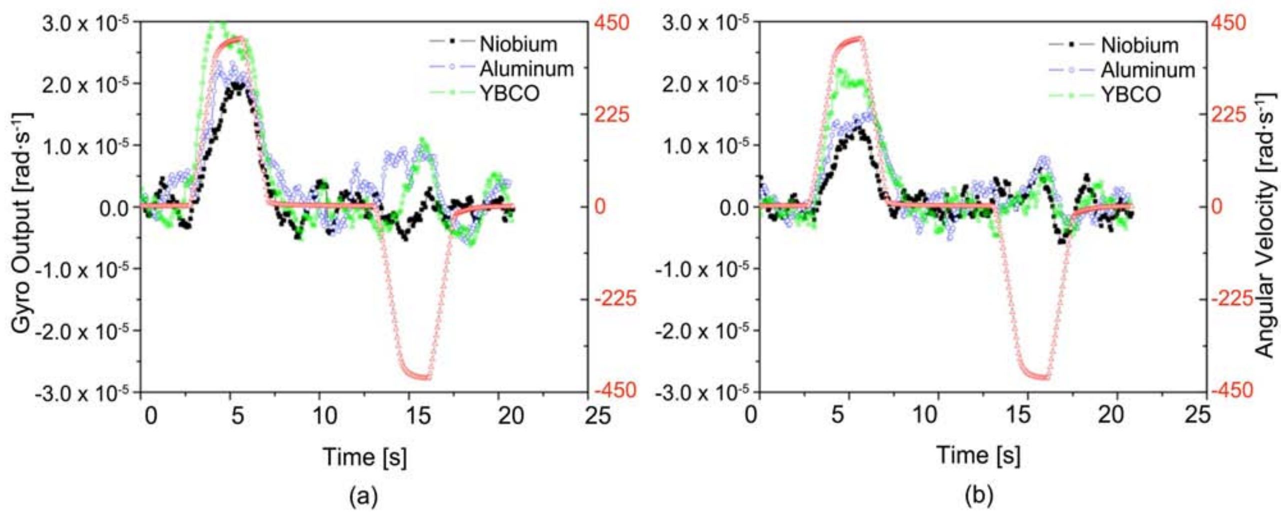

Figure 6. Laser Gyro output for Niobium, Aluminum, and YBCO versus *Applied Angular Velocity* (Δ) between a Temperature of 4 - 6 Kelvin. (a) LG 1 (Reference); (b) LG 2 (Middle).

An unexpected result was the detection of parity: the gyro outputs show a parity violation between clockwise and counterclockwise rotation (the CW signal is larger than the CCW signal), independent of the gyro's orientation. At 4 K and a top speed of 420 rad/s the anomalous gyro signal is as large as one third of the Earth's signal. The gyro follows the applied angular velocity, but only if the ring is rotated in the clockwise orientation. For example, at 4.2 K they performed 40 successive clockwise rotations, and the gyro effect could always be measured. Then (again at 4.2 K) they performed 40 CCW rotations, but any effects were an order of magnitude reduced compared to CW results. In any case, an independent experiment using the world's most precise laser gyro (in a different experiment configuration) shows the gyro's response to the speed of the spinning superconductor, but the parity violation is greater for the counterclockwise rotation—the *opposite* of the above experiments. The fact that the Canterbury ring laser experiment was carried out in the southern hemisphere, while the above experiments were carried out in the northern hemisphere, suggests the origin of the parity effect is Earth's C-field-inducing rotation.

Figure 6(a) depicts the reference Laser Gyro while Figure 6(b) shows the signal from another Laser Gyro that is placed further above the spinning disk, and is therefore yields a weaker signal.

In 2006 Tajmar, Plesescu, Marhold, and de Matos, [14] reported that the niobium ring:

"*reached 30 orders of magnitude higher than what general relativity predicts classically*!"

In 2008, Tajmar, Plesescu, and Siefert [15] concluded that the gyro signal follows the rotating ring velocity with high correlation.

"*Compared to classical frame-dragging spin-coupling predictions*, *our signals are up to 18 orders of magnitude larger.*"

Tajmar and others have written papers discussing their theory behind the experiment and the data from the experiments. Early in the game, Tajmar and de Matos attempted to formulate theoretical explanations, mostly focused on Cooper pairs of electrons, but also including *massive photons*. McCulloch's model was based on Unruh radiation. These efforts did not pan out, so effort shifted to excluding artifacts from the data; effort devoted to systems error analysis and quantification. In the end they claim that the likelihood is that these are real physical effects *without any classical explanation so far*. In (2011) *Gravity Probe B* proved the existence of the C-field [16].

Primordial Field Theory is subject to the self-interaction principle, represented by self-interaction Equation (1) and nowhere supports a formulation of "field strength". In fact, as implied by the big bang assumption, the equation governs ultra-strong fields. Nevertheless, Einstein Geometers conceive of dropping higher order terms to linearize his GR equations, $R_{ij}-\frac{1}{2}Rg_{ij}=T_{ij}$, as producing the [erroneous] "weak field approximation". In [17] Tajmar and de Matos begin:

"*Using the weak field approximation, we can express the theory of general relativity in a Maxwell-type structure comparable to electromagnetism.*"

They follow this with: "*The volume integrals in* Equations (*9*) *and* (*12*) *assume point masses.*"

I believe assumption of the "weak field approximation" and assumption of "point masses" preclude a proper ontological understanding of the Primordial Field Theory and its conceptualization of the Meissner effect of "flux exclusion". In the *Momentum-space Crystal* analysis note that each line between rows of momenta shows suppressed C-field energy density in the interior of the crystal; the C-field flux energy excluded from the interior appears outside of the crystal.

6. Meissner Exclusion of Gravitomagnetic Field from Crystal

The Meissner Effect (1933) is typically associated with the total exclusion of any electromagnetic flux from the interior of a superconductor. It is one of the defining features of superconductivity. In the above we have postulated the exclusion of gravitomagnetic flux from the interior of a "frozen lattice of momenta". We have not made any assumptions about superconductivity associated with the C-field but will find an interesting correlation of C-field exclusion and superconductivity when we analyze the Tajmar anomaly. Knorzer, *et al.* [18] remark:

"*Electron-phonon interactions lie at the heart of several phenomena in condensed matter physics, including Cooper pairing* (…) *Generally, the low-energy excitations of electrons in solids are modified by this coupling to lattice vibrations, which alters the transport and thermodynamics behavior.*"

McColloch [19] notes that the Tajmar anomaly is an unexplained acceleration observed by gyroscopes close to, but isolated from, rotating rings cooled to 5 K. The Tajmar effect…

"*…is similar to the Lense-Thirring effect (frame-dragging) predicted by General Relativity but is* ***20 orders of magnitude larger*** *and shows the added parity violation.*"

This was initially called the gravitomagnetic London effect, but it has been

"*…discredited because the inception of the Tajmar effect (at about 25 K) does not coincide with the superconducting transition temperature, only with very low temperatures.*"

Thus, in agreement with our common sense or intuition the C field is not absolutely banished from the 2D array but vanishes midway between the neighboring momenta as seen in Figure 7. We multiply the energy of two rows by N to sum the energies excluded between $N+1$ rows of frozen momenta (Figure 8). Here we show only 10 momenta per row. The same approach works for N_{col} momenta per row but smooths out the energy "bumps" between the rows.

The diameter of the niobium atom is approximately 150 picometers or 0.15 nanometers. Since the material is approximately 15 mm thick, then we determine the number of rows as follows:

$$\frac{15\times10^{-3}}{150\times10^{-12}}=\frac{1}{10}\times10^{9}=10^{8}\quad \text{rows of niobium atoms}$$

This is where the 10^8 arises.

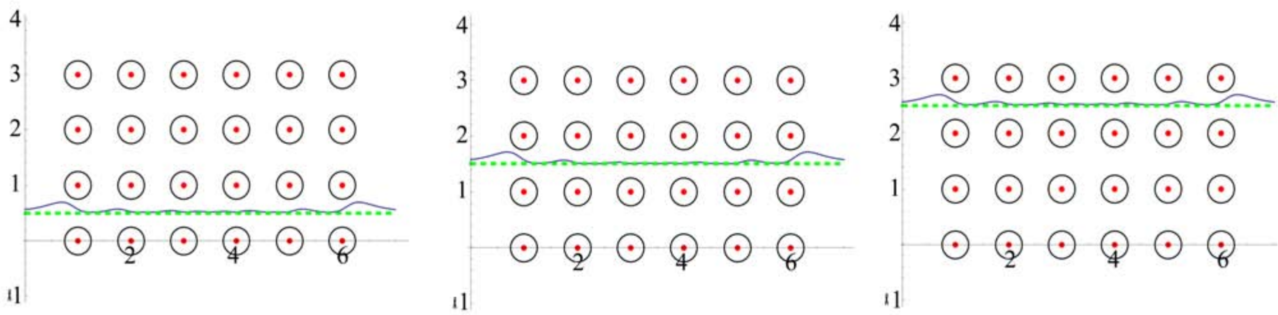

Figure 7. Clarifying the situation for a 4 × 6 momentum array. The left diagram shows the field as sampled *midway* between the first and second rows of momentum. As expected, the field is excluded. Next, we sample the field **midway** between the second and third row of momentum. Again, the field vanishes due to the inherent cancellation of the chiral circulation.

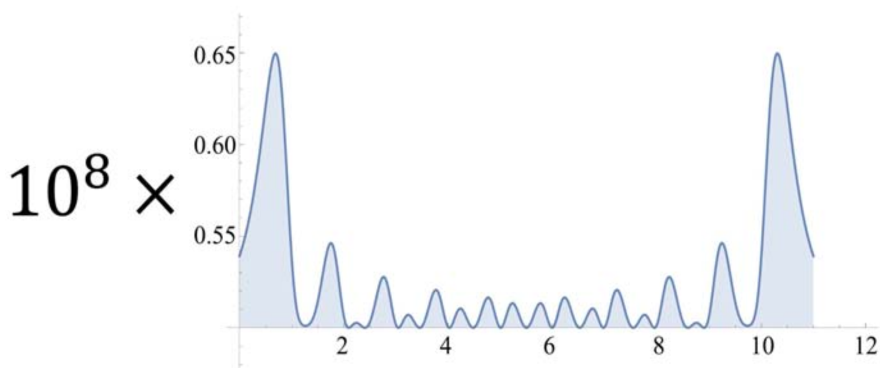

Figure 8. Depicting the multiplication of energy per row times the number of rows.

7. Summary

The primordial Equation (1) has two parametric solutions, a scalar and a vector. In Hestenes' *Geometric Calculus* these are dual with complex "*i*" the duality operator. When treated as such, Heaviside's equations are derived from the primordial field equation. Heaviside derived his gravitational equations from Newton's equation in analogy with Maxwell's electromagnetic equations, which are satisfied for $E + iB$ where E is the electric field and B is the magnetic field. Heaviside's $G + iC$ represents gravity field G and gravito-magnetic field C, both of which are physical fields that have been experimentally detected; the C field by NASA's 2011 *Gravity Probe B* experiment.

Primordial field $\psi = \boldsymbol{G} + i\boldsymbol{C}$ energy density is proportional to field amplitude squared, $\sim \boldsymbol{G} \cdot \boldsymbol{G}$ and $\sim \boldsymbol{C} \cdot \boldsymbol{C}$. Gravitational field $\boldsymbol{G}$ is effectively constant over the measurement device, whereas gravito-magnetic field $\boldsymbol{C}$ at any point in local space is the sum of the local fields induced by local momentum, in this case the momentum density of the atomic nuclei [*niobium*]. When the nuclei are perfectly arranged on the (crystal) lattice, the field midway between the rows of nuclei cancel, and local field energy is minimum. In **Figure 4**, the nuclei are not in a perfect lattice arrangement [due to thermal motion] and therefore do not cancel at every midway point between the rows. The positioning of the nuclei is essentially random, so the local field at the midway point is effectively random, and the square of the local field is energy density, shown as the shaded portion between the green midway line and the blue energy density line. As shown in **Figure 5** and **Figure 7**, when nuclei are positioned at the lattice points, internal energy is minimized, and the gravito-magnetic field is *excluded* from the material. When this occurs for superconducting materials, the exclusion of the magnetic field is known as the Meissner effect. Tajmar's experiments proved that gravito-magnetic field energy density ($\sim \boldsymbol{C} \cdot \boldsymbol{C}$) is excluded so I interpret this as *a gravitomagnetic Meissner effect*. No other interpretation has successfully explained Tajmar's results.

A reviewer stated that the "change operator" seems weird and asks if it has any physical meaning. It is designed to emulate standard physics equations, relating changes in one field to interactions with parameterized sources. Since the primordial field is the *only* field existing at the big bang, then it can interact only with itself, and this leads to the primordial field self-interaction equation, which has two formal solutions, as shown in Equation (1). We intuitively associate the scalar parameter as *time* and the vector parameter as *position* in space, and this leads to the Heaviside interpretation of gravity. What about emergent phenomena? If the primordial field is the *only* field in existence at the big bang, and today's universe has evolved/emerged from the big bang, then the entire universe we live in today has *emerged* from this field equation. A number of my papers describe key examples of emergent phenomena; the gravito-magnetic Meissner effect observed in this paper is such a key example.

The reviewer claims that cosmological and astrophysical aspects emerge from quantum gravity (that may be true, although it has not yet been shown to be true) and wonders about the effects described in this manuscript and quantum gravity. The Meissner effect is a quantum gravity effect in primordial field theory, derived from Equation (1). This topic is explored in reference [7], "*The Ontology of Quantum Gravity*", wherein the quantum wave function is interpreted to be the induced gravito-magnetic wave, *a real physical field*, whereas the quantum "wave function" of today's quantum gravity is unknown—no one is sure whether the nature of the wave function is epistemological (abstract) or ontological (physically real). As for the question, "any unification?", the primordial field unifies the physics of the universe, with examples of such unification presented in paper after paper, with more to come. As for "What is gravity?", as noted initially, there is no need for a geometric interpretation of gravity; the *G*-field solution to the primordial equation is Newton's gravitational field, and the gravito-magnetic *C*-field is Heaviside's gravito-magnetic analogy with electro-magnetism. These emerge as the primordial field at the big bang.

In summary, primordial field theory is not an abstract theory based on mathematics; it is an ontological theory of physical reality, based on the appearance of a universal primordial physical field, quickly shown to be compatible with Newton's gravity and Maxwell's electromagnetism. Unlike today's key theories—which are essentially paradoxical and incomplete, with no unified representation—primordial field theory does not give rise to paradoxes (logical inconsistencies) and is believed to unify quantum theory, gravitational physics, and particle physics. Some of this has been demonstrated in previous papers, some is yet to be presented.

8. Conclusions

Ontological concepts of "weak field approximation" to general relativity and "point masses" preclude proper ontological understanding of gravitomagnetism. Point masses have very little mass but "infinite" mass density. "Weak fields" place unrealistic limits on linearized gravity. Primordial field theory does not mention "field strength"—it applies to <u>all</u> field strengths equally. For example, the strength of the C-field circulation is determined by the momentum density, *i.e.*, the velocity of the relevant mass density. This concept fails when "point mass" is assumed. For extended particles (such as neutrons) finite densities yield C-field wave functions appropriate to quantum gravity, and field strengths at particle levels that have been ignored for over a century, due to the erroneous conception of "weak field approximation". The circulation induced by linear velocity is identical to kinetic energy, *i.e.*, energy previously linked to "motion" exists as C-field circulation. Normally, C-field circulation <u>inside</u> a solid mass is not measurable, per se, but our analysis of the primordial field leads to "flux exclusion" of the sort measured by Tajmar, de Matos, and others. The result is seen to be many orders of magnitude greater than that predicted by general relativity, with its "weak field" assumption.

Early experimenters assumed that Meissner-like flux exclusion occurred at onset of superconductivity. McColloch points out however that "*the inception of the Tajmar effect* (*at about 25 K*) *does not coincide with the superconductivity transition temperature*." I interpret this as follows:

The "freezing of the lattice" applies to the niobium nuclei, with atomic number 41 and atomic weight 92.906. Pure niobium is a superconductor when it is cooled below 9.25 K. The frozen lattice implies that the nuclei exist at lattice points and, as a result, exclude the C-field "flux" inside the material (except that immediately circling each nucleus' momentum). This behavior is uncoupled from superconductivity in the sense that the niobium nuclei are ~169,000 more massive than electrons; therefore, it takes much less thermal energy to move electrons in random fashion. To get rid of this energy, it is necessary to continue to cool the material until the 9.25 K temperature is reached and niobium becomes superconducting, which is characterized by Meissner exclusion of electromagnetic fields from inside the material.

In conclusion, the experimenters claim that the likelihood is that these are real physical effects *without any classical explanation so far*, while the primordial field theory explains the Tajmar anomaly in quite sensible fashion, compatible with ontological aspects of C-field developed in a number of my earlier papers.

Conflicts of Interest

The author declares no conflicts of interest regarding the publication of this paper.

References

[1] Armas, J. (2021) Conversations on Quantum Gravity. Cambridge U Press, Cambridge. https://doi.org/10.1017/9781316717639

[2] Einstein, A. (1952) Relativity: The Special and General Theory. Crown Publishers Inc., New York.

[3] Klingman, E. (2021) *Journal of Modern Physics*, **12**, 65-81. https://www.scirp.org/journal/jmp https://doi.org/10.4236/jmp.2021.122007

[4] Heaviside, O. (1893) *The Electrician*, **31**, 281-282.

[5] Klingman, E. (2021) *Journal of Modern Physics*, **12**, 1190-1209. https://doi.org/10.4236/jmp.2021.129073

[6] Klingman, E. (2023) *Journal of Modern Physics*, **14**, 1003-1017. https://doi.org/10.4236/jmp.2023.146055

[7] Klingman, E. (2023) *Journal of Modern Physics*, **14**, 1392-1408. https://doi.org/10.4236/jmp.2023.1411080

[8] Tajmar, M. and de Matos, C. (2003) *Physica C*, **385**, 551-554. https://doi.org/10.1016/S0921-4534(02)02305-5

[9] Klingman, E. (2023) *Journal of Applied Mathematics and Physics*, **11**, 514-524. https://doi.org/10.4236/jamp.2023.112031

[10] Hestenes, D. and Sobczyk, G. (1984) Clifford Algebra to Geometric Calculus. Reidel Pub., Boston. https://doi.org/10.1007/978-94-009-6292-7

[11] Klingman, E. (2023) *Open Journal of Philosophy*, **13**, 531-543. https://doi.org/10.4236/ojpp.2023.133035

[12] Arfkin, G. (1966) Mathematical Methods for Physicists. Academic Press, New York.

[13] Wang, J., *et al*. (2022) *Physical Review Letters*, **128**, Article ID: 157202. https://doi.org/10.1103/PhysRevLett.128.134101

[14] Tajmar, M., *et al*. (2006) Experimental Detection of the Gravitomagnetic London Moment.

[15] Tajmar, M., Plesescu, F. and Seifert, B. (2008) *Journal of Physics*: *Conference Series*, **150**, Article ID: 032101. https://doi.org/10.1088/1742-6596/150/3/032101

[16] Everitt, C., *et al*. (2011) *Physical Review Letters*, **106**, Article ID: 221101. https://doi.org/10.1103/PhysRevLett.106.221101

[17] Tajmar, M. and de Matos (2001) Coupling of Electromagnetism and Gravitomagnetism in the Weak Field Approximation.

[18] Knorzer, J., *et al*. (2022) *Physical Review Letters*, **128**, Article ID: 120404. https://doi.org/10.1103/PhysRevLett.128.120404

[19] McColloch, M. (2018) The Tajmar Effect from Quantized Inertia.

Journal of Modern Physics, 2023, 14, 1735-1740
https://www.scirp.org/journal/jmp
ISSN Online: 2153-120X
ISSN Print: 2153-1196

Turbulence and Anomalous Transport

Bin Liang

College of Science, Chongqing University of Posts and Telecommunication, Chongqing, China
Email: liangbin@cqupt.edu.cn

How to cite this paper: Liang, B. (2023) Turbulence and Anomalous Transport. *Journal of Modern Physics*, **14**, 1735-1740.
https://doi.org/10.4236/jmp.2023.1413102

Received: November 5, 2023
Accepted: December 15, 2023
Published: December 18, 2023

Abstract

Turbulence is a thermodynamic system composed of a lot of vorticons rather than disturbance to random moving particles. The transport coefficients derived from the definition on turbulence show that the anomalous transport is a natural result of present turbulence in Tokamak plasma and provides an important theoretical reference for the design and operation of Tokamak.

Keywords

Turbulence, Vorticon, Anomalous Transport, Transport Coefficient

1. Introduction

The experimental results show that the transverse transport coefficient of Tokamak plasma is much greater than the neo-classical transport coefficient derived from the present theory, and this is called anomalous transport of Tokamak plasma. It is generally believed that turbulence causes anomalous transport in the Tokamak plasma, enhancing the loss of particles and heat. The study of turbulence is not only a difficult problem in fluid mechanics, but also an important practical problem, because the appearance of turbulence in Tokamak plasma is unavoidable, but now there is no unified theory that can explain the experimental data of anomalous transport. The starting point of previous studies on turbulence is to regard turbulence as the disturbance of random moving particles, and attempt to describe turbulence by nonlinear mathematical methods [1]-[8]. However, after more than half a century, the turbulence theory has failed to provide a statistical ensemble definition to compute average value of physical quantities, because the vortices in turbulence are not disturbances to random moving particles. Regardless of mass or energy, even small vortices are much greater than individual particles. Turbulence is a thermodynamic system composed of a lot of vorticons. The transport coefficients derived from the definition on turbulence show that the anomalous transport is a natural result of present turbulence in

Tokamak plasma and provides an important theoretical reference for the design and operation of Tokamak.

2. Vorticons in Turbulence

In 1852, Joule and Thomson discovered the cooling effect of throttling. In the 1970s, people made use of this effect to make micro refrigeration and widely used in scientific research and production activities. Why does the fluid temperature drop after passing through the orifice? It turns out that there must be turbulence in the fluid passed through the throttle hole, and the turbulence is composed of large and small vorticons, which reduce the temperature of the fluid. The explanation is as follows.

As shown in Figure 1, the X-axis is the interface of two flow layers with velocity u_2, u_1, whose direction is the direction of fluid. The circle centered at point O in the figure represents a medium element with mass m and rotational inertia J in the incompressible fluid, and point A is the contact point between the medium element and the interface.

The experimental results show that the tangential force acting on the unit interface area of the adjacent flow layers is [9]

$$f = \pm \eta \frac{\mathrm{d}u}{\mathrm{d}y}, \tag{1}$$

where $\frac{\mathrm{d}u}{\mathrm{d}y}$ is velocity gradient, η is coefficient of viscosity, the positive and negative signs indicate the tangential force acting on the flow layer with larger or smaller flow velocity, respectively. Suppose $u_2 > u_1$, the tangential force acting on micro-area s at point A is

$$F = -s\eta \frac{\mathrm{d}u}{\mathrm{d}y}, \tag{2}$$

the minus sign indicates the tangential force to the left. When point A is at rest instantaneously, the force acting on point O is the same as above, but in the opposite direction. Since the dimension of $\frac{\mathrm{d}u}{\mathrm{d}y}$ is the same as the frequency, write $\omega = 2\pi \frac{\mathrm{d}u}{\mathrm{d}y}$. Suppose the circle radius is r, so

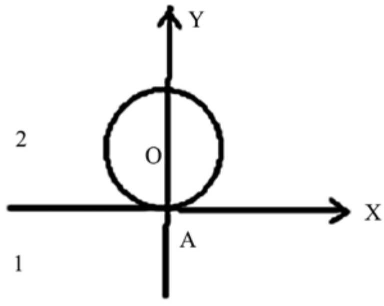

Figure 1. A medium element in fluid.

$$J\frac{\mathrm{d}\omega}{\mathrm{d}t}=\frac{s\eta r}{2\pi}\omega\ . \tag{3}$$

Integrate the above equation and get

$$\omega=\omega_0\mathrm{e}^{\frac{s\eta r}{2\pi J}t}\ , \tag{4}$$

this is the angular velocity of the medium element in the vortex motion, where $\omega_0=2\pi\left(\frac{\mathrm{d}u}{\mathrm{d}y}\right)_0$ is the initial angular velocity. It can be seen that as long as the flow velocity of flow layers is different, there will be viscous effect, and vortices will be produced. We call the medium element in the vortex motion the vorticon. A lot of vorticons constitute turbulence. The angular velocity of a three-dimensional vorticon is

$$\boldsymbol{\omega}=\boldsymbol{\omega}_0\mathrm{e}^{\frac{s\eta r}{2\pi J}t}\ , \tag{5}$$

where $\boldsymbol{\omega}_0=2\pi\sum_{\substack{i,j,k=1,2,3\\ i\neq j\neq k}}\left(-\xi_{ijk}\right)\frac{\partial u_i}{\partial x_j}\boldsymbol{e}_k$, symbol ξ_{ijk} obeys the rules: $\xi_{123}=\xi_{231}=\xi_{312}=1$, otherwise it's minus 1.

In the absence of external fields (such as electromagnetic fields, gravitational fields, etc.), the kinetic energy of a vorticon is

$$\varepsilon=\frac{1}{2}mu^2+\frac{1}{2}J\omega^2\ , \tag{6}$$

The first term on the right of the above equation is the translational kinetic energy of the vorticon, and the second term is the rotational energy.

We know that temperature is a measure of the average translational energy of molecules. As can be seen from the above equation if there is turbulence in a fluid in the advection state under adiabatic conditions, it means that a part of the molecular translational energy is transformed into the rotational energy of the vorticons, thus reducing the molecular translational energy of the fluid and lowering the fluid temperature. This is why where the Joule-Thomson throttling cooling effect occurs. Suppose the temperature of the unimolecular ideal gas is T and the temperature of the gas after turbulence is T'. According to the conservation of energy, there is

$$N\frac{3}{2}kT'+N_t\frac{3}{2}kT'=N\frac{3}{2}kT\ , \tag{7}$$

where N is the number of gas molecules and N_t is the number of vorticons, obviously there is $T'<T$.

It is well known that the molecules in an ideal gas do not interact with each other except collisions. There is no other interaction between vorticons in turbulence except viscous action and collision, and the viscous action has been reflected in the rotational energy of vorticons, thereby the turbulent can be regarded as an approximate ideal vortex system.

Assuming that the turbulent is in thermodynamic equilibrium and the Maxwell vorticon energy distribution law is

$$f(\varepsilon)=\frac{1}{\sqrt{2\pi}(kT)^{3/2}}\sqrt{\varepsilon}\mathrm{e}^{-\frac{\varepsilon}{2kT}}. \tag{8}$$

The above equation satisfies the normalization condition $\int_0^\infty f(\varepsilon)\mathrm{d}\varepsilon=1$. The average kinetic energy of vorticons in the turbulence is

$$\bar{\varepsilon}=\int_0^\infty \varepsilon f(\varepsilon)\mathrm{d}\varepsilon=3kT. \tag{9}$$

It is noted that the vorticon has 6 spatial degrees of freedom, so the above equation is consistent with the equipartition theorem of energy. The maximum probability energy of vorticons is kT. It can be seen that there are few vorticons with large energy in turbulent in thermodynamic equilibrium, and this is consistent with the actual situation.

The cooling of fluid accompanied by turbulence has a very important adverse effect on the stable operation of Tokamak plasma, this needs further study.

3. Anomalous Transport in Tokamak Plasma

The lateral drifted velocity of charged particles in electromagnetic field is [1]

$$\boldsymbol{\upsilon}_\perp=\frac{1}{B^2}(\boldsymbol{E}\times\boldsymbol{B}), \tag{10}$$

It's perpendicular to both the magnetic field and the electric field, and the magnitude is $E_\perp/B$.

Charged particles in electromagnetic fields may be also affected by non-electromagnetic force $\boldsymbol{F}$. Introducing an equivalent electric field

$$\boldsymbol{E}_{eff}=\boldsymbol{F}/q, \tag{11}$$

formula (10) can be written as

$$\boldsymbol{\upsilon}_\perp=\frac{1}{qB^2}(\boldsymbol{F}\times\boldsymbol{B}). \tag{12}$$

1) Diffusion coefficient

In Tokamak plasma, the Debye sphere with the radius equals Debye λ_D has weak electricity, so it is easy to form a particle cluster with the Debye sphere as the core, and the particle cluster is called the smallest vorticon. Since the electric potential $V(r)=\frac{q}{4\pi\varepsilon_0 r}\mathrm{e}^{-\frac{r}{\lambda_D}}$ of the Debye sphere is almost zero at $r=5\lambda_D$ [10], the smallest vorticon with radius $r=5\lambda_D$ is almost an electrically neutral cluster of particles, so the force on the smallest vorticon is mainly the plasma pressure

$$\boldsymbol{F}=-\frac{1}{n}\nabla p, \tag{13}$$

where n is the particle number density of the plasma. Substituting the above equation into Equation (12), since $\boldsymbol{B}\cdot\nabla p=0$ in plasma equilibrium, there is

$$\boldsymbol{\upsilon}_{\perp} = -\frac{1}{nqB}\nabla p. \tag{14}$$

Substituting $p = nkT$ into the above equation and supposing the temperature is uniform in space, the particle number flux across the magnetic field is obtained

$$n\boldsymbol{\upsilon}_{\perp} = -\frac{kT}{qB}\nabla n. \tag{15}$$

Writing the particle number flux as

$$n\boldsymbol{\upsilon}_{\perp} = -D_{\perp}^{n}\nabla n, \tag{16}$$

there is

$$D_{\perp}^{n} = \frac{kT}{qB}. \tag{17}$$

This is the diffusion coefficient caused by the gradient of particle number density. If $n = 10^{20}/\mathrm{m}^3$, $T = 10\ \mathrm{keV}$, Debye radius $\lambda_D = 7.4\times10^{-5}\ \mathrm{m}$, then the number of particles in the smallest vorticon is $n_D = \frac{4\pi}{3}(5\lambda_D)^3 n = 2.13\times10^{10}$, electric quantity $q = \frac{1}{2}n_D e$, the introduction factor 1/2 is due to the recombination of particles in the vorticon, thus obtaining

$$D_{\perp}^{n} = 50.64(T/B)(\mathrm{m}^2/\mathrm{s})(\mathrm{keV}). \tag{18}$$

This is similar to Bohm's empirical formula $D_B = 62.5(T/B)(\mathrm{m}^2/\mathrm{s})(\mathrm{keV})$. Factor 1/16 was artificially introduced into Bohm's formula [11]. If the introduction is 1/20 rather than 1/16, then Bohm's formula becomes
$D_B = 50.0(T/B)(\mathrm{m}^2/\mathrm{s})(\mathrm{keV})$. This is almost the same as Formula (18).

2) Coefficient of heat conduction

Supposing the particle number density is uniform in space, and as said before, the average energy of vorticons is $3kT$, so the energy flux density across the magnetic field is

$$\left(\frac{n}{n_D}\right)3kT\boldsymbol{\upsilon}_{\perp} = -3k\left(\frac{n}{n_D}\right)\frac{kT}{qB}\nabla T = -\boldsymbol{\kappa}\nabla T. \tag{19}$$

Therefore, the coefficient of heat conduction of plasma due to temperature gradient is

$$\boldsymbol{\kappa} = -3k\left(\frac{n}{n_D}\right)\frac{kT}{qB}. \tag{20}$$

3) Coefficient of viscosity

The appearance of turbulence in Tokamak plasma indicates that there are flow layers with different velocity along the ring in the plasma. Supposing the velocity difference of smallest vorticons on both sides of a flow layer interface is Δu, then the viscous force along the interface is

$$F = \frac{n}{n_D}m_D\Delta u\upsilon_{\perp} = \rho\Delta u\upsilon_{\perp}, \tag{21}$$

where m_D is the mass of smallest vorticon, and ρ is the plasma mass density. Suppose the flow velocity difference Δu occurs within a radius of smallest vorticon on each side of the interface, *i.e.*

$$\frac{\Delta u}{l} = \frac{\mathrm{d}u}{\mathrm{d}r}, \tag{22}$$

where $l = 10\lambda_D$ is the diameter of smallest vorticon. Substitute the above equation into Equation (21), and get

$$F = \rho \upsilon_{\perp} l \frac{\mathrm{d}u}{\mathrm{d}r} \tag{23}$$

so we get the coefficient of viscosity

$$\eta = \rho \upsilon_{\perp} l . \tag{24}$$

Since Reynolds number $R_e = \rho \upsilon_{\perp} L/\eta$, the Reynolds number of Tokamak is

$$R_e = \frac{L}{10\lambda_D}, \tag{25}$$

where L is the maximum radius of cross-section of Tokamak plasma. That provides an important theoretical reference for the design and operation of Tokamak. For example, if the maximum radius of cross-section of Tokamak plasma is 1 m, Debye radius $\lambda_D = 7.4 \times 10^{-5}\ \mathrm{m}$, then Reynolds number $R_e = 1351$. It's below the critical Reynolds number but it's not too low.

Conflicts of Interest

The author declares no conflicts of interest regarding the publication of this paper.

References

[1] Qin, Y.-W. (2011) The Physical Basis of Tokamak Experiments. Atomic Energy Press, Beijing, p. 14, 38, 46, 190, 197.

[2] Landau, L.D. and Lifshitz, E.M. (1984) Fluid Dynamics. Third Edition, Chapter Three.

[3] Pope, S.B. (2000) Turbulent Flows. Cambridge University Press, Cambridge.

[4] Sitenko, A. and Malnev, V. (1995) Plasma Physics Theory. Chapman & Hall, New York.

[5] Braginskii, S.I. (1965) Transport Processes in a Plasma. Reviews of Plasma Physics, Vol. 1, Consultants Bureau, New York, p. 205.

[6] Tsytovich, V.N. (1977) Theory of Turbulent Plasma. Consultants Bureau, New York & London.

[7] Connor, J.W. and Wilson, H.R. (1994) *Plasma Physics and Controlled Fusion*, **36**, 719. https://doi.org/10.1088/0741-3335/36/5/002

[8] Connor, J.W. (1988) *Plasma Physics and Controlled Fusion*, **30**, 619. https://doi.org/10.1088/0741-3335/30/6/001

[9] Liang, B. (2016) General Physics. Scholar's Press, Saarbrücken, p. 211.

[10] Li, D., *et al.* (2006) Plasma Physics. Higher Education Press, Beijing, p. 9.

[11] Okazaki, T. (2022) Fusion Reactor Design. University of Science and Technology of China Press, Hefei, p. 135. (In Chinese)

Journal of Modern Physics, 2023, 14, 1741-1754
https://www.scirp.org/journal/jmp
ISSN Online: 2153-120X
ISSN Print: 2153-1196

Understanding the Formation of Galaxies with Warm Dark Matter

Bruce Hoeneisen

Universidad San Francisco de Quito, Quito, Ecuador
Email: bhoeneisen@usfq.edu.ec

How to cite this paper: Hoeneisen, B. (2023) Understanding the Formation of Galaxies with Warm Dark Matter. *Journal of Modern Physics*, **14**, 1741-1754.
https://doi.org/10.4236/jmp.2023.1413103

Received: October 9, 2023
Accepted: December 19, 2023
Published: December 22, 2023

Abstract

The formation of galaxies with warm dark matter is approximately adiabatic. The cold dark matter limit is singular and requires relaxation. In these lecture notes, we develop, step-by-step, the physics of galaxies with warm dark matter, and their formation. The theory is validated with observed spiral galaxy rotation curves. These observations constrain the properties of the dark matter particles.

Keywords

Warm Dark Matter, Galaxy, Galaxy Formation

1. Introduction

The formation of galaxies is qualitatively different if dark matter is warm instead of cold. The cold dark matter limit is singular. It turns out that understanding galaxies, and the formation of galaxies, is *less difficult* if dark matter is warm. So we add to the cold dark matter ΛCDM cosmology one more parameter, namely the temperature-to-mass ratio of dark matter, and let observations decide whether dark matter is warm or cold. These lecture notes do bring new understanding of dark matter, and constrain the properties of the dark matter particles.

There is an extensive literature on warm dark matter, e.g. [1] and references therein. Here, our main focus of attention is the understanding of a relation between observables and an adiabatic invariant in the early universe, which is either an unlikely coincidence, or the solution to the long-standing dark matter problem.

2. Warm Dark Matter

Let us consider warm dark matter as a non-relativistic classical noble gas of particles of mass *m*, density ρ and temperature T. By "classical" we mean that the velocity distribution of the non-relativistic particles of dark matter in the early universe is assumed to be the Maxwell distribution, *i.e.* is not degenerate. For a discussion on how dark matter might have acquired the Maxwell distribution of velocities, see [2]. By "noble" we mean that collisions, if any, do not excite internal states of the particles. Recall that for a non-relativistic gas, $\frac{1}{2}m\langle v^2\rangle = \frac{3}{2}kT$. $\sqrt{\langle v^2\rangle}$ is the root-mean-square thermal velocity of the dark matter particles. Recall that for adiabatic expansion of a noble gas, $TV^{\gamma-1} = TV^{2/3} = \text{constant}$ (here V is the volume), so

$$\sqrt{\langle v^2\rangle}\rho^{-1/3} = \text{constant} \tag{1}$$

is an adiabatic invariant. We will review these concepts in more detail in the next lecture. We want to stress that Equation (1) is valid for a collisionless or collisional gas, and is valid whether, or not, the particles are bouncing off the walls of an expanding box of volume V.

To verify these statements, let us now consider a free particle in a homogeneous universe with expansion parameter $a(t)$, normalized to $a(t_0) = 1$ at the present time t_0. The particle has velocity v at the space point $\boldsymbol{r}$. In time $\mathrm{d}t$ the particle advances $v\mathrm{d}t$ and arrives at the space point $\boldsymbol{r}'$. Due to the expansion of the universe, $\boldsymbol{r}'$ moves away from $\boldsymbol{r}$ with velocity

$$Hv\mathrm{d}t = \frac{1}{a}\frac{\mathrm{d}a}{\mathrm{d}t}v\mathrm{d}t = \frac{\mathrm{d}a}{a}v. \tag{2}$$

So the velocity of the free particle relative to $\boldsymbol{r}'$, when it coincides with $\boldsymbol{r}'$, is reduced by $-\mathrm{d}v = (\mathrm{d}a/a)v$, so

$$va = \text{constant}. \tag{3}$$

Note that this expression is in agreement with Equation (1). As the universe expands, velocities decrease in proportion to a^{-1}, the temperature decreases in proportion to a^{-2}, and the density decreases in proportion to a^{-3}.

It is not necessary to invoke General Relativity. The preceding arguments are valid also in the non-relativistic physics of Newton. During galaxy formation, the dark matter particles have a velocity field in addition to the thermal velocity. Whenever the velocity field diverges, dark matter cools as described in the preceding paragraph.

We define the "adiabatic invariant" of warm dark matter as the comoving root-mean-square thermal velocity of the dark matter particles:

$$v_{h\mathrm{rms}}(1) \equiv v_{h\mathrm{rms}}(a)a = v_{h\mathrm{rms}}(a)\left(\frac{\Omega_c\rho_{\mathrm{crit}}}{\rho_h(a)}\right)^{1/3}. \tag{4}$$

$\Omega_c\rho_{\mathrm{crit}}$ is the mean dark matter density of the universe at the present time (throughout we use the notation and the values of parameters of [3]). The sub-index *h* stands for the dark matter halo. We will use the sub-index *b* for "baryons", mostly hydrogen and helium. These sub-indices will be used only when needed.

Consider a free observer in a density peak in the early universe. This observer feels no gravity and "sees" warm dark matter expand adiabatically, reach maximum expansion, and then contract adiabatically into the core of a galaxy. The adiabatic invariant (4) in the early universe remains constant in the core of the galaxy throughout the formation of the galaxy. This statement is non-trivial, so we will study it in detail in the following lectures, and finally will validate it with observations.

To the cold dark matter cosmology ΛCDM, that has six parameters [3], we add one more parameter, namely the adiabatic invariant $v_{hrms}(1)$, and obtain the warm dark matter cosmology ΛWDM. As we shall learn in the following lectures, we are able to measure v_{hrms} and ρ_{0h} in the core of spiral galaxies, and will therefore be able to obtain $v_{hrms}(1)$, and then decide whether dark matter is warm or cold.

3. The Exponential Isothermal Atmosphere

This lecture is included to remind the reader of results we will be using later on. (For more background, I recommend studying the awe inspiring Feynman Lectures on "The exponential atmosphere" [4].)

James Clerk Maxwell presented several clever arguments to obtain the distribution of velocities of the particles in a gas in thermal equilibrium. The number of particles per unit phase space volume $\mathrm{d}^3\boldsymbol{r}\mathrm{d}^3\boldsymbol{p} \equiv \mathrm{d}x\mathrm{d}y\mathrm{d}z\mathrm{d}p_x\mathrm{d}p_y\mathrm{d}p_z$ is proportional to $\exp\left[-p^2/(2mkT)\right]$:

$$\frac{\mathrm{d}n}{\mathrm{d}^3\boldsymbol{r}\mathrm{d}^3\boldsymbol{p}} \propto \exp\left[-\frac{p^2}{2mkT}\right], \tag{5}$$

where $\boldsymbol{p} = m\boldsymbol{v}$ is the particle momentum. The momenta $\boldsymbol{p}$ are assumed isotropic (later on we will lift this assumption when needed). This Maxwell distribution has been validated experimentally (which settles the issues of the clever arguments), and is our point of departure in these lectures. Using the definite integrals

$$\int_0^\infty \mathrm{e}^{-x^2} x^2 \mathrm{d}x = \frac{\sqrt{\pi}}{4}, \quad \int_0^\infty \mathrm{e}^{-x^2} x^4 \mathrm{d}x = \frac{3\sqrt{\pi}}{8}, \tag{6}$$

the following well known results are readily obtained:

$$\frac{1}{2}m\langle v^2\rangle = \frac{3}{2}kT, \quad P = \frac{\rho}{m}kT \quad \text{with } \rho \equiv \frac{N}{V}m, \tag{7}$$

where the pressure P is defined as twice the momenta p_z of particles with $p_z > 0$ traversing unit area in unit time.

Let N/V be the number of particles per unit volume of the gas. Then the normalized Maxwell distribution is

$$\frac{\mathrm{d}n}{\mathrm{d}^3\boldsymbol{r}\mathrm{d}^3\boldsymbol{p}} = \frac{N}{V}\frac{1}{(2\pi mkT)^{3/2}}\exp\left[\frac{-p^2}{2mkT}\right]. \tag{8}$$

The number of particles with z-momenta in the interval p_z to $p_z + \mathrm{d}p_z$, traversing unit area in unit time, obtained from (8), is

$$\mathrm{d}F = v_z \mathrm{d}p_z \int \frac{N}{V} \frac{1}{(2\pi mkT)^{3/2}} \exp\left[\frac{-p^2}{2mkT}\right] \mathrm{d}p_x \mathrm{d}p_y. \tag{9}$$

Now consider gas in equilibrium in a column in a uniform gravitational field $\boldsymbol{g} = g_z \boldsymbol{e}_z$ with $g_z < 0$. The potential energy of a particle at altitude $z = h$ is $\Phi(h) = m(-g_z)h$. We wish to obtain the distribution of momenta at altitude h. We consider particles at altitude 0 with $p_z > 0$ and $p_z^2/(2m) > \Phi(h)$, with z-momenta in the interval p_z to $p_z + \mathrm{d}p_z$. These particles reach altitude h with z-momenta in the interval p'_z to $p'_z + \mathrm{d}p'_z$, where

$$\frac{p_z^2}{2m} = \frac{p_z'^2}{2m} + \Phi(h) \quad \text{and} \quad \frac{(p_z + \mathrm{d}p_z)^2}{2m} = \frac{(p'_z + \mathrm{d}p'_z)^2}{2m} + \Phi(h). \tag{10}$$

Subtracting these two equations, and keeping first order terms, obtains

$$v_z \mathrm{d}p_z = v'_z \mathrm{d}p'_z. \tag{11}$$

Multiplying by $\mathrm{d}t$ obtains

$$\mathrm{d}z\mathrm{d}p_z = \mathrm{d}z'\mathrm{d}p'_z. \tag{12}$$

This equation is Liouville's theorem in one dimension: the volume of phase space occupied by a set of particles moving in a conservative field is a constant of the motion.

In the steady state, the flux $\mathrm{d}F'$ of particles at altitude h with z-momenta in the interval p'_z to $p'_z + \mathrm{d}p'_z$ is the same as the flux $\mathrm{d}F$ of particles at altitude 0 with z-momenta in the interval p_z to $p_z + \mathrm{d}p_z$, since these are the same particles. Therefore, expressing $\mathrm{d}F$ in terms of variables at altitude h, we obtain:

$$\mathrm{d}F = \mathrm{d}F' = v'_z \mathrm{d}p'_z \int \left(\frac{N}{V}\right)' \frac{1}{(2\pi mkT)^{3/2}} \exp\left[\frac{-p'^2}{2mkT}\right] \mathrm{d}p'_x \mathrm{d}p'_y. \tag{13}$$

where

$$\left(\frac{N}{V}\right)' = \frac{N}{V} \exp\left[\frac{-\Phi(h)}{kT}\right] \tag{14}$$

So, the density varies with altitude as

$$\rho(h) = \rho(0) \exp\left[\frac{-\Phi(h)}{kT}\right]. \tag{15}$$

Comparing (13) with (9), we obtain the distribution of particles at any altitude:

$$\frac{\mathrm{d}n}{\mathrm{d}^3\boldsymbol{r}\mathrm{d}^3\boldsymbol{p}} \propto \exp\left[-\frac{E}{kT}\right], \tag{16}$$

where the energy of a particle is

$$E = \frac{p^2}{2m} + \Phi(\boldsymbol{r}). \tag{17}$$

Equation (16) is the Boltzmann distribution. The proportionality constant in (16) is independent of altitude. Note that *T* in (16) is the same *T* as in (8), so the column of gas is isothermal! These equations are valid for general potential energies $\Phi(\boldsymbol{r})$ not explicitly dependent on *t*.

An amazing result of these calculations is that the root-mean-square velocity $\sqrt{\langle v^2 \rangle}$ of the particles of the gas is independent of altitude! This is because only the more energetic particles with the Maxwell distribution reach a higher altitude. Another amazing result is that the column of gas is isothermal because of the Maxwell distribution of momenta, not because of thermal contact, or not, with the walls (if any) of the gas column.

We have not considered particle collisions. It turns out that results are unchanged because collisions conserve energy (another non-trivial statement).

If the particles are collisionless, the thermal velocities may not be isotropic, in which case we will consider separately each component of the thermal velocity.

One more equation that we will be using in the sequel is

$$\frac{\mathrm{d}P}{\mathrm{d}z} = \frac{mg_z}{kT} P = \rho g_z, \tag{18}$$

in agreement with (15). This equation expresses that the difference of pressure $P(z) - P(z + \mathrm{d}z)$ supports the weight of the gas between z and $z + \mathrm{d}z$. This result may again be surprising since there are no membranes at z and $z + \mathrm{d}z$ on which the particles can bounce off. Equation (18) expresses conservation of momentum.

4. The Cored Isothermal Sphere

Let us repeat the arguments of the preceding lecture, but this time we consider a self-gravitating gas with spherical symmetry. The equations to be solved are

$$\nabla \cdot \boldsymbol{g} = \frac{1}{r^2} \frac{\mathrm{d}}{\mathrm{d}r}\left(r^2 g_r\right) = -4\pi G \rho, \quad \nabla P = \frac{\mathrm{d}P}{\mathrm{d}r} \boldsymbol{e}_r = \rho \boldsymbol{g}, \quad P = \left\langle v_r^2 \right\rangle \rho. \tag{19}$$

The rotation velocity $V(r)$ of a test particle in a circular orbit of radius r is given by

$$-g_r(r) = \frac{V(r)^2}{r}. \tag{20}$$

First we seek a particular solution of the form $\rho(r) \propto r^n$, with $\left\langle v_r^2 \right\rangle$ independent of *r*, *i.e.* we limit the scope of the present lectures to the isothermal case. There is a single well known solution of this form (with $n = -2$):

$$\rho(r) = \frac{kT}{2\pi G m r^2}, \quad M(r) = \frac{2kT}{Gm} r, \quad V = \sqrt{\frac{2kT}{m}} = \sqrt{2\left\langle v_r^2 \right\rangle}. \tag{21}$$

The potential energy difference between particles at r and a reference r_c is $\Phi(r) = 2kT \ln(r/r_c)$, so (15) is valid. Note that to obtain a solution it is necessary to provide $\left\langle v_r^2 \right\rangle$.

The total mass of the halo can be defined as $M(r_{\max})$ with $\rho(r_{\max}) = \Omega_c \rho_{\text{crit}}$. Then $M(r_{\max}) \propto T^{3/2} \propto V^3$, which is the Tully-Fisher relation if $M(r_{\max})$ is proportional to the absolute luminosity.

Let us review Liouville's theorem for the problem at hand. Let dn be the number of particles occupying the phase-space volume $\mathrm{d}^3\boldsymbol{r}\mathrm{d}^3\boldsymbol{p}$. If the force field is conservative, *i.e.* if (17) is satisfied with $\Phi(\boldsymbol{r})$ not explicitly dependent on t, then, in the course of the motion of the dn particles, the corresponding volume of phase-space moves in phase-space, and may change shape, but its volume turns out to be a constant of the motion. Also, no particles cross the boundary of this phase-space volume, so dn is also a constant of the motion. The phase-space density $\left(\mathrm{d}n/\left(\mathrm{d}^3\boldsymbol{r}\mathrm{d}^3\boldsymbol{p}\right)\right)$ at time t is equal to the phase-space density $\left(\mathrm{d}n/\left(\mathrm{d}^3\boldsymbol{r}\mathrm{d}^3\boldsymbol{p}\right)\right)'$ at time t', and so can only be a function of constants of the motion, e.g. the energy E. If this function of E is exponential the system is isothermal, *i.e.* $\left\langle v^2\right\rangle$ is independent of $\boldsymbol{r}$. In the present case of the isothermal sphere, E does not depend on the directions of $\boldsymbol{r}$ or $\boldsymbol{p}$, so the phase-space volume can be written as $4\pi r^2\mathrm{d}r\cdot 4\pi p^2\mathrm{d}p$, with $\boldsymbol{v}\cdot\mathrm{d}\boldsymbol{p}=\boldsymbol{v}'\cdot\mathrm{d}\boldsymbol{p}'$, and, in particular, $v_r\mathrm{d}p_r=v_r'\mathrm{d}p_r'$. If convenient, the phase-space volume can also be written as $4\pi r^2\mathrm{d}r\cdot\mathrm{d}p_r\cdot 2\pi p_T\mathrm{d}p_T$, where $\boldsymbol{p}_T$ is the momentum transverse to $\boldsymbol{e}_r$. Then the flux at r per unit area and time of particles with p_r in $\mathrm{d}p_r$, and similarly at r', are

$$\mathrm{d}F\equiv\frac{\mathrm{d}n}{4\pi r^2\mathrm{d}t}=v_r\mathrm{d}p_r\int\left(\frac{\mathrm{d}n}{\mathrm{d}^3\boldsymbol{r}\mathrm{d}^3\boldsymbol{p}}\right)2\pi p_T\mathrm{d}p_T, \tag{22}$$

$$\mathrm{d}F'\equiv\frac{\mathrm{d}n}{4\pi r'^2\mathrm{d}t'}=v_r'\mathrm{d}p_r'\int\left(\frac{\mathrm{d}n}{\mathrm{d}^3\boldsymbol{r}\mathrm{d}^3\boldsymbol{p}}\right)'2\pi p_T'\mathrm{d}p_T', \tag{23}$$

Note that $\mathrm{d}t\equiv\mathrm{d}r/v_r=\mathrm{d}r'/v_r'\equiv\mathrm{d}t'$, so $4\pi r^2\mathrm{d}F=4\pi r'^2\mathrm{d}F'$.

Equations (19) can be solved numerically in radial steps dr, starting from $r_{\min}$. To start the numerical integration we need to provide two boundary conditions, e.g. $g_r\left(r_{\min}\right)$ and $\rho\left(r_{\min}\right)$, in addition to $\left\langle v_r^2\right\rangle$. For solutions with no black hole at $r=0$ we can take $g_r\left(r_{\min}\right)\approx -G4\pi r_{\min}\rho\left(r_{\min}\right)/3$. For these isothermal spheres with a core the solution for $r\gg r_c$ is (21), while the solution for $r\ll r_c$ is

$$\rho\left(r\ll r_c\right)=\rho_0,\quad V\left(r\ll r_c\right)=\sqrt{\frac{4}{3}\pi G\rho_0}\,r,\quad \Phi\left(r\ll r_c\right)\equiv 0. \tag{24}$$

The two asymptotes meet at a "core radius"

$$r_c=\sqrt{\frac{3\left\langle v_r^2\right\rangle}{2\pi G\rho_0}}. \tag{25}$$

We note that the adiabatic invariant (1) is a minimum at $r=0$ where $\Phi(r)$ is a minimum. Since the cored isothermal sphere has formed from a density perturbation in the early universe, its two parameters ρ_0 and $\left\langle v_r^2\right\rangle=kT/m$ are related by the adiabatic invariant (4):

$$v_{hrms}(1)=\sqrt{3\left\langle v_r^2\right\rangle}\left(\frac{\Omega_c\rho_{\mathrm{crit}}}{\rho_0}\right)^{1/3}. \tag{26}$$

Further justification of (26), and observational validation, will be given in following lectures. Therefore, in the present work, the cored isothermal sphere, and its Boltzmann distribution of dark matter particles, is defined by a single independent parameter, ρ_0 or $\langle v_r^2 \rangle = kT/m$. Equation (26) assumes isotropic velocities (valid in the core due to spherical symmetry, and also valid if the dark matter halo is isothermal).

We note that a measurement of $V(r \gg r_c)$ obtains $\sqrt{\langle v_r^2 \rangle}$, and a measurement of $\mathrm{d}V(r \ll r_c)/\mathrm{d}r$ obtains ρ_0, and together they obtain the adiabatic invariant $v_{h\mathrm{rms}}(1)$.

5. An Example

As an extreme example, with a very large ρ_{0h}, let us consider the spiral galaxy UGC11914 (note that our final measurements of $v_{h\mathrm{rms}}(1)$ are obtained from rotation curves of dwarf galaxies [6]). The rotation curves of UGC11914, observed by the SPARC collaboration [5], are presented in **Figure 1**. We fit these rotation curves by solving the equations:

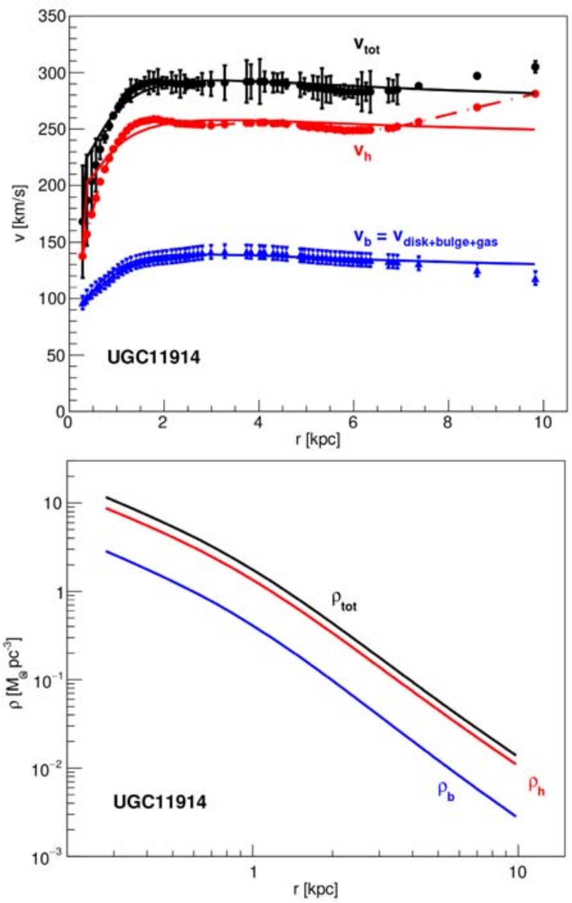

Figure 1. Top: Observed rotation curve $V_{\mathrm{tot}}(r)$ (dots) and the baryon contribution $V_b(r)$ (triangles) of galaxy UGC11914 [5]. The solid lines are obtained by numerical integration as explained in the text. Bottom: Mass densities of baryons and dark matter obtained by the numerical integration.

$$\nabla \cdot \boldsymbol{g}_b = -4\pi G \rho_b, \quad \nabla \cdot \boldsymbol{g}_h = -4\pi G \rho_h, \tag{27}$$

$$\boldsymbol{g} = \boldsymbol{g}_b + \boldsymbol{g}_h, \quad g_b \equiv -\frac{v_b^2}{r}, \quad g_h \equiv -\frac{v_h^2}{r}, \quad V^2 = v_b^2 + v_h^2, \tag{28}$$

$$\nabla P_b = \rho_b \left(\boldsymbol{g} + \kappa_b \frac{V^2}{r} \hat{\boldsymbol{e}}_r \right), \quad \nabla P_h = \rho_h \left(\boldsymbol{g} + \kappa_h \frac{V^2}{r} \hat{\boldsymbol{e}}_r \right), \tag{29}$$

$$P_b = \left\langle v_{rb}^2 \right\rangle \rho_b \quad \text{and} \quad P_h = \left\langle v_{rh}^2 \right\rangle \rho_h. \tag{30}$$

$\boldsymbol{g}_b$ and $\boldsymbol{g}_h$ are the contributions of baryons and dark matter to the gravitation field $\boldsymbol{g}$. We have included κ_b and κ_h to account for rotation. These parameters are quite uncertain, though a rough estimate is $\kappa_b \approx 0.98$ and $\kappa_h \approx 0.15$ [7] or less [8]. We can eliminate κ_b and κ_h from the numerical integration by replacing $\left\langle v_{rb}^2 \right\rangle \to \left\langle v_{rb}^2 \right\rangle / (1-\kappa_b)$, and $\left\langle v_{rh}^2 \right\rangle \to \left\langle v_{rh}^2 \right\rangle / (1-\kappa_h)$. We start the numerical integration at the first measured point at $r_{\min}$, and end at the last measured point, in steps d*r*. To start the numerical integration we need six boundary conditions: $\left\langle v_{rb}^2 \right\rangle / (1-\kappa_b)$, $\left\langle v_{rh}^2 \right\rangle / (1-\kappa_h)$, $\rho_b(r_{\min})$, $\rho_h(r_{\min})$, M_{bBH} and M_{hBH}, where

$$g_b(r_{\min}) = -G(4/3)\pi r_{\min} \rho_b(r_{\min}) - GM_{bBH} / r_{\min}^2, \tag{31}$$

$$g_h(r_{\min}) = -G(4/3)\pi r_{\min} \rho_h(r_{\min}) - GM_{hBH} / r_{\min}^2, \tag{32}$$

to include the possibility of a black hole at the center. Good fits are obtained assuming $\left\langle v_{rb}^2 \right\rangle / (1-\kappa_b)$ and $\left\langle v_{rh}^2 \right\rangle / (1-\kappa_h)$ are independent of *r*. We vary the six boundary conditions to minimize the χ^2 between the observed and calculated rotation velocities, and obtain:

$$\sqrt{\frac{\left\langle v_{rb}^2 \right\rangle}{1-\kappa_b}} = 193.9 \pm 1.7 \text{ km/s}, \quad \sqrt{\frac{\left\langle v_{rh}^2 \right\rangle}{1-\kappa_h}} = 197.5 \pm 0.8 \text{ km/s}, \tag{33}$$

$$\rho_b(r_{\min}) = 2.86 \pm 0.22 \text{ M}_\odot/\text{pc}^3, \quad \rho_h(r_{\min}) = 8.75 \pm 0.29 \text{ M}_\odot/\text{pc}^3, \tag{34}$$

$$M_{bBH} = (2.85 \pm 0.95) \times 10^8 \text{ M}_\odot, \quad M_{hBH} = (18.6 \pm 2.0) \times 10^8 \text{ M}_\odot. \tag{35}$$

Uncertainties are statistical from the fit. The core radius is 0.70 kpc. The core dark matter density $\rho_h(r_{\min})$ is 2.6×10^8 times the mean dark matter density of the universe $\Omega_c \rho_{\text{crit}}$. We note that this galaxy indeed has a black hole at its center. From $\left\langle v_{rh}^2 \right\rangle$ and $\rho_h(r_{\min})$ we obtain the adiabatic invariant (26):

$$v_{h\text{rms}}(1) = \sqrt{1-\kappa_h} \cdot (535 \pm 8(\text{stat}))\text{m/s}, \tag{36}$$

where the uncertainty is statistical only.

Let us mention that similar results are obtained from galaxies spanning 3.5 orders of magnitude in absolute luminosity [6], validating that the adiabatic invariant in the core of galaxies is conserved, confirming that $v_{h\text{rms}}(1)$ is of cosmological origin, and that dark matter is indeed warm!

If we add an *r*-dependence to $\left\langle v_{rh}^2 \right\rangle$ we generally obtain a higher χ^2 of the fit, so indeed, within uncertainties, the dark matter halo is isothermal, at least out to the observed rotation curves, indicating that the particles have the Maxwell-Boltzmann momentum distribution. We note that $\sqrt{\langle v_{rb}^2 \rangle / (1-\kappa_b)}$ is of the same order of magnitude as $\sqrt{\langle v_{rh}^2 \rangle / (1-\kappa_h)}$, because dark matter and baryons fall into the same potential well. Since thermal equilibrium implies $\frac{1}{2} m_p \langle v_{rb}^2 \rangle = \frac{1}{2} m_h \langle v_{rh}^2 \rangle$, we conclude that, unless $m_p (1-\kappa_b) \approx m_h (1-\kappa_h)$, dark matter is not in thermal equilibrium with baryons (mostly hydrogen atoms). So, on galactic scales, we can neglect dark matter-baryon interactions. If dark matter feels only the gravitational interaction, it can be shown that deviations of its trajectory due to particle-particle encounters, or interchange of energy with baryons, can be neglected on galactic scales. We also note that the ratio of dark matter to baryon densities in the galaxy is generally of the order of the universe average.

The galaxy density (21) reaches $\Omega_c \rho_{\text{crit}}$ at

$$r_{\max} = \left(\frac{\langle v_{rh}^2 \rangle}{2\pi G \Omega_c \rho_{\text{crit}}} \right)^{1/2} \approx 6.6 \text{ Mpc}. \tag{37}$$

The age of the universe at, say, redshift $z = 6$, is 3×10^{16} s. In this time a particle with constant velocity 198 km/s reaches 0.2 Mpc, less than $r_{\max}$, and much farther than the last observed rotation velocity.

From (36), neglecting κ_h, we estimate that dark matter becomes non-relativistic at expansion parameter

$$a_{h\text{NR}} \equiv \frac{v_{h\text{rms}}(1)}{c} \approx 1.8 \times 10^{-6}, \tag{38}$$

i.e. after e^+e^- annihilation, and while the universe is still dominated by radiation [3].

Now let us do the following back-of-the-envelope approximate calculations. An ultra-relativistic gas with zero chemical potential has a number density of particles $n(T) = 0.1218 \cdot (kT/(\hbar c))^3 (N_b + 3N_f/4)$ [3]. At expansion parameter a_{hNR} the temperature is $T_h(a_{h\text{NR}}) \approx m_h c^2/(3k)$. The present number density is $n(1) = n(a_{h\text{NR}}) a_{h\text{NR}}^3 = \Omega_c \rho_{\text{crit}}/m_h$, if dark matter particles do not decay or annihilate at $\approx a_{h\text{NR}}$, *i.e.* if there is no "freeze-out". From these equations we obtain

$$m_h \approx \left(\frac{\Omega_c \rho_{\text{crit}} (3\hbar)^3}{0.1218 \cdot v_{h\text{rms}}^3(1)} \right)^{1/4} (N_b + 3N_f/4)^{-1/4}, \tag{39}$$

or

$$\frac{m_h c^2}{e} \approx 107.3 \text{ eV} \left(\frac{760 \text{ m/s}}{v_{h\text{rms}}(1)} \right)^{3/4} (N_b + 3N_f/4)^{-1/4}. \tag{40}$$

For scalar dark matter, *i.e.* $N_b = 1$ and $N_f = 0$, and neglecting κ_h, we estimate the mass of the dark matter particles from (36): $m_h c^2/e \approx 140 \text{ eV}$. At expansion parameter $a_{h\text{NR}}$ the photon temperature is $T_\gamma(a_{h\text{NR}}) = T_0/a_{h\text{NR}}$. From the preceding equations we obtain

$$\frac{T_h(a_{h\text{NR}})}{T_\gamma(a_{h\text{NR}})} \approx 0.386 \left(\frac{v_{h\text{rms}}(1)}{760 \text{ m/s}} \right)^{1/4} (N_b + 3N_f/4)^{-1/4}, \tag{41}$$

or, for our example, $T_h(a_{h\mathrm{NR}})/T_\gamma(a_{h\mathrm{NR}}) \approx 0.354$. That this ratio is of order 1, given that the dark matter particle mass m_h is uncertain over 89 orders of magnitude [3], is surely telling us something! Furthermore, note that dark matter is sufficiently cooler than photons to (marginally) evade the "thermal relic" mass limits obtained from the Lyman-α forest [9], and sufficiently cool to not spoil the success of Big-Bang Nucleosynthesis [7]. Finally, within experimental uncertainties, dark matter is in thermal and diffusive equilibrium with the Standard Model sector, and decouples from this sector, at T somewhere between the top quark mass m_t and the temperature T_C of the deconfinement-confinement transition from quarks to hadrons (decoupling at a lower temperature compromises the agreement with Big Bang Nucleosynthesis [7]). For a proper treatment of the preceding estimates see [2] [10]. It turns out that Equations (40) and (41) change by less than 1%. For a summary of measurements and their interpretation, see [11]. For details of each measurement see the citations in [9].

Excersize to test the Boltzmann factor $\exp(-\Phi/(kT)) \approx (r_c/r)^2$: From the measured dark matter density in the vecinity of the sun [3], and other Milky Way data that you can find in the literature, estimate $v_{hrms}(1)/\sqrt{1-\kappa_h}$. Is your answer consistent with (36)?

Exersizes: The isothermal assumption can be lifted by using the observed galaxy density runs $\rho_h(r)$ and $\rho_b(r)$ [12] [13]. Study these articles and obtain the adiabatic invariant $v_{hrms}(1)/\sqrt{1-\kappa_h}$ from each of them. Are your answers consistent with (36)?

6. Galaxy Formation

Let us solve, by numerical integration, the following equations that describe the formation of a galaxy: Newton's equation

$$\nabla \cdot \boldsymbol{g} = -4\pi G(\rho_h + \rho_b), \tag{42}$$

the continuity equations

$$\frac{\partial \rho_h}{\partial t} = -\nabla \cdot (\boldsymbol{v}_h \rho_h), \tag{43}$$

$$\frac{\partial \rho_b}{\partial t} = -\nabla \cdot (\boldsymbol{v}_b \rho_b), \tag{44}$$

and Euler's equations

$$\frac{\mathrm{d}\boldsymbol{v}_h}{\mathrm{d}t} = \frac{\partial \boldsymbol{v}_h}{\partial t} + (\boldsymbol{v}_h \cdot \nabla)\boldsymbol{v}_h = (1-\kappa_h(t))\boldsymbol{g} - \frac{1}{\rho_h}\nabla\left(\left\langle v_{rh}^2\right\rangle \rho_h\right), \tag{45}$$

$$\frac{\mathrm{d}\boldsymbol{v}_b}{\mathrm{d}t} = \frac{\partial \boldsymbol{v}_b}{\partial t} + (\boldsymbol{v}_b \cdot \nabla)\boldsymbol{v}_b = (1-\kappa_b(t))\boldsymbol{g} - \frac{1}{\rho_b}\nabla\left(\left\langle v_{rb}^2\right\rangle \rho_b\right). \tag{46}$$

$\boldsymbol{g}(\boldsymbol{r},t)$ is the gravitation field, $\boldsymbol{r}$ is the proper (not comoving) coordinate vector, $\rho_h(\boldsymbol{r},t)$ and $\rho_b(\boldsymbol{r},t)$ are the mass densities, $\boldsymbol{v}_h(\boldsymbol{r},t)$ and $\boldsymbol{v}_b(\boldsymbol{r},t)$ are the velocity fields, and $\sqrt{\left\langle v_{rh}^2\right\rangle(t)}$ and $\sqrt{\left\langle v_{rb}^2\right\rangle(t)}$ are the radial (1-dimensional) velocity dispersions, *i.e.* thermal velocities, of dark matter and baryons (mostly hydrogen), respectively. Equations (45) and (46) express the conservation of momentum. The static limits of Equations (42) - (46) are Equations (27) - (30). These equations need to be supplemented by the equations of state of dark matter and baryons at $r_{\min}$ in order to obtain a solution. The Maxwell distributions of baryons and dark matter have different temperatures $kT_b = m_p \langle v_{rb}^2 \rangle$ and $kT_h = m_h \langle v_{rh}^2 \rangle$, respectively. The dark matter velocity field converging onto the core has two consequences: it increases both the core density ρ_{0h} and temperature T_h, maintaining constant the dark matter adiabatic invariant (26) (as explained in lecture 2), and similarly for baryons. When the dark matter halo reaches a final stationary state its cored isothermal halo is defined by a single parameter ρ_{0h}.

An example, discussed in [15], is presented in **Figure 2**. For baryons we take $v_{b\text{rms}}(1) = 21\,\text{m/s}$, corresponding to hydrogen decoupling from photons at $z \approx 150$ [16]. We set the initial $\rho_h(r)$ and $\rho_b(r)$ as shown in **Figure 2**. We integrate the equations in steps d*t*, and for each *t*, in steps d*r*, starting at $r_{\min}$, to calculate the new $\rho_b(r, t + \mathrm{d}t)$ and $\rho_h(r, t + \mathrm{d}t)$. The above equations need to be supplemented by the adiabatic conditions, so, for each step of *t*, we set, only once, *i.e.* for all *r*:

$$\sqrt{\langle v_{rh}^2 \rangle (t)} = \frac{v_{h\text{rms}}(1)}{\sqrt{3}} \left(\frac{\rho_h(r_{\min}, t)}{\Omega_c \rho_{\text{crit}}} \right)^{1/3}, \tag{47}$$

and

$$\sqrt{\langle v_{rb}^2 \rangle (t)} = \frac{v_{b\text{rms}}(1)}{\sqrt{3}} \left(\frac{\rho_b(r_{\min}, t)}{\Omega_b \rho_{\text{crit}}} \right)^{1/3}. \tag{48}$$

Equation (47) is justified out to at least the last observed rotation velocity by the nearly flat rotation curves. The isothermal prescription (47) cannot be correct beyond $r_{\max}$ where the universe is expanding homogeneously. However, this is not a problem since, beyond $r_{\max}$, $\nabla(\langle v_{rh}^2 \rangle \rho_h)$ and $\nabla(\langle v_{rb}^2 \rangle \rho_b)$ are zero. While the hydrogen and helium gas remains adiabatic, *i.e.* until excitations, ionization, radiation, shocks and star formation become significant, we require (48). **Figure 2** illustrates the formation of a core, and how the galaxy reaches a stationary isothermal state starting from $r = 0$ and progressing outwards. For additional examples, see [14] and [15].

Note that, independently of the details of how the core reaches its final density ρ_{0h}, including spherical or filament collapse and galaxy mergers, this density fully specifies the cored isothermal sphere with its temperature, core radius, Boltzmann distribution, and adiabatic invariant $v_{h\text{rms}}(1)$ (up to a rotation, and perhaps also a relaxation, correction ≤ 1, that observationally is found to be in the approximate range 1 to 0.5 [6]).

Finally, let us mention that in the cold dark matter scenario, *i.e.* in the limit $\langle v_{rh}^2 \rangle \to 0$, we are left with no hydrostatic Equations (27) - (30), or hydrodynamical Equations (42) - (46).

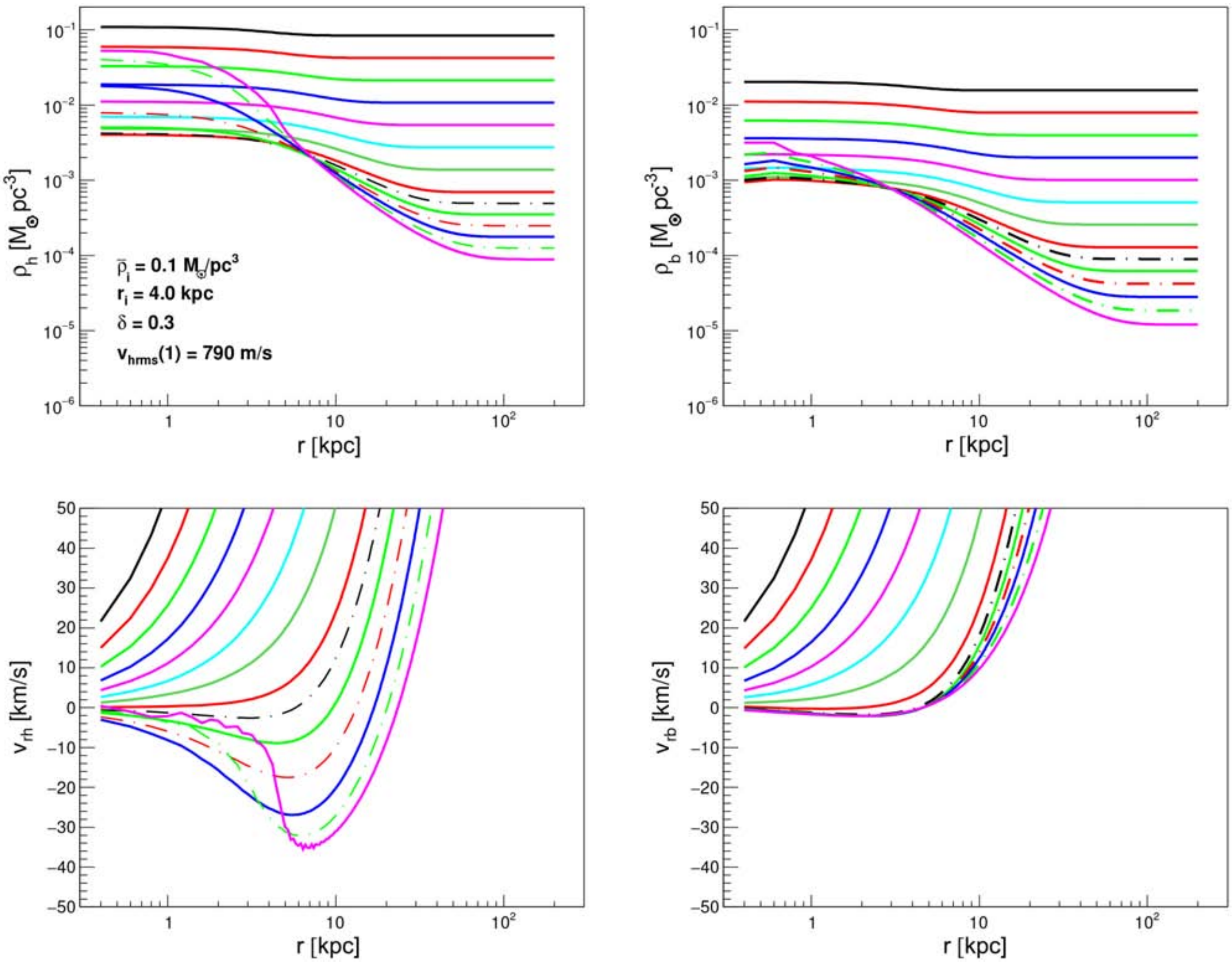

Figure 2. Shown is the formation of a warm dark matter plus baryon galaxy. The densities $\rho_h(r)$ and $\rho_b(r)$, and velocity fields $v_{rh}(r)$ and $v_{rb}(r)$, are presented at time-steps that increase by factors 1.4086 (or $\sqrt{1.4086}$ for the dot-dashed lines). The initial density perturbations are Gaussian, with parameters listed in the figure. In this example, dark matter is warm with $v_{hrms}(1) = 790\ \mathrm{m/s}$. $\kappa_h(t) = 0$. $\kappa_b(t)$ is increased from 10^{-4} to 1 keeping constant baryon angular momentum. Note the initial velocity field corresponding to the expansion of the universe. Note that both warm dark matter and baryons acquire cores. The baryon core is due to the baryon angular momentum conservation. The warm dark matter core is due to the adiabatic invariant feedback (47). Note the effect of this feedback on $v_{rh}(r)$ at the final times shown (studied in [14]). An isothermal steady state is reached for both warm dark matter and baryons, starting at $r = 0$ and then extending out to larger r, at least out to the observed rotation curves. This Figure is taken from [15].

7. Conclusions

We have studied galaxies, and galaxy formation, assuming that dark matter is warm. This scenario requires the addition of one parameter to the cold dark matter ΛCDM cosmology, namely the adiabatic invariant $v_{hrms}(1)$ defined in (4). We find that the formation of galaxies, all the way from linear perturbations in the early universe, until the galaxies reach an isothermal stationary state, conserves the adiabatic invariant $v_{hrms}(1)$ in the core to a good approximation. The arguments in favor of this view are not without objections, so observational validation is necessary. This adiabatic invariant feedback and the initial conditions determine the final core density ρ_{0h}, and hence the entire cored isothermal sphere including its core radius and temperature (at least out to the observed spiral galaxy rotation curves). Note that it is not necessary to invoke dark matter self interactions, baryonic feedback, or fermionic dark matter quantum degeneracy, to justify a core (though these phenomena may influence the core). The observed spiral galaxy rotation curves allow measurements of $v_{hrms}(1)$ (up to a rotation, and perhaps also a relaxation, correction ≤ 1, that observationally is found to be in the approximate range 1 to 0.5 [6]). These measurements are consistent for galaxies with absolute luminosities spanning 3.5 orders of magnitude [6], so the analysis is validated by observations, and the interpretation that $v_{hrms}(1)$ is of cosmological origin is confirmed. Independent measurements of $v_{hrms}(1)$ are obtained by studying the consequences of the warm dark matter free-streaming suppression factor $\tau^2(k)$ of the cold dark matter power spectrum of density perturbations, *i.e.* galaxy stellar mass distributions, galaxy rest-frame ultra-violet luminosity distributions, first galaxies, and their effect on the reionization optical depth [17]. All of these measurements of $v_{hrms}(1)$ are consistent, solve the small scale problems of ΛCDM [18], and constrain the warm dark matter particle properties [9] [11] [19].

Conflicts of Interest

The author declares no conflicts of interest regarding the publication of this paper.

References

[1] Destri, C., de Vega, H.J. and Sanchez, N.G. (2013) *Physical Review D*, **88**, Article ID: 083512. https://doi.org/10.1103/PhysRevD.88.083512

[2] Paduroiu, S., Revaz, Y. and Pfenniger, D. (2015) Structure Formation in Warm Dark Matter Cosmologies Top-Bottom Upside-Down. https://arxiv.org/pdf/1506.03789.pdf

[3] Particle Data Group, Zyla, P.A., *et al.* (2020) *Progress of Theoretical and Experimental Physics*, **2020**, 083C01.

[4] Feynman, R.P., Leighton, R.B. and Sands, M. (1963) The Feynman Lectures on Physics. Vol. 1, Addison-Wesley Publishing Company, Reading, Mass.

[5] Lelli, F., McGaugh, S.S. and Schombert, J.M. (2016) *The Astronomical Journal*, **152**, 157. https://doi.org/10.3847/0004-6256/152/6/157

[6] Hoeneisen, B. (2022) *International Journal of Astronomy and Astrophysics*, **12**, 363-381. https://doi.org/10.4236/ijaa.2022.124021

[7] Hoeneisen, B. (2019) *International Journal of Astronomy and Astrophysics*, **9**, 71-96. https://doi.org/10.4236/ijaa.2019.92007

[8] Tonini, C., Lapi, A., Shankari, F. and Salucci, P. (2006) *The Astrophysical Journal*, **638**, L13-L16. https://doi.org/10.1086/500556

[9] Hoeneisen, B. (2023) Comparing Measurements and Limits on the Warm Dark Matter Temperature-to-Mass Ratio. arxiv: 2308.10356.

[10] Hoeneisen, B. (2022) *International Journal of Astronomy and Astrophysics*, **12**, 94-109. https://doi.org/10.4236/ijaa.2022.121006

[11] Hoeneisen, B. (2023) *European Journal of Applied Sciences*, **11**, 473-481. https://doi.org/10.18272/aci.v15i1.2961

[12] Karukes, E.V. and Salucci, P. (2017) *MNRAS*, **465**, 4703-4722. https://doi.org/10.1093/mnras/stw3055

[13] Borzou, A. (2021) *Journal of Cosmology and Astroparticle Physics*, **8**, 23. https://doi.org/10.1088/1475-7516/2021/08/023

[14] Hoeneisen, B. (2021) *International Journal of Astronomy and Astrophysics*, **11**, 489-508. https://doi.org/10.4236/ijaa.2021.114026

[15] Hoeneisen, B. (2022) *Journal of Modern Physics*, **13**, 932-948. https://doi.org/10.4236/jmp.2022.136053

[16] Weinberg, S. (2008) Cosmology. Oxford University Press, Oxford. https://doi.org/10.1093/oso/9780198526827.001.0001

[17] Hoeneisen, B. (2022) *International Journal of Astronomy and Astrophysics*, **12**, 258-272. https://doi.org/10.4236/ijaa.2022.123015

[18] Hoeneisen, B. (2023) *International Journal of Astronomy and Astrophysics*, **13**, 25-38. https://doi.org/10.4236/ijaa.2023.131002

[19] Hoeneisen, B. (2023) *International Journal of Astronomy and Astrophysics*, **13**, 217-235. https://doi.org/10.4236/ijaa.2023.133013

Journal of Modern Physics, 2023, 14, 1755-1761
https://www.scirp.org/journal/jmp
ISSN Online: 2153-120X
ISSN Print: 2153-1196

The Yukawa and Exponential Potentials for a Galaxy's Spherical Central Bulge*

José Luis Garrido Pestaña

Departamento de Física, Universidad de Jaén, Campus Las Lagunillas, Jaén, España
Email: jlg@ujaen.es

How to cite this paper: Pestaña, J.L.G. (2023) The Yukawa and Exponential Potentials for a Galaxy's Spherical Central Bulge. *Journal of Modern Physics*, **14**, 1755-1761.
https://doi.org/10.4236/jmp.2023.1413104

Received: October 25, 2023
Accepted: December 24, 2023
Published: December 27, 2023

Abstract

By adding an extra term to the Newtonian potential, matter outside the orbit of a star adds to the gravitational acceleration acting on that star. In this work, we solve the Poisson equation for non-Newtonian potentials of a spherically symmetric distribution of mass. We derive equations for calculating the centripetal acceleration and velocity of galactic disk stars that are due to the Newtonian and exponential potentials of the galaxy's central bulge.

Keywords

Galaxies: Kinematics and Dynamics, Gravitation, General Physics (Physics Education)

1. Introduction

In Book III of Principia, Newton [1] published proofs of two theorems that afford an easy calculation of the gravitational potential of any spherically symmetric distribution of matter and to calculate excellent approximations of the potential for approximately spherical distributions of matter such as the central bulge of a spiral galaxy. Thus, since 1687 we have known that the Newtonian acceleration of an orbiting object depends only on the mass inside the orbit. Any uniform spherical shell of matter outside the orbit has no effect on the orbital dynamics. These useful Newtonian theorems are not valid for other gravitational potentials proposed over the past decade to explain anomalous galactic dynamics. For example, with a linear potential [2], the centripetal acceleration of a disk star is sensitive to the halo mass outside its orbit and, even more inconveniently, to the mass of the entire Universe.

*This article is dedicated to the fond memory of Don Eckhardt, who passed away in the morning of 21st October 2023. He was my friend and collaborator, and a true visionary.

The foci of our exposition are two other non-Newtonian gravitational models that are more tractable than the linear potential. The first is a Yukawa potential [3] which, for a point mass M at $r = 0$, has the form

$$V_{\mathrm{Y}}(r) = -\alpha G \mathrm{e}^{-\mu r} / r,$$

where G is the Newtonian gravitational constant, α is a dimensionless constant, and μ is the wave number ($2\pi/\mu$ is the Compton wavelength). The second is an exponential potential [4] [5] which is actually the superposition of two Yukawa potentials with coupling constants $\pm\alpha G$ that are identical except for their signs: an attractive potential, $V_{\mathrm{Y}}^{\mathrm{A}} = -\alpha G \mathrm{e}^{-\mu_{\mathrm{A}} r}$, and a repulsive potential, $V_{\mathrm{Y}}^{\mathrm{R}} = \alpha G \mathrm{e}^{-\mu_{\mathrm{R}} r}$. Their wave numbers are different, but almost identical: $\delta\mu = \mu_{\mathrm{R}} - \mu_{\mathrm{A}} > 0$ and $\mu = (\mu_{\mathrm{A}} + \mu_{\mathrm{R}})/2 \gg \delta\mu$. Then

$$V_{\mathrm{E}}(r) = (\partial V_{\mathrm{Y}} / \partial \mu)\delta\mu. \tag{1}$$

In this paper, we present the mathematical development that has allowed us to resolve for the exponential potential the same problem that Newton solved for the Newtonian potential. That is, given the mass distribution of a spherically symmetric central bulge and halo, then what are their contributions to the specific forces on disk matter that are due to the exponential potential? With this distribution, how much does the exponential potential contribute to the orbital velocity of disk matter? In fact, we provide a route to the potential, and then to the acceleration, that is often more convenient than the iteration by Eckhardt [5]. This model assumes that the central bulge of a galaxy is spherically symmetric, that the mass of the galaxy disk is negligible or is treated separately [6], and that there is an exponential potential as well as a Newtonian potential. To make it clear, the same approach is used to model the shell for the Newtonian potential, then the Yukawa potential, and finally the exponential potential. Although the solution for the Newtonian potential is trivial, it is presented as a guide for the approach for solving the other potentials.

2. Newtonian Potential

The governing equation for the [1] potential V_{N}, which is mediated by the massless graviton, is Poisson's equation:

$$\nabla^2 V_{\mathrm{N}} = 4\pi G \rho,$$

The potential of a point source with mass $\mathrm{d}M$ at a distance R from the source is $-G\mathrm{d}M/R$. (That is, the appropriate Green's function that vanishes at $R = \infty$ is $-G/R$.) Thus the potential at $r = 0$ of a shell at $r = a$ with mass

$$\mathrm{d}M = \mathrm{d}M(a) = 4\pi\rho(a) a^2 \mathrm{d}a$$

is

$$\mathrm{d}V_{\mathrm{N}}(0) = -G a^{-1} \mathrm{d}M.$$

Because of the spherical symmetry, Laplace's Equation ($\rho = 0$) is

$$\frac{1}{r^2}\frac{\mathrm{d}}{\mathrm{d}r}\left[r^2\frac{\mathrm{d}V_\mathrm{N}}{\mathrm{d}r}\right]=0.$$

The two solutions to this equation are of the form *constant* and $constant\times r^{-1}$. The solution that remains finite at $r=0$ is $V_\mathrm{N}=constant$, so for $r\le a$, we have

$$\mathrm{d}V_\mathrm{N}(r)=\mathrm{d}V_\mathrm{N}(0)=-Ga^{-1}\mathrm{d}M,\quad r\le a. \tag{2}$$

The solution that remains finite at $r=\infty$ is $V_\mathrm{N}=constant\times r^{-1}$, so for $r\ge a$, we have

$$\mathrm{d}V_\mathrm{N}(r)=\frac{a}{r}\mathrm{d}V_\mathrm{N}(a)=\frac{a}{r}\mathrm{d}V_\mathrm{N}(0)=-Gr^{-1}\mathrm{d}M,\quad r\ge a. \tag{3}$$

3. Differential Equation for the Exponential Potential

We define the operators

$$\mathcal{D}=\frac{\mathrm{d}}{\mathrm{d}r}$$

and

$$\mathcal{L}=\mathcal{D}^2+\frac{2}{r}\mathcal{D}-\mu^2.$$

With spherical symmetry, the differential equations for the Yukawa potentials $V_\mathrm{Y}^\mathrm{A}(r)$ and $V_\mathrm{Y}^\mathrm{R}(r)$ are then

$$\left[\mathcal{L}+\left(\mu^2-\mu_\mathrm{A}^2\right)\right]V_\mathrm{Y}^\mathrm{A}=\left[\mathcal{L}+\mu\delta\mu\right]V_\mathrm{Y}^\mathrm{A}=4\pi\alpha G\rho$$

and

$$\left[\mathcal{L}+\left(\mu^2-\mu_\mathrm{R}^2\right)\right]V_\mathrm{Y}^\mathrm{R}=\left[\mathcal{L}-\mu\delta\mu\right]V_\mathrm{Y}^\mathrm{R}=-4\pi\alpha G\rho.$$

In addition to $V_\mathrm{E}=V_\mathrm{A}+V_\mathrm{R}$, we define $V_\mathrm{D}=V_\mathrm{A}-V_\mathrm{R}$. We then have

$$\mathcal{L}V_\mathrm{E}+\mu\delta\mu V_\mathrm{D}=0,$$

and

$$\mathcal{L}V_\mathrm{D}+\mu\delta\mu V_\mathrm{E}=8\pi\alpha G\rho.$$

It is obvious that $|V_\mathrm{D}|\gg|V_\mathrm{E}|$, so we neglect the $\mu\delta\mu V_\mathrm{E}$ term and then define

$$V_\mathrm{C}=\mu\delta\mu V_\mathrm{D},$$

and finally derive

$$\mathcal{L}V_\mathrm{E}=-V_\mathrm{C}, \tag{4}$$

and

$$\mathcal{L}V_\mathrm{C}=8\pi\gamma\mu^2G\rho. \tag{5}$$

The exponential potential satisfies the fourth order differential equation

$$\mathcal{L}^2V_\mathrm{E}=-8\pi\gamma\mu^2G\rho.$$

4. The Yukawa and Exponential Potentials of a Thin Spherical Shell

For a thin spherical shell of mass M at $r=a$, the Yukawa potential (coupling constant αG) at the origin is

$$V_{\mathrm{Y}}(0)=-\alpha GM\frac{\exp(-\mu a)}{a}.$$

In free space, the Yukawa potential satisfies the homogeneous equation $\mathcal{L}V_{\mathrm{Y}}=0$, whose solutions are linear combinations of $\exp(\pm\mu r)/r$. The only combination that is finite and equal to unity at the origin is $\sinh(\mu r)/(\mu r)$, so the Yukawa potential inside the shell is

$$V_{\mathrm{Y}}(r)=-\alpha GM\frac{\exp(-\mu a)}{a}\frac{\sinh(\mu r)}{\mu r},\quad r\le a. \tag{6}$$

The solution interval is closed at the shell because the potential (but not its derivative) is continuous there. Thus

$$V_{\mathrm{Y}}(a)=-\alpha GM\frac{\exp(-\mu a)\sinh(\mu a)}{\mu a^2}.$$

The homogeneous solution that is equal to unity at the shell boundary and remains finite outside the shell is $(a/r)\exp\left[-\mu(r-a)\right]$, so the Yukawa potential outside the shell is

$$V_{\mathrm{Y}}(r)=-\alpha GM\frac{\sinh(\mu a)}{\mu a}\frac{\exp(-\mu r)}{r},\quad r\ge a. \tag{7}$$

Note that Equation (6) becomes Equation (7) on interchanging r and a.

The derivative of $V_{\mathrm{Y}}(r)$ is discontinuous at $r=a$. Let δa be the shell thickness, and let $a_-=a-\delta a/2$ represent r just inside the shell, while $a_+=a+\delta a/2$ represents r just outside the shell. Then

$$\mathcal{D}V_{\mathrm{Y}}(r)\big|_{a_+}-\mathcal{D}V_{\mathrm{Y}}(r)\big|_{a_-}=4\pi\alpha G\rho\delta a.$$

For $\mu=0$, this is the Gauss divergence theorem.

Setting $\gamma=\alpha\delta\mu/\mu$ in Equation (1), the exponential potential is

$$V_{\mathrm{E}}(r)=-\gamma\mu GM\frac{\exp(-\mu a)}{\mu a}\left[(1+\mu a)\frac{\sinh(\mu r)}{\mu r}-\cosh(\mu r)\right],\quad r\le a, \tag{8}$$

and, on interchanging r and a and then rearranging terms,

$$V_{\mathrm{E}}(r)=-\gamma\mu GM\left[\frac{\sinh(\mu a)}{\mu a}\exp(-\mu r)+\left(\frac{\sinh(\mu a)}{\mu a}-\cosh(\mu a)\right)\frac{\exp(-\mu r)}{\mu r}\right],\quad r\ge a. \tag{9}$$

The operators $\mathcal{D}$ and $\partial/\partial\mu$ commute, so

$$\begin{aligned}\mathcal{D}V_{\mathrm{E}}(r)\big|_{a_+}-\mathcal{D}V_{\mathrm{E}}(r)\big|_{a_-}&=\frac{\partial}{\partial\mu}\left[\mathcal{D}V_{\mathrm{Y}}(r)\big|_{a_+}-\mathcal{D}V_{\mathrm{Y}}(r)\big|_{a_-}\right]\delta\mu\\&=\frac{\partial(4\pi\alpha G\rho\delta a)}{\partial\mu}\delta\mu=0.\end{aligned}$$

Thus, unlike $\mathcal{D}V_{\mathrm{Y}}(r)$, the derivative of $V_{\mathrm{E}}(r)$ is continuous at $r=a$. This is the reason why $V_{\mathrm{E}}(r)$ cannot be modeled with a second order differential equation. Note that in the far field, where $1/(\mu r)$ is negligible, Equation (9) becomes

$$V_{\mathrm{E}}(r) = -\gamma\mu GM \frac{\sinh(\mu a)}{\mu a} \exp(-\mu r);$$

and, for $\mu a \ll 1$,

$$V_{\mathrm{E}}(r) = -\gamma\mu GM \exp(-\mu r).$$

All the variables in Equations (8) and (9) are linear combinations of $\exp(\pm\mu r)$ and $\exp(\pm\mu r)/r$. Thus, because

$$\mathcal{L}\exp(\pm\mu r) = \left[\mathcal{D}^2 - \mu^2\right]\exp(\pm\mu r) + \frac{2}{r}\mathcal{D}\exp(\pm\mu r)$$
$$= \frac{2}{r}\mathcal{D}\exp(\pm\mu r) = \pm 2\mu \frac{\exp(\pm\mu r)}{r}$$

and

$$\mathcal{L}\left[\frac{\exp(\pm\mu r)}{r}\right] = 0,$$

the equation

$$\mathcal{L}^2 V_{\mathrm{E}}(r) = 0$$

is satisfied wherever $\rho = 0$.

5. Specific Forces and Galaxy Rotation Velocities

The centripetal specific force (acceleration) due to the Newtonian and exponential potentials of the spherically symmetric bulge is

$$g = \frac{\partial\left[V_{\mathrm{N}} + V_{\mathrm{E}}\right]}{\partial r},$$

where

$$V_{\mathrm{N}} + V_{\mathrm{E}} = \int_0^r \mathrm{d}\left[V_{\mathrm{N}} + V_{\mathrm{E}}\right] + \int_r^\infty \mathrm{d}\left[V_{\mathrm{N}} + V_{\mathrm{E}}\right].$$

From Equations (3) and (9),

$$\int_0^r \mathrm{d}\left[V_N + V_E\right] = -r^{-1}G\int_0^r \mathrm{d}M - \gamma\mu G\exp(-\mu r)\int_0^r \frac{\sinh(\mu a)}{\mu a}\mathrm{d}M$$
$$-\gamma\mu G\frac{\exp(-\mu r)}{\mu r}\int_0^r \frac{\sinh(\mu a)}{\mu a}\mathrm{d}M$$
$$+\gamma\mu G\frac{\exp(-\mu r)}{\mu r}\int_0^r \cosh(\mu a)\,\mathrm{d}M,$$

and from Equations (2) and (8),

$$\int_r^\infty \mathrm{d}\left[V_{\mathrm{N}} + V_{\mathrm{E}}\right] = -G\int_r^\infty a^{-1}\mathrm{d}M - \gamma\mu G\frac{\sinh(\mu r)}{\mu r}\int_r^\infty \frac{\exp(-\mu a)}{\mu a}\mathrm{d}M$$
$$-\gamma\mu G\frac{\sinh(\mu r)}{\mu r}\int_r^\infty \exp(-\mu a)\,\mathrm{d}M$$
$$+\gamma\mu G\cosh(\mu r)\int_r^\infty \frac{\exp(-\mu a)}{\mu a}\mathrm{d}M.$$

Thus

$$
\begin{aligned}
g = {} & Gr^{-2}\int_0^r \mathrm{d}M + G\gamma\left(1+\mu r+\mu^2 r^2\right)\frac{\exp(-\mu r)}{r^2}\int_0^r \frac{\sinh(\mu a)}{\mu a}\mathrm{d}M \\
& - G\gamma(1+\mu r)\frac{\exp(-\mu r)}{r^2}\int_0^r \cosh(\mu a)\mathrm{d}M \\
& - G\frac{\gamma\left[\mu r\cosh(\mu r)-\sinh(\mu r)-\mu^2 r^2\sinh(\mu r)\right]}{r^2}\int_r^\infty \frac{\exp(-\mu a)}{\mu a}\mathrm{d}M \\
& - G\frac{\gamma\left[\mu r\cosh(\mu r)-\sinh(\mu r)\right]}{r^2}\int_r^\infty \exp(-\mu a)\mathrm{d}M .
\end{aligned}
$$

The sum of the two last terms (dominated by the last one), which is negative, represents a very small outward force due to the exponential potential of matter further from the origin than *r*; they vanish at the origin. In modeling spiral galaxies with a combination of Newtonian and exponential potentials [7], we have estimated that $\gamma = 12.5$ and $\lambda = \mu^{-1} = 20\ \text{kpc}$, roughly one order of magnitude larger than the radius of the central bulge, so a good approximation is

$$g = \left[r^{-2} + \gamma\mu^2 \exp(-\mu r)\right] GM(r),$$

where

$$M(r) = \int_0^r \mathrm{d}M .$$

If a star is in a circular orbit a distance r from the origin with velocity v, then $v^2 = gr$. Setting $\xi = \mu r$, we then have

$$v = \left\{\mu GM(r)\left[\xi^{-1} + \gamma\xi \mathrm{e}^{-\xi}\right]\right\}^{1/2}.$$

6. Conclusions

Whereas the Poisson equation for a spherically symmetric Newtonian potential is of second order in r, the corresponding equation for the exponential potential is of fourth order. We have derived rigorous and precise mathematical solutions to calculate the exponential potential of a spherically symmetric distribution of mass such as a galactic bulge or halo. Moreover, we have derived a simple and efficient algorithm to closely approximate the associated radial gradients in galaxies. Using the Abel transform, all integrations of spherically symmetric models are relatively simple.

Combined with our technique for modeling the gravitational field of a galactic disk [6], we have found it easy to use in evaluating the effects of Newtonian and exponential potentials for numerous spiral galaxies [7]. Furthermore, it is evident that our approach will be convenient to apply at other distance scales, smaller and larger, such as globular clusters, elliptical galaxies and galaxy clusters.

Conflicts of Interest

The author declares no conflicts of interest regarding the publication of this paper.

References

[1] Newton, I. (1687) Philosophiae Naturalis Principia Mathematica. Royal Society. https://doi.org/10.5479/sil.52126.39088015628399

[2] Mannheim, P.D. (1993) *ApJ*, **419**, 150-154. https://doi.org/10.1086/173468

[3] Yukawa, H. (1935) *Progress of Theoretical Physics*, **17**, 48.

[4] Fischbach, E., Talmadge, C. and Krause, D. (1991) *Physical Review D*, **43**, 460. https://doi.org/10.1103/PhysRevD.43.460

[5] Eckhardt, D.H. (1993) *Physical Review D*, **48**, 3762. https://doi.org/10.1103/PhysRevD.48.3762

[6] Eckhardt, D.H. and Pestaña, J.L.G. (2002) *ApJ*, **572**, L135. https://doi.org/10.1086/341745

[7] Pestaña, J.L.G. and Eckhardt, D.H. (2011) *ApJ*, **741**, L31. https://doi.org/10.1088/2041-8205/741/2/L31

Journal of Modern Physics, 2023, 14, 1762-1770
https://www.scirp.org/journal/jmp
ISSN Online: 2153-120X
ISSN Print: 2153-1196

Logical Conflict between Bell's Locality and Probability Theory

Karl Hess

Center for Advanced Study, University of Illinois, Urbana, IL, USA
Email: k-hess@illinois.edu

How to cite this paper: Hess, K. (2023) Logical Conflict between Bell's Locality and Probability Theory. *Journal of Modern Physics*, **14**, 1762-1770.
https://doi.org/10.4236/jmp.2023.1413105

Received: November 18, 2023
Accepted: December 24, 2023
Published: December 27, 2023

Abstract

Based on "locality" considerations, John Stuart Bell and his followers have derived inequalities and theorems that, when taken together with actual experiments that have been performed by Aspect and others, appear to contradict physical reality as defined by Einstein. However, their specifically applied concept of locality is in conflict with the Fundamental Model of probability theory and the set theoretic definition of conditional probabilities. Bell-type inequalities are, therefore, not adequate to decide ponderous questions regarding physical reality.

Keywords

Bell's Inequalities, Quantum Entanglement, EPR Experiments

1. Introduction

The well-known inequalities and corresponding theorems of Bell [1] and Clauser-Horne-Shimony-Holt (CHSH) [2] have been based on mathematical reasoning involving probability spaces and physical reasoning involving Einstein's separation principle. The mathematical reasoning has been shown to involve a number of issues with respect to the premises used in the Bell-CHSH proofs [3] [4]. These mathematical issues should have been sufficient to relegate the Bell-CHSH theorems to a place of lesser importance, if Bell would not have reformulated his theorem purely in terms of the attributes of "local" and "not-local" [5]:

> "But if [a hidden variable theory] is local it will not agree with quantum mechanics, and if it agrees with quantum mechanics it will not be local."

The notion of "hidden variable theory" relates to "elements of physical reality" as defined by Einstein, Podolsky and Rosen (EPR) [6]. They stated:

> "If without in any way disturbing a system, we can predict with certainty… the value of a physical quantity, then there exists an element of physical reality corresponding to this physical quantity."

The "hidden variables" that have taken center stage in the well-known Einstein-Bohr debate, are just mathematical representations of these elements of physical reality that Einstein presented as alternative to "spooky" influences at a distance.

Key to the EPR arguments are Gedanken-experiments performed in two spatially distant stations. Aspect and others [7] have performed such measurements, using photon-pairs emitted from a source and subsequently passing polarizers and being detected at certain times determined by synchronized clocks. The photon pairs are prepared at the source S in a special way and said to be entangled when so prepared.

The locality-postulates of Bell and followers are usually based on the fact that the entangled pairs may not in any way be related to or depend on the configuration of the measurement equipment including polarizer-angles and detector outcomes in the respective stations. To show this fact, Aspect and others have involved very fast switching of the polarizer angles just before the pair-measurement. As soon as one accepts Einstein's separation principle [6] that is based on the limitation of all velocities by the velocity of light c in vacuum, the fast switching proves indeed that the photon-pair properties must be independent of the polarizer angles just before measurement. Unfortunately, and incorrectly, any such dependence is chastised in the well-known Alice-Bob tutorials and labeled "spooky", even after the sorting by the measurements, using Einstein's own words against his elements of physical reality.

I will show, however, that the evaluation of Einstein's elements of physical reality by polarizers and detector clicks leads to a separation of these elements into distinct sub-sets even for trivially local computer models. This fact contradicts Bell's definition of locality. I will further show that other definitions of locality that have been used by Bell, Aspect, CHSH and many researchers in papers and text-books, are in direct conflict with set-theoretic probability theory and fail, therefore, as well.

2. Einstein- and Bell-Type Models of Quantum Entities

The nature of experiments involving quantum entities is complicated by the well-known facts: 1) That these entities are not directly accessible to our senses, 2) That they are possibly disturbed (meaning changed with respect to their physical properties) by any instrument that we use to experimentally investigate them and 3) That the physical properties associated with them may only be defined in connection with the measuring instruments and the procedure of measurement. We discuss these factors specifically for models related to Aspect-type experiments.

2.1. Einstein's Gedanken-Experiments

Naturally, one cannot speak about a photon-polarization such as "horizontal", as long as one has not defined "horizontal" by the configuration of a polarizer in ordinary space and performed an evaluation of a photon with that polarizer. Bohr's postulate that no property of quantum entities exists before measurement may be interpreted that way. Einstein constructed his Gedanken-experiments in a way that acknowledged the three points of the previous paragraph. He involved two related distant measurements of especially prepared correlated (procedurally entangled) quantum entities that are generated at a common source. Each entity is measured only once and any involved disturbance is, therefore, of no direct consequence. The pair-measurement is important, because one measurement evaluates a physical property of one quantum-entity and the second measurement recognizes that property of the correlated entity by a confirming measurement outcome. If that outcome can be predicted with certainty, then EPR postulate that an element of physical reality must have transferred the information, while otherwise we would need to accept "spooky" influences; instantaneous influences at a distance.

In the theory of relativity, evaluations of distant elements of physical reality by use of local instruments and photons are defined only *relative* to each other. The nonlocality that is inherent in the word relative is acceptable within Einstein's methods and space-time system. Interestingly, the Bell-CHSH inequalities are also derived by only considering measurement-outcomes *relative* to each other and are, therefore, (as will be shown below in detail) subject to a more subtle interpretation of the concepts "local" and "not-local".

2.2. Einstein's vs Bell's "Locality" and Aspects "Nonlocality"

The derivation of the Bell-CHSH inequalities deals with model-function values $A = \pm 1$ in station S_A and $B \pm 1$ in S_B, respectively, for given polarizer angles (e.g. $j = a$ and $j' = b$). It is, however, not the values of the functions by themselves that matter but only the fraction of $A = B$ versus the fraction of $A \neq B$, as determined by the measurement. Because the functions only possible values are ±1 and because Bell's derivations involve only the products $A \cdot B$, the Bell-CHSH procedure is entirely equivalent to the asking for the outcomes of B relative to those of A (and vice versa).

The $A \cdot B$ products also encompass the notion that both A and B (seen as model events) occur, which is in set theoretic probability denoted by $A \cap B$. Any such statement involves necessarily both distant stations and, therefore, a nonlocality in the broadest sense of the word. Bell's theorem (as stated in the introduction) is, thus, trivially true as soon as we deal with such products.

Bell-CHSH and their followers have, however, narrowed their definition of "local" by two further postulates that are used for the derivation of their inequalities. A model is Bell-CHSH-local (**BC-local**):

1) If and only if the properties of the photon-pairs and their corresponding mathematical variable that Bell denoted by λ neither depend on the polarizer angles nor the function-outcomes corresponding to detector clicks.

And

2) If and only if the conditional probability of B to assume a certain value in station S_B does not depend on the fact that A assumes any value in S_A and vice versa.

I will prove in two separate sections below that (1) is incorrect, because (as mentioned) a careful distinction needs to be made between the elements of reality before and after their evaluations by polarizers and detectors. The distinction is necessary, in general, even if the act of measurement does not alter the elements of physical reality. Einstein's hypothesis is that the photon pairs do have properties that are recognized by the measurement instruments. The assumption of Bell and followers that their variable λ (and the sets of values λ_s that the variable exhibits under different circumstances) may *never* show any relation to the measurement instruments, denies Einstein's hypothesis from the start and without physical or mathematical reason.

Furthermore, I will show that (2) is incorrect because it entails, even for trivially local models, serious mathematical problems with respect to the definition of conditional probabilities in the Kolmogorov framework. The Bell-CHSH definition of "local" is, therefore, not acceptable from a mathematical point of view.

As an alternative, I propose a definition of "local" that is free of these contradictions and denote it by the term ST-local. We denote the measurement time by t_s (which may also stand for two different times t'_s, t''_s [4]). The subscript $s = 1,2,3,\cdots,N$ labels a particular pair-measurement and N is a very large number. Furthermore, I denote the properties of the photons that determine the detector clicks after passing the polarizers by the mathematical model value λ_s.

A model of the Aspect-type experiments is defined as **ST-local:**

3) If and only if the function value of B is deduced entirely from facts available in S_B, yet relative to the value of A that also must be derived in S_B from the value of λ_s for any imaginable polarizer angle in S_A at the time t_s.

The idea of **ST-local** is the following. The theorist, relying on space-time, may derive in station S_B a law of nature for the product $A \cdot B$ by imagining all possible equipment configurations in S_A. After all the measurements are done, the actual equipment configurations of the measurements can be determined from the registered clock-times t_s. The theory is then judged from the consistency with a large number of measurements. This underlying idea is probably as old as the existence of time-measurement. The amazing feature is just that it is applicable to random photon-pair emanations.

Finally, we define the extreme opposites. A model is trivially Einstein-local (**TE-local**):

4) If and only if the objects sent out from the source are at all times accessible to our senses and identified as the direct cause for the outcomes in the distant stations.

A model is **spooky:**

5) If and only if the (model) measurement of B with given polarizer angle at time t_s, alters the model value of the function A for that same measurement-time. (The definition is also valid with A and B exchanged).

A majority of physicists, including Aspect himself have, unfortunately, accepted that the true nature of Aspect-type experiments is spooky as defined by (5), while they found Bell's (1) and (2) acceptable and did not consider (3).

3. The Fundamental Model of Probability Theory and the Quantum Result

These rather abstract definitions are best explained by a specific example of the Fundamental Model of probability theory. I use and follow the notation of Bell-CHSH. However, in contrast to them, I strictly distinguish Bell's variable λ from the specific mathematical model values λ_s that (together with the polarizer angles at the time t_s) determine the detector outcomes and, thus, the values of A, B. There are two detectors related to any given polarizer angles. One for detecting "horizontal" in station S_A, whose clicks we model by the function-outcomes $A(j,\lambda_s)=+1$, while "horizontal" in station S_B is denoted by the function $B(j',\lambda_s)=+1$. Clicks of the second detector are modeled by the same functions, with a value of -1 instead and called "vertical". Bell-CHSH considered mostly two possible polarizer angles in each station: $j=a$ or a' in station S_A and $j'=b$ or b' in S_B and also equal polarizer angles in both stations. While Bell's variable λ must not depend in any way on the instrument configurations, the values λ_s may be clearly linked to both detector outcomes and polarizer angles, as described in the following mathematical model (computer experiment).

The Fundamental model represents the λ_s by a real number, randomly and uniformly chosen from the interval $\Omega=[0,1]$ for each separate model-measurement (see [4] and the explanations in Williams' textbook "Weighing the Odds" [8]). Following Williams, we also may introduce a probability measure x corresponding to the statement "a chosen number is less than or equal to x". We may use that probability measure to determine approximate data averages as well as corresponding theoretical expectation values for $N\to\infty$. The particular choice of λ_s out of [0, 1] permits great flexibility in modeling or simulating properties of the elements of physical reality and, in particular, permits us to develop an infinite variety of mathematical models, one of which may hopefully fit the physics of the problem.

Consider first the following **TE-local** computer-model with both polarizer angles fixed and equal a. Let the λ_s be random numbers created by an excellent random number generator from the interval [0, 1] and let them be sent from the source to the two computers. We consider now a mathematical model with the following features. The "mathematical" polarizers evaluate only a certain digit of λ_s in its binary representation, depending on the time t_s. For reasons of simplicity, we discuss the example that at time t_s it is the digit of number (s + 10) that is being evaluated (it may be a different digit for a different polarizer angle).

Consider now the measurement number $s = 10$. Then it is the 20th digit of λ_{10} that will be evaluated. If that random number features a 0 in the 20th digit of its binary representation, we denote λ_s by λ_{10}^0 and evaluate it such that $A\left(a, \lambda_{10}^0\right) = +1$ as well as $B\left(a, \lambda_{10}^0\right) = -1$. Had the 20th digit been 1, we would have denoted it by λ_{10}^1 and evaluated it such that $A\left(a, \lambda_{10}^1\right) = -1$ and $B\left(a, \lambda_{10}^1\right) = +1$. Bell's reasoning that deterministic outcomes lead (among other factors) to his inequalities can, thus, be turned against him: determinism leads, even for trivially local (**TE-local**) models, to a dependence of the properties of sets of λ_s (as for λ_{10} above) on polarizer angles and function outcomes, which invalidates postulate (1).

We are also able to construct a more general **ST-local** model. Two separated computers evaluate the functions A and B with the only external input of λ_s. We keep the polarizer angle fixed to a for the computer in station S_A, while rotating the angle of the polarizer in S_B during random times t_k toward the angle j', where j' may have any value (and even be switched between any number of values). For simplicity we discuss only $j' = b$. We evaluate B locally in station S_B relative to the value of the function A and conditional to a fixed and arbitrary polarizer angle a in S_A as follows: analog to the procedure above, we introduce (locally in station S_B) the Lebesgue probability measure x for the outcome-product such that $A(a, \lambda_k) \cdot B(b, \lambda_k) = -1$ if and only if $\lambda_k \le x = \cos^2(b - a)$ and +1 otherwise. This choice of probability measure for B relative to A, represents a Malus-type natural law.

We obtain for N model measurements:

$$A \cdot B = -1 \text{ for } \approx N \cos^2(b - a) \tag{1}$$

while the number of positive product outcomes is about:

$$A \cdot B = +1 \text{ for } \approx N \sin^2(b - a) \tag{2}$$

For the single outcomes we may choose $A\left(a, \lambda_k^0\right) = +1$ and $A\left(a, \lambda_k^1\right) = -1$. The marginals ($A$ and B separately) are then in good approximation randomly equal to ±1 by the definitions of the Fundamental Model. The probabilities yield, therefore, the results of quantum mechanics for both the averages of the marginals and for the product averages and may also be used to model actual experiments.

A standard Bell-CHSH (Alice and Bob) objection is that I keep the polarizer angle in station S_A fixed and that my choices in S_B are conditional to that fixed angle in S_A, while Bob "cannot know" the polarizer angle of Alice at the time of measurement t_k. Bob can, however, explore a law of nature conditional to the instrument configurations in S_A and is justified to do so if he is only interested in his outcomes relative to those induced in S_A by λ_k at the time t_k. In fact, the experimenters collect, after all is done, the outcomes for 4 pairs of fixed polarizer angles and determine the averages of N measurements for each pair. The polarizer angles and measurement outcomes that form pairs are identified by the clock-times t_k. The switching of polarizer angles in between the registered measurements has no effect [7].

Another objection arises from the claim of Bell-CHSH that the experimenters have the freedom to choose any polarizer angle (and angle pair) to measure the properties of one given photon pair [4]. For the Fundamental Model, Alice and Bob have no freedom at all to choose the property that is to be evaluated, such as λ_{10}^{0}. That property is entirely determined by the random choice of λ_s and the assumed law of nature and will be different for any other measurement. There exists no freedom to investigate λ_{10}^{0} by using different polarizer angles.

Why is it then that the Bell-CHSH locality conditions are so important for a majority of physicists. One reason has been discussed in [4]: it is simply not possible to find four outcome products $A \cdot B$ for the four CHSH polarizer-angle pairs consistent with a probabilistic Malus type law and for the same λ_s, which has nothing to do with locality considerations. To avoid this problem, we have fixed the angle in station S_A and need, therefore, at any measurement-time t_s only one outcome-pair consistent with Malus. There exists, however, one more argument in Bell's definition of "local", which is postulate (2) that appears to clearly show why my Equations (1) and (2) above must be "not-local". In fact, however, it is postulate (2) which contains a deep-seated mathematical problem and can, therefore, not be applied.

4. Error of the Second Bell-CHSH Locality Postulate

As explained in (2) above, Bell and his followers have postulated that, assuming locality, the probability of $B(j', \lambda_s) = +1$ must not depend on whether $A = +1$ or $A = -1$ for all λ_s and that, therefore, Equations (1) and (2) must be non-local. Gisin [9] appears to clearly proof this fact. Following Bell, Gisin uses the following conditional probabilities (given in my notation):

$$P_{AB}^{cd}(A, B \mid j, j', \lambda_s) = P_A^{cd}(A \mid j, \lambda_s) P_B^{cd}(B \mid j', A, \lambda_s) \tag{3}$$

The vertical line | indicates that A and B assume certain values conditional to the values that the symbols after the vertical line assume. Gisin continues that, owing to locality-postulate (2), we must have in addition:

$$P_B^{cd}(B \mid j', A, \lambda_s) = P_B^{cd}(B \mid j', \lambda_s) \tag{4}$$

This equation is crucial and leads to:

$$P_{AB}^{cd}(A, B \mid j, j', \lambda_s) = P_A^{cd}(A \mid j, \lambda_s) P_B^{cd}(B \mid j', \lambda_s), \tag{5}$$

from which Gisin derives the Bell-CHSH-type inequalities.

However, The Bell-Gisin locality-argument (2) (which results in the crucial Equation (4)) is in conflict with the *set theoretic definition* of conditional probabilities P_B^{cd} of B given A, which is [8]:

$$P_B^{cd}(B \mid A) := \frac{P(A \cap B)}{P(A)} \tag{6}$$

If and only if $P(A) \neq 0$.

To appreciate the necessity of $P(A) \neq 0$ that Bell and Gisin did not include into their derivations, consider the following completely **TE-local** model. Just send out, randomly and exclusively, actual numbers of opposite sign (+1, −1 or −1, +1) toward the two distant stations. Here is the problem: The conditional probability on the left-hand side of Equation (4) is only defined if we have $A \cdot B = -1$ and is ill defined otherwise, namely a 0/0 (zero over zero) problem, while the right-hand side of Equation (4) is always equal to 0 or 1. Gisin's other derivations depend, in addition on BC-locality condition (1) that was also shown to be invalid.

In my **ST-local** computer example, the probability $P\left(A\left(a, \lambda_s\right) = +1\right)$ vanishes for all subsets λ_s^1 according to expression (2). Gisin's Equation (4) involves, thus, for our **ST-local** model and an infinite number of trivial **TE-local** models, conditioning to events with probability 0 which is equivalent to dividing by 0. Because the range of the functions is restricted to $A, B = \pm 1$, Equation (4) is incorrect for a large fraction of the λ_s (50% in the above examples) and, therefore, must not be used to derive the Bell-CHSH inequalities.

Based on these findings, the original experiments on entangled photons by Kocher and Commins [10] assume new importance and appear to support the existence of Einstein's elements of physical reality.

Perhaps it is useful to discuss, by another example, why even respectable researchers and their writings go awry for any number of reasons, when discussing Bell's theorem. Take the two-computer model of Susskind and Friedman [11]. They let the experimenters press a button at each of two computers, in order to "measure" at any moment. However, there is no guarantee that a correlated pair is available at these moments. Of course, such a guarantee may be provided by their "instantaneous cable" that is installed between the computers. But why not using clocks as the experimenters do? Their experimenters (Alice & Bob) may also choose any arbitrary equipment configurations such as the polarizer angles for any given photon pair (λ_s). This, however, is not possible, because the λ_s are randomly chosen and evaluated (e.g. $\lambda_{10}^0, \lambda_{10}^1$) for each new event in the Fundamental Model.

Furthermore, Susskind and Friedman do not discuss that, from all the possible choices of such random equipment configurations, only four pairs are used to derive all averages and the corresponding inequalities of Bell-CHSH. The only randomness of the actually used measurements is that of the sequence of these four pairs, and it is known from the actual experiments that the sequence of the measurements plays no role. Why, then, not accept a model for which the sequence plays no role in the first place. Susskind did emphasize, however, that the locality concepts of Einstein and Bell differ greatly.

5. Conclusions

It is this author's conviction that classical set-theoretic probability theory is indeed applicable to the physics of the Einstein-Bohr debate in contrast to the claims of Bell-CHSH and followers such as Aspect, Gisin, Clauser and many others. However, great care is required when defining conditional probabilities based on physical concepts that have no precise meaning within the Kolmogorov framework. Great care is also required for the physical definitions of "local" and "spooky".

It has been an unfortunate coincidence of factors that made the incorrect Bell-CHSH interpretations prevail for more than half a century: There exists indeed a powerful mathematical theory [3] that leads to Bell-CHSH type theorems, just not for the precise Bell-CHSH premises. Also, the disagreement of Bell-CHSH with experiments was for many a welcome confirmation of Bohr's conviction that the quantum world requires a completely new conceptual net, different from all classical thinking. The very wish to confirm Bohr's notions and to prove Einstein is wrong has led a large number of researchers to throw all caution in the wind and to abandon not only classical thinking but also the classical calculus.

Acknowledgements

I would like to thank Mårten Wikström for valuable discussions.

Conflicts of Interest

The author declares no conflicts of interest regarding the publication of this paper.

References

[1] Bell, J.S. (1964) *Physics*, **1**, 195-200. https://doi.org/10.1103/PhysicsPhysiqueFizika.1.195

[2] Clauser, J.F., Horne, M.A., Shimony, A. and Holt, R.A. (1969) *Physical Review Letters*, **23**, 880-884. https://doi.org/10.1103/PhysRevLett.23.880

[3] Hess, K. (2022) *Symmetry*, **14**, 1-28. https://doi.org/10.3390/sym14010163

[4] Hess, K. (2023) *Journal of Modern Physics*, **14**, 1167-1176. https://doi.org/10.4236/jmp.2023.148064

[5] Bell, J.S. (1976) *Epistemological Letters*, **2**, 2-7.

[6] Einstein, A., Podolsky, B. and Rosen, N. (1935) *Physical Review*, **16**, 777-780. https://doi.org/10.1103/PhysRev.47.777

[7] Aspect, A. (2015) *Physics*, **8**, 123. https://doi.org/10.1103/Physics.8.123

[8] Williams, D. (2001) Weighing the Odds. Cambridge University Press, Cambridge, p. 44, 73, 110.

[9] Gisin, N. (2012) *Foundations of Physics*, **42**, 80-85. https://doi.org/10.1007/s10701-010-9508-1

[10] Kocher, C.A. and Commins, E.D. (1967) *Physical Review Letters*, **18**, 575-577. https://doi.org/10.1103/PhysRevLett.18.575

[11] Susskind, L. and Friedman. A. (2014) Quantum Mechanics. Basic Books, New York, 227-235.

Journal of Modern Physics, 2023, 14, 1771-1782
https://www.scirp.org/journal/jmp
ISSN Online: 2153-120X
ISSN Print: 2153-1196

How to Achieve a Warp Drive

Juan A. Miranda-Colón

Independent Researcher, Puerto Rico, USA
Email: maruca397@yahoo.com

How to cite this paper: Miranda-Colón, J.A. (2023) How to Achieve a Warp Drive. *Journal of Modern Physics*, **14**, 1771-1782.
https://doi.org/10.4236/jmp.2023.1413106

Received: September 30, 2023
Accepted: December 24, 2023
Published: December 27, 2023

Abstract

In this paper, we delve into the intrinsic nature of mass and gravity, as per the amplitude modulation interpretation of the quantum theory. We explore the idea that the elementary constituent is an electromagnetic configuration that interacts with the quantum field, leading to the emergence of inertia and gravity as a reaction to the exchange with the quantum field. While these two phenomena have a common origin, they are distinct. Our proposal suggests manipulating the connection between the quantum field and the particle using high-frequency electromagnetic fields, thereby making a warp drive possible.

Keywords

Photon, Inertia, Gravity, Maxwell's Equations, Magnetic Monopoles, Fine Structure Constant, Warp Drive, *Zitterbewegung*

1. Introduction

As we delve deeper into our analysis, previously discussed in a paper regarding the amplitude modulation hypothesis of the quantum theory, we mention the possibility of manipulating inertia and gravity [1] [2]. Controlling a characteristic or property of a physical object at volition often requires specific knowledge about what we desire to modify. We develop a "toy" model incorporating crucial details from the amplitude modulation interpretation to elucidate the nature of gravity and inertia and propose a method to surmount them. The description or meaning of the fine structure constant and a definition of magnetic monopoles are the foundation on which we build this conjecture. Indeed, inertia is subtly in the fundamental equations concerning classical electrodynamics, and we argue that gravity and inertia are electromagnetic phenomena. In the proposed view of the quantum theory, the elementary constituent is a consequence of an amplitude modulation phenomenon. Hence, associating a second wave to the elementary particle analogous to the signal wave in communications the author refers to as Castellano's wave. In essence, Castellano's wave modulates the amplitude of the de Broglie wave. We, therefore, posit that the second wave is the hidden variable, whose absentia has caused a plethora of interpretations to explain the counterintuitive quantum behaviors or observations. The foundations of quantum physics are a contentious subject where some interpretations are as bizarre as the events they are supposed to explain. Indeed, Schrödinger exemplified the absurdity of the most acknowledged rendition with his cat thought experiment. In the amplitude modulation interpretation, the cat oscillates between dead and alive. Namely, the system oscillates between its possible states. A comparable physical prediction would be the oscillation of the photon's polarization, which explains the observations in the entanglement experiments. The Quantum entanglement phenomenon is a form of synchronicity; no strange or spooky connections link quantum particles. In the following, we will use the mathematical framework of geometric algebra, because it is more natural, less arduous, and straightforward when dealing with these concepts. Moreover, we shall not address controversies or historical debates related to the previous assertions. However, instead, we focus on information regarding how to achieve a warp drive.

2. Fine-Structure Constant

As per our understanding of Schrödinger's *Zitterbewegung* equation [3], the elementary constituent is an amplitude-modulated wave. The amplitude modulation thesis is essential to this paper because it proposes a linear momentum, velocity, force, energy, and mass, among others, for each wave involved in the modulation. The quantum entity is a dynamical system that oscillates among its various possible states and has an information capacity of one bit. Furthermore, the particle is an emergent phenomenon whose radius is the relativistic reduced Compton wavelength. The boundary shares similarities with a quantum oscillator; the particle is in breathing mode. To be precise, its surface vibrates at the broadband frequency, two times the frequency of the signal, carrier, and mass. Given its persistence in fundamental factors, the Compton frequency is the system's natural frequency and remains crucial in our analysis. The Dirac theory presents an intriguing aspect involving certain equations viewed as curiosities without clear physical significance or relevance [4]. These equations have been mainly disregarded due to a lack of understanding of their physical meaning. However, two specific equations warrant closer examination. In particular, one equation we deem fundamental in comprehending the manipulation of inertia and the Sommerfeld constant. The equation in question is as follows, where the Dirac Hamiltonian H_c represents the dynamics of the carrier wave. In the Heisenberg picture, regarding the Dirac Hamiltonian with electromagnetic interactions, there is a dependence on time;

$$\frac{\mathrm{d}H_c}{\mathrm{d}t} = -qc\boldsymbol{\alpha}' \cdot \boldsymbol{E} = -q\boldsymbol{u} \cdot \boldsymbol{E} \tag{1}$$

According to the interpretation we bestow on the power equation, the quantum entity emits and absorbs energy, even though it is supposed to be a constant of motion. This behavior suggests an interaction between the quantum entity and its surroundings, as it communicates with the quantum vacuum field by engaging with it. The vacuum field and the elementary constituent constitute a self-contained system and can be treated as a closed system for quantum mechanical analysis. Namely, the particle is not within or surrounded by the field but an integral part of it. To formulate the toy model, we propose the following Hamiltonian, which takes a purely mechanical perspective on the system. The amplitude represents the zero-point energy of the quantum system, while the unitary operator describes a self-contained quantum system's time evolution or propagation. A critical characteristic of this operator is that it is a unitary transformation, meaning that it is reversible. This property has important implications in the study of quantum mechanics, as it allows for the conservation of information. We conclude that the sign of the exponent of the oscillation is positive, owing to a discernible relationship between the reduced Compton wavelength and the Hamiltonian from the *Zitterbewegung* term in Schrödinger's equation. The multiplication of operators results in a constant, which further supports our determination of the positive sign ($H\lambda_r = c\hbar$). Additionally, regarding the imaginary unit, it ensures the correct sign in the calculations and shifts the oscillation phase. It enables us to describe an oscillation that is real accurately.

$$H = \frac{1}{2}\omega\hbar i \mathrm{e}^{2\omega i t} \tag{2}$$

This equation is equivalent to the Dirac Hamiltonian with electromagnetic interactions, considering the quantum entity's fields, potentials, and rest mass, where the parameter β represents the fourth Dirac matrix.

$$H_c = \boldsymbol{u}\cdot\boldsymbol{\zeta} - qV + m_0 c^2 \beta \tag{3}$$

With the Hamiltonian (2) and simplifying Equation (1), we determined the oscillating electric field, which encompasses the particle resulting from its interaction with the quantum field, where the Schwinger limit is a particular case.

$$E = \frac{\omega^2\hbar}{qu}\mathrm{e}^{2\omega i t} \tag{4}$$

By applying basic principles of electrostatics, one can also ascertain the electric field on the surface of the quantum object, where the following expression is tantamount to the previous amplitude.

$$E = \frac{q}{4\pi\epsilon_0\lambda_r^2} \tag{5}$$

Moreover, when we compare the magnitude of the two, we come to the subsequent correlation.

$$\frac{c}{u} = \frac{q^2}{4\pi\epsilon_0 c\hbar} \tag{6}$$

Assuming that the charge in the previous equation is that of the electron, and the relation regarding the phase velocity and group velocity, $uv = c^2$, we can arrive at the fine-structure constant. This constant is a product of the relativistic analysis of the hydrogen atom's spectral lines. Sommerfeld discovered that the constant is the ratio of the electron's tangential speed in the first circular orbit of the relativistic Bohr atom to the speed of light in the vacuum. It is important to note that the electron in the first circular orbit is in resonance and is a standing wave. However, the result obtained is for a free particle. Therefore, the speed is the magnitude of the minimum translational velocity for the free electron. By analysis of the equation, we infer that the constant is unique to the electron and relates to its intrinsic parameters, including the ratio of external to internal fundamental physical parameters.

$$\frac{c}{u} = \frac{v}{c} = \frac{e^2}{\varrho^2} = \frac{\varepsilon}{\varepsilon_0} = \alpha \tag{7}$$

Hence, there is a Planck charge in the interior of all the elementary constituents, including the photon.

3. Photon Charge

Despite the widespread belief that photons do not have an inherent electric charge, surprisingly, a fact that is not widely known, researchers can still nondestructively detect them in resonant cavities because they display an electric charge when confined or trapped. There are other phenomena, such as Delbrück scattering and photon deflection by magnetic fields in certain mediums or photon molecules, where the photon mimics the behavior of particles possessing an electric charge [5]-[10]. It is worth mentioning that each of these phenomena has a corresponding theory, which reminds the author of the infamous epicycles. According to physicist Dr. V. Brown, he adduced the emergence of a charge in trapped photons for years and heard of its confirmation. However, when he inquired with researchers about their observations, they suggested he should forget it, as it is considered or perceived as a perilous concept (personal communication, April 13, 2002). Some inconvenient observations contrary to our current paradigms are censored, thus hindering progress. Understanding that photons acquire an electric charge in specific circumstances simplifies the explanation of numerous observations using a unified theoretical framework. To effectively understand the behavior of photons in cavities, we use the canonical momentum and the Liénard-Wiechert potential of the carrier wave in the modeling process.

$$\boldsymbol{\zeta} \equiv \boldsymbol{p} - q\boldsymbol{A} \tag{8}$$

For a photon displacing across the vacuum, the momentum is $\boldsymbol{p}$. However, when it is in a high-Q cavity;

$$\boldsymbol{\zeta} = -q\boldsymbol{A} = -q\frac{V}{c^2}\boldsymbol{u} \tag{9}$$

Since for the photon,

$$H = \boldsymbol{u} \cdot \boldsymbol{p} \tag{10}$$

From which the energy-momentum relation follows and will be helpful in the following sections.

$$\mathcal{E}^2 = c^2 p^2 \tag{11}$$

Therefore,

$$H = -q\boldsymbol{A} \cdot \boldsymbol{u}$$

$$\hbar\omega = -qV$$

With the voltage on the surface of the photon in the high-Q cavity;

$$\hbar \frac{c}{\lambda_r} = -q\left(-\frac{q}{4\pi\varepsilon_0\lambda_r}\right)$$

Thus,

$$q = \pm\sqrt{4\pi\varepsilon_0 c\hbar} \tag{12}$$

The charge that enables researchers continuously observe and count nondestructively photons in high-Q cavities is the Planck charge ϱ [11].

4. Photon Rest Energy

The photon's energy and that of the other elementary constituents regarding the amplitude modulation interpretation is twice the observed amount. Each wave in the modulation process contributes the same energy to the system, half observed in each cycle of the photon's *Zitterbewegung*. The following is the energy of the electromagnetic field, and we associate it with the carrier wave:

$$\mathcal{E} = \frac{1}{2}\int\left(\varepsilon_0 E^2 + \frac{1}{\mu_0}B^2\right)\mathrm{d}\tau \tag{13}$$

The mathematical formulas pertaining to the energy stored in electric charge and current distributions follow.

$$\mathcal{E}_{elec} = \frac{1}{2}\int(V\rho)\mathrm{d}\tau = \frac{\varepsilon_0}{2}\int E^2\mathrm{d}\tau + \frac{\varepsilon_0}{2}\int(V\boldsymbol{E})\cdot\mathrm{d}\boldsymbol{a} \tag{14}$$

$$\mathcal{E}_{mag} = \frac{1}{2}\int(\boldsymbol{A}\cdot\boldsymbol{J})\mathrm{d}\tau = \frac{1}{2\mu_0}\int B^2\mathrm{d}\tau - \frac{1}{2\mu_0}\int(\boldsymbol{A}\times\boldsymbol{B})\cdot\mathrm{d}\boldsymbol{a} \tag{15}$$

Equation (13) and an additional term result from the summation of the previous expressions. Indeed, according to the literature [12], the integration over all space implies that the surface integrals are supposed to tend towards zero, leaving behind only the volume integrals. However, there is no rigorous formal proof regarding the previous assertion. Arguments intend to discard the surface integral terms to obtain the well-known conclusion that the energy in circuits is in the fields. Regardless, the surface integrals are zero for the photon, yet not because of the aforementioned arguments.

$$\frac{1}{2}\int\left(\varepsilon_0 V\boldsymbol{E} - \frac{1}{\mu_0}\boldsymbol{A}\times\boldsymbol{B}\right)\cdot\mathrm{d}\boldsymbol{a} = 0 \tag{16}$$

We will demonstrate that the previous discarded terms correlate directly to the free photon's rest energy, which regarding the formula, is ultimately equal to zero—Scilicet, the inertial mass, is subtly found in discarded terms from fundamental electrodynamics.

5. Photon Internal Forces

The stability of the elementary constituent depends on two opposing entropic forces, with equal magnitude and out of sync with each other. However, in the case of the photon, they are not out of phase and cancel each other; there is perfect equilibrium. Moreover, these forces are in plain sight in the fundamental equations relating to the photon's electric and magnetic components.

$$\boldsymbol{E} = -\boldsymbol{u}\times\boldsymbol{B},\ \boldsymbol{u}\cdot\boldsymbol{E} = 0,\ \boldsymbol{B} = \frac{1}{c^2}\boldsymbol{u}\times\boldsymbol{E},\ \boldsymbol{u}\cdot\boldsymbol{B} = 0,\ \|\boldsymbol{u}\| = c \tag{17}$$

It is acknowledged that the expressions denote the known conventional fact that the velocity and the field for the photon are mutually orthogonal. However, there is a more profound meaning to the previous relations since, along with Formula (1), the following puzzling attractive Lorentz-type force also surges from the Heisenberg picture.

$$\boldsymbol{F}_c = -q\left(\boldsymbol{E} + \boldsymbol{u}\times\boldsymbol{B}\right) \tag{18}$$

Therefore,

$$\frac{\mathrm{d}H_c}{\mathrm{d}t} = \boldsymbol{u}\cdot\boldsymbol{F}_c \tag{19}$$

Furthermore,

$$F_c = -\frac{\omega^2\hbar}{u}\mathrm{e}^{2\omega it}$$

where,

$$m = \frac{1}{2}\frac{\omega\hbar}{c^2}i\mathrm{e}^{2\omega it},\ a_c = 2\omega vi \tag{20}$$

We resolve that this force is one of the two entropic forces holding together the elementary constituent. Indeed, it is zero for the photon, and since (1) is also zero for the photon, we end up with the first and second terms in (17). The third relation results from equating to zero the following repulsive magnetic Lorentz-type force.

$$\boldsymbol{F}_s = q_m\left(\boldsymbol{B} - \frac{1}{c^2}\boldsymbol{v}\times\boldsymbol{E}\right) \tag{21}$$

Thus, the second entropic force also follows from the Heisenberg picture, however, with a Hamiltonian and momentum, which describes the behavior of the signal wave. Additionally, the matrix χ is associated with the time component of the group velocity, while the rest mass pertains to the magnetic field.

$$H_s = \boldsymbol{v}\cdot\boldsymbol{\zeta}' + q_m V_s + m_0' c^2\chi \tag{22}$$

We define the electric vector potential A_s regarding the magnetic scalar potential V_s.

$$\zeta' \equiv m_0'\boldsymbol{u} + q_m \frac{V_s}{c^2}\boldsymbol{v} = \boldsymbol{p}' + q_m \boldsymbol{A}_s.$$

where,

$$\boldsymbol{B} = \nabla V_s + \frac{\partial \boldsymbol{A}_s}{\partial t},\ \ \boldsymbol{E} = -\nabla \times \boldsymbol{A}_s$$

Furthermore, in geometric algebra, the magnetic charge and the magnetic scalar potential are trivectors.

$$q_m \equiv cq\acute{\imath},\ \ V_s \equiv \frac{V}{c}\acute{\imath}$$

There is also time dependence upon analyzing the Hamiltonian of the signal in the Heisenberg picture; the fourth term in Equation (17) directly results from this time dependence.

$$\frac{\mathrm{d}H_s}{\mathrm{d}t} = q_m \boldsymbol{v}\cdot\boldsymbol{B} = \boldsymbol{v}\cdot\boldsymbol{F}_s \tag{23}$$

Therefore, it is crucial to acknowledge the existence of a magnetic charge in addition to the electric charge.

6. Magnetic Monopoles

Succinctly, regarding magnetic charges, they are essentially oscillating electric charges that generate a homogeneous field with zero polarity. The Planck charge oscillates in the interior of the elementary constituent in a loop with a Planck radius. The oscillation is akin to a current loop, therefore for two current loops, and according to magnetostatics, the force that each loop feels is:

$$\boldsymbol{F} = -\frac{\mu_0}{4\pi} I_1 I_2 \oint\oint \frac{\hat{\boldsymbol{r}}}{r^2}\mathrm{d}\boldsymbol{l}_1\cdot\mathrm{d}\boldsymbol{l}_2$$

The electric current loops are equivalent;

$$R_1 = R_2 = R$$

And assuming the simples configuration between the loops,

$$\boldsymbol{F} = -\frac{\mu_0}{4\pi} I_1 I_2 \oint\oint \frac{\hat{\boldsymbol{r}}}{r^2}\mathrm{d}l_1\mathrm{d}l_2$$

Therefore, let $I = \frac{q}{T} = qf$, and $\mathrm{d}l = R\mathrm{d}\theta$;

$$\boldsymbol{F} = -\frac{\mu_0 q^2 f_1 f_2 R^2}{4\pi r^2}\left(\oint \mathrm{d}\theta\right)^2 \hat{\boldsymbol{r}}$$

$$\boldsymbol{F} = -\frac{\pi\mu_0 q^2 f_1 f_2 R^2}{r^2}\hat{\boldsymbol{r}}$$

Since the system's frequency is the Compton frequency; therefore, according to the Einstein-de Broglie relation, $fh = mc^2$.

$$\boldsymbol{F} = -\frac{\pi\mu_0 q^2 c^4 m_1 m_2 R^2}{h^2}\frac{\hat{\boldsymbol{r}}}{r^2}$$

Hence, because the radius R is the plank length and q is the Planck charge, gravity is a magnetic force due to magnetic monopoles.

$$\boldsymbol{F} = -G\frac{m_1 m_2}{r^2}\hat{\boldsymbol{r}}$$

The interaction of the Planck charge that resides in the particle's interior with the surrounding environment is the source of gravity and inertia, which is the gist of the conjecture. Modifying gravity's effects on objects, whether to weaken or intensify them, necessitates the implementation of magnetic fields. Therefore, by applying the same methodology that led to Equation (4) development, we arrive at a new equation that contains pertinent information regarding the magnetic field necessary to achieve this objective. This equation also incorporates the Schwinger magnetic field limit as a unique condition in its amplitude.

$$B = \frac{\omega^2 \hbar}{q_m v}\mathrm{e}^{2\omega i t} \tag{24}$$

where the magnetic Lorentz force is:

$$F_s = \frac{\omega^2 \hbar}{v}\mathrm{e}^{2\omega i t} \tag{25}$$

And,

$$m' = \frac{1}{2}\frac{\omega \hbar}{c^2} i\mathrm{e}^{2\omega i t},\ a_s = -2\omega u i \tag{26}$$

Regarding the acceleration, if we require the mass associated with the force to be positive, the acceleration must be negative. In the previous article, multiplying the amplitude of the waves involved in the modulation process yielded the square of the particle radius. Similarly, the product of the acceleration of the waves must result in the square of the *Zitterbewegung* acceleration. Therefore, we add the imaginary units to the acceleration to obtain the correct result. However, this introduces the imaginary unit in the oscillating mass equation to balance the equation, resulting in an eigenvalue of Equation (2). In the following, we will establish expressions for the inertial mass in representations of electric and magnetic fields.

7. Inertial Mass

We will obtain Maxwell's equations in the vacuum, and the approach involves Geometric algebra and applying the energy and momentum operators of the quantum theory to the photon's field component equations. Consequently, we obtain expressions for inertial mass regarding electromagnetic fields and potentials as a byproduct. The initial point of departure will be the components derived from the Lorentz magnetic force, enabling us to acquire Gauss and Faraday's law.

$$\boldsymbol{B} = \frac{\boldsymbol{u}}{c^2} \times \boldsymbol{E}$$

With the geometric product,

$$\boldsymbol{up} = \boldsymbol{u}\cdot\boldsymbol{p} + \acute{\imath}\boldsymbol{u}\times\boldsymbol{p}$$

Since for the photon $\boldsymbol{u} = \boldsymbol{v}$,

$$\boldsymbol{up} = \boldsymbol{u}\cdot\boldsymbol{p} = H$$

$$\boldsymbol{u} = H\frac{\boldsymbol{p}}{|\boldsymbol{p}|^2}$$

$$H \to i\hbar\frac{\partial}{\partial t},\quad \boldsymbol{p} \to -i\hbar\nabla$$

1) Faraday's Law

$$\boldsymbol{B} = \frac{H\boldsymbol{p}}{c^2|\boldsymbol{p}|^2}\times\boldsymbol{E}$$

$$H\boldsymbol{B} = \boldsymbol{p}\times\boldsymbol{E}$$

$$i\hbar\frac{\partial}{\partial t}\boldsymbol{B} = -i\hbar\nabla\times\boldsymbol{E}$$

$$\therefore \frac{\partial\boldsymbol{B}}{\partial t} = -\nabla\times\boldsymbol{E}$$

2) Gauss's Law for Magnetism

$$\boldsymbol{p}\cdot\boldsymbol{B} = \boldsymbol{p}\cdot\left(\frac{\boldsymbol{u}}{c^2}\times\boldsymbol{E}\right)$$

$$-i\hbar\nabla\cdot\boldsymbol{B} = -i\hbar\nabla\cdot\left(\frac{\boldsymbol{u}}{c^2}\times\boldsymbol{E}\right)$$

$$\nabla\cdot\boldsymbol{B} = 0$$

Careful adherence to the outline procedure mentioned above, with the electric force field components, allows us to obtain the remaining relations: Ampere's and Gauss's law. We can take things further by incorporating the Hamiltonian of the signal (22) and carrier (3). Consequently, this approach has allowed us to derive Maxwell's equations again and the subsequent unique set of promising relations.

$$-qV\boldsymbol{E}\beta - mc^2\boldsymbol{E} + qc^2\boldsymbol{A}\times\boldsymbol{B} = 0 \tag{27}$$

$$-m_0'c^2\boldsymbol{B}\chi - q_m\boldsymbol{A}_s\times\boldsymbol{E} + q_mV_s\boldsymbol{B} = 0 \tag{28}$$

With Gauss's law and assuming that the matrices β and χ are the identity matrix in the previous relations, the rest energy and rest mass for the photon articulated in terms of electromagnetic fields and potentials are the following. We conjecture that this concept overarches all the elementary constituents.

$$m_0c^2 = \int\left[\varepsilon_0V\boldsymbol{E} - \frac{1}{\mu_0}\boldsymbol{A}\times\boldsymbol{B}\right]\cdot\mathrm{d}\boldsymbol{a} \tag{29}$$

$$m_0'c^2 = -\frac{1}{\mu_0}\int\left[V_s\boldsymbol{B} + \boldsymbol{A}_s\times\boldsymbol{E}\right]\cdot\mathrm{d}\boldsymbol{a} \tag{30}$$

Equation (16) is a specific instance of Equation (29), indicating that a free photon has no rest mass. However, the derivation process suggests that if the photon obtains a charge, it might also acquire mass. Since the electric mass is nil, we conclude that the magnetic inertial mass (30) is also zero and consequently.

$$\int\left[\frac{V\boldsymbol{B}}{\mu_0 c}+\varepsilon_0 c\left(\boldsymbol{A}\times\boldsymbol{E}\right)\right]\cdot \mathrm{d}\boldsymbol{a}=0 \tag{31}$$

Nonetheless, by utilizing the principles of vector identities, we arrive at the equation for the aggregate energy of the magnetic charge and current distributions, the magnetic analog of Equations (14) and (15).

$$\mathcal{E}_{mag}=\frac{1}{2c}\int V\rho_{mag}\,\mathrm{d}\tau \tag{32}$$

$$\mathcal{E}_{elec}=-\frac{c}{2}\int \boldsymbol{A}\cdot\boldsymbol{J}_{mag}\,\mathrm{d}\tau \tag{33}$$

Hence, the magnetic monopole is undergoing an oscillatory motion, which may result in the emergence of an electric charge. This eventuality would then serve as the origin of the particle's intrinsic charge.

8. Conclusion

The realm of science fiction often alludes to hypothetical technological devices that enable vehicles to circumvent the limitations or restrictions on motion imposed by inertia. With these devices, vehicles accelerate and displace at high speeds or even surpass the speed of causality. Among these apparatuses, the most prominent is the warp drive. Researchers have proposed several warp-type mechanisms based on our current comprehension of gravity, as there are no explicit hypotheses about its nature. Nonetheless, this paper presents an intriguing assumption regarding the fundamental nature of gravity and inertia. Indeed, the research suggests that these two phenomena are intricately linked to electromagnetic forces and can be influenced by applying highly intense high-frequency electromagnetic fields according to Equations (4) and (24). Although this concept may seem reminiscent of previous theories, this paper's approach is unique. The concepts and ideas presented by the author are open to falsification and not limited to gravity and inertia but also include the fine structure constant, magnetic monopoles, the Photon, and entropic forces that play an essential role in holding the particle together. As a result, this paper takes the field of physics closer to a plausible ontology. In a forthcoming paper, we shall further delve deeper into these concepts and explore the potential for a theory of almost everything where the vacuum field interacts with itself, generating an electromagnetic configuration whose properties and characteristics are emergent. Namely, the particle and the field are the same thing in different states. As per our presentation, we did not provide the blueprints for a warp drive-type mechanism; however, we propose that the technological feat of generating potent electric and magnetic fields around an object with the *Zitterbewegung* frequency will disrupt or distort the connection with the ubiquitous quantum field. This will render the entity impervious to the vacuum field, permitting or opening up previously impossible avenues for displacement, acceleration, and even cloaking, making it feasible to achieve a warp drive.

Acknowledgements

The author expresses utmost gratitude regarding Professor Dr. Castellanos's mentorship and assistance. His sagacious counsel and invaluable guidance have been instrumental in fostering the author's professional growth and development.

Conflicts of Interest

The author declares no conflicts of interest regarding the publication of this paper.

References

[1] Miranda-Colón, J. (2022) *Journal of Modern Physics*, **13**, 301-314. https://doi.org/10.4236/jmp.2022.133021

[2] Miranda-Colón, J. (1994) About the Nature of the Wave Function and the New Developments in Quantum Mechanics. Master's Thesis, University of Puerto Rico, Mayagüez, PR.

[3] Schrödinger, E. (1930) Über die Kräftefreie Bewegung in der Relativistischen Quantenmechanik. Sitzungsberichte Akad, Berlin, 418.

[4] Sakurai, J.J. (1967) Advanced Quantum Mechanics. Addison-Wesley, Boston.

[5] Haywood, R. (2023) *Journal of Modern and Applied Physics*, **6**, No. 1.

[6] Zhou, D.L., Zhou, L., Wang, R.Q., Yi, S. and Sun, C.P. (2007) *Physical Review A*, **76**, Article ID: 055801. https://doi.org/10.1103/PhysRevA.76.055801

[7] Brzobohatý, O., Karásek, V., Šiler, M., *et al.* (2013) *Nature Photon*, **7**, 123-127. https://doi.org/10.1038/nphoton.2012.332

[8] Burke, D.L., Field, R.C., Horton-Smith, G., Spencer, J.E., Walz, D., Berridge, S.C., Bugg, W.M., Shmakov, K., Weidemann, A.W., Bula, C., McDonald, K.T., Prebys, E.J., Bamber, C., Boege, S.J., Koffas, T., Kotseroglou, T., Melissinos, A.C., Meyerhofer, D.D., Reis, D.A. and Ragg, W. (1997) *Physical Review Letters*, **79**, 1626-1629. https://doi.org/10.1103/PhysRevLett.79.1626

[9] Mann, C., Horsley, S.A.R. and Mariani, E. (2020) *Nature Photonics*, **14**, 669-674. https://doi.org/10.1038/s41566-020-0688-8

[10] Shen, J.-T. and Fan, S.H. (2007) *Physical Review Letters*, **98**, Article ID: 153003. https://doi.org/10.1103/PhysRevLett.98.153003

[11] Haroche, S. (1995) *Annals of the New York Academy of Sciences*, **755**, 73-86. https://doi.org/10.1111/j.1749-6632.1995.tb38957.x

[12] Griffiths, D.J. (1981) Introduction to Electrodynamics. Prentice-Hall, New Jersey.

Nomenclature

u phase velocity, v group velocity, $c\alpha'$ Dirac velocity, p group velocity momentum, p' phase velocity momentum, q electric charge, q_m magnetic charge, ϱ Planck charge, H Hamiltonian, H_s signal Hamiltonian, H_c carrier Hamiltonian, t time, R radius, r position, $\hat{r}$ radial unit vector, c speed of light, ω angular frequency, f frequency, T period, $\hbar$ reduce Planck constant, h Planck constant, λ_r reduce Compton wavelength, ϵ_0 permittivity in free space, μ_0 magnetic susceptibility in free space, ε permittivity in the interior of the electron, θ or ϕ angle, a the fine structure constant, V electric scalar potential, V_s magnetic scalar potential, í geometric factor, i imaginary number, A magnetic vector potential, A_s electric vector potential, $\mathcal{E}$ energy, τ volume, a area, j current, l loop length, ρ_m magnetic charge density, ρ electric charge density, G gravitational constant, E electric field, B magnetic field, ζ group velocity canonical momentum, ζ' phase velocity canonical momentum, F force, F_c electric force, F_s magnetic force, a_c carrier acceleration, a_s signal acceleration, m carrier mass, m' signal mass, m_0 and m'_0 rest mass.